Signal Processing in Arrayed MIMO Systems

Xiao Lei Wang

A thesis submitted for the degree of
Doctor of Philosophy (PhD)
in the Faculty of Engineering of Imperial College London
and the Diploma of Imperial College(DIC)

2009

Communications and Array Processing
Department of Electrical and Electronic Engineering
Imperial College London

Abstract

Multiple-Input Multiple-Output (MIMO) systems, using antenna arrays at both receiver and transmitter, have shown great potential to provide high bandwidth utilization efficiency. Unlike other reported research on MIMO systems which often assumes independent antennas, in this thesis an arrayed MIMO system framework is proposed, which provides a richer description of the channel characteristics and additional degrees of freedom in designing communication systems.

Firstly, the spatial correlated MIMO system is studied as an array-to-array system with each array (Tx or Rx) having predefined constrained aperture. The MIMO system is completely characterized by its transmit and receive array manifolds and a new spatial correlation model other than Kronecker-based model is proposed. As this model is based on array manifolds, it enables the study of the effect of array geometry on the capacity of correlated MIMO channels.

Secondly, to generalize the proposed arrayed MIMO model to a frequency selective fading scenario, the framework of uplink MIMO DS-CDMA (Direct-Sequence Code Division Multiple Access) systems is developed. DOD estimation is developed based on transmit beam rotation. A subspace-based joint DOA/TOA estimation scheme as well as various spatial temporal reception algorithms is also proposed.

Finally, the downlink MIMO-CDMA systems in multiple-access multipath fading channels are investigated. Linear precoder and decoder optimization problems are studied under different criterions. Optimization approaches with different power allocation schemes are investigated. Sub-optimization approaches with close-form solution and thus less computation complexity are also proposed.

Contents

Abstract **2**

Contents **3**

List of Figures **6**

List of Tables **9**

Acknowledgements **10**

Abbreviations and Acronyms **11**

Notation **13**

List of Symbols **15**

1 Introduction **17**
1.1 Space-Time Characteristics of Multipath Fading Channels 17
1.2 Diversity 18
1.2.1 Classification of Diversity 19
1.2.2 Space Diversity 20
1.3 Space-Time Arrayed Communications 24
1.3.1 Space-Time Array Processing 24
1.3.2 Classification of Space-Time Wireless Channels 26
1.4 Motivation and Organization of the research 28
Appendix 1.A Field Regions of Antenna 34
Appendix 1.B Selectivity and Coherence of Wireless Channels 36

2 Arrayed MIMO Modelling **39**
2.1 Introduction 39
2.1.1 Kronecker-based Model 40
2.1.2 Weichselberger's Model 42
2.1.3 Sayeed's Model 43
2.1.4 Müller's Models 45
2.2 System Modelling 47
2.2.1 Propagation with DOD and DOA 48
2.2.2 Cluster Model 51
2.3 Spatial Correlation Studies 58

2.3.1 Comparison with Kronecker-based model 60
2.3.2 Comparison with Weichselberger's model 62
2.4 Capacity and Array Geometry 63
2.5 Number of Multipaths and Spatial Degree of Freedom 71
2.6 Summary 74
Appendix 2.A Kronecker Product 76
Appendix 2.B Degree of Freedom 78

3 Space-time Design in Arrayed MIMO-CDMA Uplink Systems 84
3.1 Introduction 84
3.2 Arrayed CDMA-MIMO System Modeling 85
3.3 MIMO-CDMA STAR Receivers 94
3.4 Channel Estimation 104
3.4.1 Blind STAR Estimation of DOA and TOA 104
3.4.2 Cooperative Beamforming: Estimation of DODs 110
3.5 Summary 113
Appendix 3.A Decision variables of different space-time receivers for MIMO-CDMA with QPSK modulation 114

4 Precoder and Decoder Optimization in Arrayed MIMO-CDMA Downlink Systems 116
4.1 Introduction 116
4.2 Channel Modelling 118
4.3 Optimization Objectives 125
4.3.1 Optimal Multiplexing Order 126
4.3.2 Optimal Precoder and Decoder 128
4.4 Iterative Optimization 130
4.4.1 Iterative Joint Precoder-Decoder Optimization With Power Allocation Scheme-I 130
4.4.2 Iterative Precoder-Decoder Optimization With Power Allocation Scheme-II 133
4.5 Sub-optimal Close-form Optimization 133
4.5.1 Close-form SNIR Optimization 134
4.5.2 Close-form Tx Power Minimization 136
4.6 Numerical Studies 137
4.7 Summary 143
Appendix 4.A Proof of Lemma 4.1 144
Appendix 4.B Proof of Theorem 4.1 145
Appendix 4.C Proof of Eqn. (4.19) 146
Appendix 4.D Proof of Eqn. (4.63) 147

5 Conclusions and Further Work 148
5.1 Thesis Summary 148
5.2 List of Contributions 150
5.3 Suggestions for Further Works 151
5.3.1 Robust Space Time Processing In Arrayed MIMO 151
5.3.2 Antenna Selection 153

5.3.3 STBC in Arrayed Correlated MIMO System 154
5.3.4 Ad-hoc distributed precoding/decoding optimization . . . 155

References **157**

List of Figures

1.1 Multipath propagation. 18
1.2 Structure of a space-only beamformer. 22
1.3 Array Patterns of a 5 element Uniform Linear Array. 23
1.4 Structure of space-time beamformer using tapped delay lines. . . . 24
1.5 Array Pattern of a space-time beamformer using a 5 element Uniform Linear Array and tapped delay lines with 31 taps. 25
1.6 Classification of space-time channels. 27
1.7 MIMO Channel 28
1.8 Illustration of Jakes' One-Ring Scattering Model 30
1.9 Spatial correlation changes with inter-element spacing in Jake's one-ring propagation model. 31
1.10 Field regions of an antenna. 34

2.1 A schematic example of (2,2)-MIMO. 41
2.2 Some idealized radio propagation environments and their corresponding coupling matrice $\mathbb{G}$ for Weichselberger model. 44
2.3 "Local area" and array manifold. 49
2.4 Schematic interpretation of the arrayed MIMO channel. 53
2.5 Modelling of diffused MIMO channel. 56
2.6 Modelling of arrayed MIMO Channel. 57
2.7 Model descrepancy factor κ as a function of the array size N for three different multipath cases. 61
2.8 The complementary $\mathrm{CDF}_{\mathrm{capacity}}$ of a $(8,8)$-MIMO system employing ULA with $0.5\lambda_c$ spacing at both the Tx and the Rx. The number of resolvable multipaths $K = 1$, 8, 16, 32, 64 and 80, $\overline{\theta}_k$ and θ_k randomly distributed on $[0, 2\pi]$, and $\overline{P}/\sigma_n^2 = 15$ dB. 65
2.9 The same as Figure 2.8 except that the inter-element spacing of Tx and Rx array is increased to $5\lambda_c$. 65
2.10 Ergodic Capacities of a (8,8)-MIMO system employing $0.5\lambda_c$ inter-antenna spacing ULA and UCA (shown in Figure 2.11) at both Tx and Rx, simulated using i.i.d. model, Kronecker-based model and proposed model. 66
2.11 Array geometries investigated in the simulation: (a) Uniform Linear Array; (b) Cross Array; (c) Uniform Circle Array, all with fixed spacing. 67

2.12 $\text{CDF}_{\text{capacity}}$ of $(8,8)$-MIMO system employing different array geometries with fixed inter-antenna spacing $0.5\lambda_c$ and $\overline{P}/\sigma_n^2 = 10$ dB, 20 dB and 30 dB. 67
2.13 Array geometries investigated in the simulations: (a) Uniform Linear Array; (b) Cross Array; (c) Uniform Circle Array, all with fixed aperture. 68
2.14 $\text{CDF}_{\text{capacity}}$ of $(8,8)$-MIMO employing different array geometries with fixed aperture $3.5\lambda_c$ and $\overline{P}/\sigma_n^2 = 10$ dB, 20 dB, and 30 dB. . 69
2.15 (a) Capacity of a (2,2)-MIMO system employing half wave spacing ULA at both Tx and Rx. There are two resolvable multipaths, one fixed at $(\text{DOD}, \text{DOA}) = (45°, 132°)$, another varies. (b) Contour figure of (a). 70
2.16 Cumulative distribution functions of capacity for a SISO and a (8,8) i.i.d. MIMO channels with $\overline{P}/\sigma_n^2 = 25$, 28, 31 and 34 dB. . . 72
2.17 Relation of Spatial Degree of Freedom and the number of antennas in Tx/Rx arrays, with the array aperture fixed at $2.5\lambda_c$, $5\lambda_c$ and $10\lambda_c$, with $\overline{P}/\sigma_n^2 = 20$ dB. 73
2.18 Relationship between Spatial Degree of Freedom.and the number of paths for SISO, (2,2)-MIMO, (3,3)-MIMO and (4,4)-MIMO. . . 74

3.1 Diagram of uplink MIMO-CDMA transmitter. 87
3.2 Uplink arrayed MIMO frequency selective channel of the i^{th} user. 89
3.3 Diagram of uplink MIMO-CDMA Receiver 90
3.4 Inter-Symbol Interference (ISI) resulted from previous and next symbols. 91
3.5 Diagram of decision variables at the output of different receivers of the MIMO-CDMA systems with BPSK modulation. for a single run of 200 data symbols. The subspace-based ST receivers show significant near-far resistant ability. 101
3.6 BER performance of different receivers in a MIMO-CDMA system with 10 users, each with 3 multipaths. $\overline{N} = 2$ and $N = 2$, with half-wavelength spacing. 102
3.7 BER performance of different receivers in a MIMO-CDMA system with 10 users, each with 3 multipaths. $\overline{N} = 2$ and $N = 4$. All arrays are ULA with half-wavelength spacing. 102
3.8 BER performance of MIMO-CDMA system of 10 and 15 users, using 2-element ULA (half-wavelength spacing) at transmitters, 3-element ULA (half-wavelength spacing) at receivers, and assuming perfect channel estimation. 103
3.9 Joint angle (DOA) and delay (TOA) estimation of all the multipath components of the desired user based on Eqn. (3.62) as shown in (a) 3D surface plot and (b) 2D contour plot of (a). 109
3.10 An example of cooperative beamforming approach: (a) DOA/TOA estimation; (b) rotated Tx beamforming while steering mainlobes towards DOA at Rx; (c) DOD information feedback; (d) Tx-Rx beamforming. 111

3.11 The gain pattern at the output of the receiver array beamformers as a function of the direction of the transmit rotating beam. . . . 112
3.12 Diagram of decision variables at the output of different receivers of the MIMO-CDMA systems with QPSK modulation. for a single run of 200 data symbols. The subspace-based ST receivers show significant near-far resistant ability. 115

4.1 System architecture of the transmitter of BS in arrayed MIMO-CDMA downlink communication systems. 119
4.2 Downlink arrayed MIMO frequency selective channel of the i^{th} user. 121
4.3 System architecture of the receiver in arrayed MIMO-CDMA downlink communication systems. 124
4.4 Convergence study for the proposed iterative LM-based optimization algorithm with and without power distribution in a 6-user MIMO-CDMA system, with input $E_b/N_0 = 0$, 5, and 10 dB. . . . 139
4.5 Convergence study for the proposed iterative LM-based optimization algorithms with different number of transmit antennas, in a 6-user MIMO-CDMA system, with input $E_b/N_0 = 10$ dB. 139
4.6 BER performance of different optimization schemes for a 6-user MIMO-CDMA system with 6 element Tx ULA and 2 element Rx ULA, $N_c = 15$, $K_i = 3$. 140
4.7 BER performance of the proposed iterative algorithms (by 30 iterations) with power allocation scheme I/II, and the eigendecomposition-based transmit precoding with RAKE/MMSE decoding. There are 6 users in the MIMO-CDMA system. 141
4.8 The same as Fig. 4.7 except there are 10 users in the MIMO-CDMA system. 142
4.9 BER performance of the proposed iterative schemes (by 30 iterations) with and without array geometry uncertainty, for a 5-user MIMO-CDMA system with 6 element Tx ULA and 2 element Rx ULA, $N_c = 15$, $K_i = 2$. 142

5.1 MIMO channel with antenna selection 153

List of Tables

2.1 DOA and DOD parameters for capacity studying example. 66

3.1 User's parameters for DOA and TOA estimation example 108
3.2 Channel parameters for DOD estimation example. 112

Acknowledgements

I am most indebted to Professor Athanassios Manikas, my supervisor, who, in the past four years, introduced me to the field of array communications. His wide knowledge and insightful thinking have been of great value for me. I am thankful for his patience and guidance. It is very unlikely I would have seen this endeavor through to its end without him.

I wish also to express my warm thanks to my colleagues in the communications and array processing group who I have worked with. Tingting Zhang, George Elissaios, George Efstathopoulos, Farrukh Rashid and Victor Li have given me useful help during enormous technical discussions.

Finally, above all, I wish to thank my family. Their support and kind encouragement have made a truly large part in my completing this work. To them I dedicate this thesis.

Abbreviations and Acronyms

3G/4G	Third/Fourth Generation
AWGN	Additive White Gaussian Noise
AIC	Akaike Information Criterion
BER	Bit Error Rate
BPSK	Binary Phase Switch Keying
BS	Base Station
$\text{CDF}_{\text{capacity}}$	Cumulative Density Function of Capacity
CDMA	Code Division Multiple Access
CSI	Channel State Information
DOA	Direction Of Arrival
DOD	Direction Of Departure
DS-CDMA	Direct Sequence Code Division Multiple Access
EGC	Equal Gain Combining
FFT	Fast Fourier Transform
STBC	Space Time Block Code
IID	Independent Identical Distribution
ISI	Inter Symbol Interference
MAI	Multiple Access Interference
MMSE	Minimum Mean Square Error

MIMO	Multiple Input Multiple Output
MISO	Multiple Input Single Output
MRC	Maximal Ratio Combining
MSE	Mean Square Error
MSLR	Maximum Signal-to-Leakage Ratio
MUSIC	Multiple Signal Classification
PN	Pseudo Noise
RX	Receiver
SC	Selection Diversity
SER	Symbol Error Rate
SIMO	Single Input Multiple Output
SISO	Single Input Single Output
SNR	Signal-to-Noise Ratio
SNIR	Signal-to-Noise-plus-Interference Ratio
S/P	Serial-to-Parallel
ST	Space Time
STAR	Spatial Temporal ARray
SVD	Singular Value Decomposition
TDD	Time Division Duplex
TDL	Tapped Delay Line
TOA	Time of Arrival
TX	Transmitter
UCA	Uniform Circle Array
UE	User Equipment
ULA	Uniform Linear Array

Notation

$\mathcal{Z}$	Set of integers
$\mathcal{R}$	Field of real numbers
$\mathcal{C}$	Field of complex numbers
a, A	Scalar
$\underline{a}$, $\underline{A}$	Column Vector
$\mathbb{A}$	Matrix
$\|A\|$	Absolute value
$\|\|\underline{A}\|\|$	Euclidian norm of vector $\underline{A}$
$\|\|\mathbb{A}\|\|_{\mathcal{F}}$	Frobenius norm of matrix $\mathbb{A}$
$\underline{A}^b$	Element by element power
$\exp(\underline{A})$	Element by element exponential of vector $\underline{A}$
$(\cdot)^*$	Complex conjugate
$(\cdot)^T$	Transpose
$(\cdot)^H$	Hermitian transpose
$\otimes$	Kronecker product
$\odot$	Hadamard product
$\oslash$	Hadamard division
$\mathbb{I}_N$	Identity matrix of $N \times N$ dimension

$\mathbb{O}_{N\times M}$	$N \times M$ matrix of all zeros
$\underline{0}_N$	$N \times 1$ vector of all zeros
$\underline{1}_N$	$N \times 1$ vector of all ones
$\mathbb{J}_N$	$N \times N$ downshifting matrix
$\text{row}_l(\mathbb{A})$	l^{th} row of the matrix $\mathbb{A}$
$[\mathbb{A}]_{ij}$	Element of the matrix $\mathbb{A}$ on the i^{th} row and j^{th} column
$[\underline{A}]_i$	i^{th} element of the vector $\underline{A}$
$\text{diag}(\underline{A})$	Diagonal matrix with the vector $\underline{A}$ as the leading diagonal
$\underline{\text{diag}}(\mathbb{A})$	Column vector with elements the diagonal elements of the matrix $\mathbb{A}$
$\mathbb{P}_{\mathbb{A}}$	Projection operator matrix onto the range space of $\mathbb{A}$
$\mathbb{P}_{\mathbb{A}}^{\perp}$	Complementary projection operator of the matrix $\mathbb{A}$

List of Symbols

$\underline{u}_{ij}$	direction vector of the j^{th} spatial subchannel of the i^{th} user
$\underline{\mathrm{k}}_k$	wavenumber vector pointing towards the DOA of the k^{th} path
$\underline{b}_i[n]$	n^{th} transmitted vector-signal
$\hat{\underline{b}}_i[n]$	n^{th} detected vector-signal
$\underline{d}_i[n]$	n^{th} decoded vector-signal of the i^{th} user
h_{ij}	channel coefficient between the j^{th} Tx antenna and the i^{th} Rx antenna
$\underline{m}_i(t)$	complex baseband transmitted vector-signal of the i'th user
$\underline{x}[n]$	n^{th} received vector-signal
$\underline{n}[n]$	n^{th} noise-vector at input of the receive array
B	bandwidth
C	capacity
C_{ergodic}	ergodic capacity
G	array gain
F_c	carrier frequency
$J_0(x)$	Bessel function of the first kind of zero order
K_i	number of spatially distinct subchannels of the i'th user
M	number of users
N	number of antennas at the receiver

$\overline{N}$	number of antennas at the transmitter
$N_i^{(s)}$	number of signal streams
N_0	power spectral density of noise
N_c	length of pseudo code
$\underline{S}_{ij}$	array manifold vector of the j^{th} spatial subchannel of the i^{th} user
T_c	chip period
T_{cs}	bit or symbol duration
$\mathbb{E}_i$	MSE matrix of the i^{th} user
$\mathbb{G}_{i,\xi}$	composite STAR channel matrix associated with current symbols
$\mathbb{G}_{i,\xi}^{(\text{prev})}$	composite STAR channel matrix associated with previous symbols
$\mathbb{G}_{i,\xi}^{(\text{next})}$	composite STAR channel matrix associated with next symbols
$\mathbb{H}$	channel coefficient matrix
$\mathbb{H}_w$	channel coefficient matrix with i.i.d. elements
$\mathbb{R}$	receiver-side covariance matrix
$\overline{\mathbb{R}}$	transmitter-side covariance matrix
$\mathbb{R}_H$	channel covariance matrix
$\overline{\mathbb{W}}_i$	precoder or transmit beamforming matrix of the i^{th} user
$\mathbb{W}_i$	decoder or receive beamforming matrix of the i^{th} user
$\underline{\beta}_{ij}$	propagation coefficient of the j^{th} multipath of the i^{th} user
ρ	correlation coefficient
λ_c	carrier's wavelength
σ_n	variance of noise
τ_{ij}	delay of the j^{th} path of the i^{th} user
θ_{ij}	nominal direction of the j^{th} spatial subchannel of the i^{th} user

Chapter 1

Introduction

1.1 Space-Time Characteristics of Multipath Fading Channels

Generally speaking, wireless channels are much more difficult and hostile than wired channels, since the former composes of multipaths which arise as the sequence of reflection, diffraction and scattering of the radiated energy off objects that lie in the propagation path. An illustrative example of these three basic propagation mechanisms is shown in Figure 1.1.

Multipaths in wireless channels create *small-scale fading* effects. Given that the receiver (Rx) antenna is located in Fraunhofer region [1] of transmitter (Tx) antenna (see Appendix 1.A), the signal received at any point in the space may consist of a large number of plane waves having randomly distributed amplitudes, phases, delay, and angles of arrival. Combination of these multipath components at the Rx antenna causes the fluctuation in received signal, thereby inducing signal distortion or *small-scale fading*.

The propagation channel introduces dispersion to the transmitted signal in

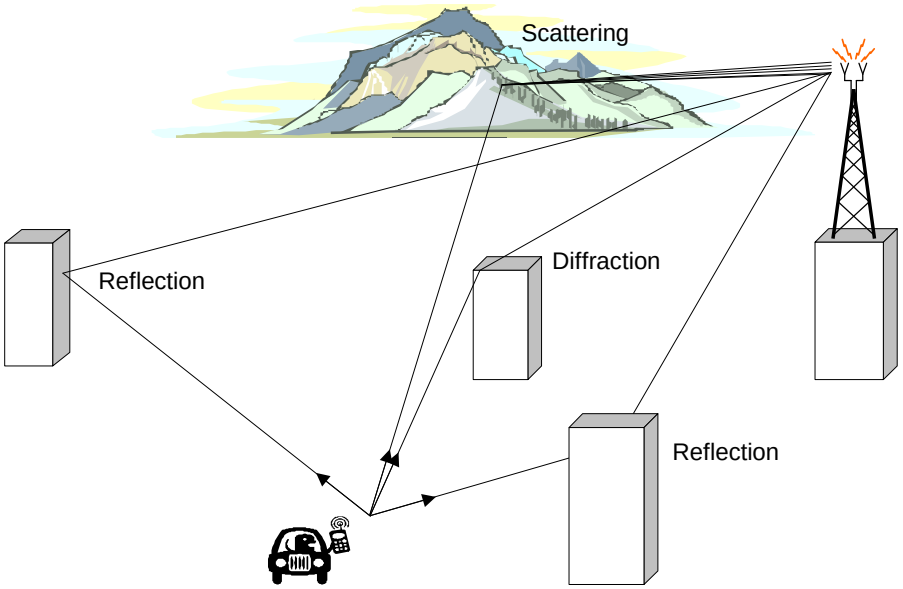


Figure 1.1: Multipath propagation.

different dimensions, e.g. frequency, time, and space. Accordingly, the channel dispersion can be characterized in terms of *delay spread*, *Doppler spread*, and *angle spread* (see Appendix 1.B and reference [2] [3] [4])

1.2 Diversity

Dispersion of multipaths in the wireless channel causes the signal at the receiver to distort or fade significantly. One of the most powerful techniques to mitigate the effects of fading is *diversity*.

Diversity is defined as a general technique that utilizes two or more copies of the signal with varying degrees of noise/interference effects to achieve, by selection or a combination scheme, higher degree of message-recovery performance than that achievable by any one of the individual copies separately.

1.2.1 Classification of Diversity

The idea behind *diversity* is to send the same data over multiple independent fading paths. For instance [3] [5],

- In *frequency diversity*, the same information (usually narrowband signal) is transmitted on different carrier frequencies which are separated by the *coherence bandwidth* of the channel; then at the receiver several replicas of the transmitted signals are combined before a decision is made. This diversity technique requires additional bandwidth and power to send signal over multiple frequency bands.

- *Time diversity* is achieved by transmitting the same information at different times, where the time difference is greater than the *coherence time* of the channel. It does not require increased bandwidth and transmit power, but does decrease the data rate.

- While some of *spread spectrum* techniques, e.g. *Frequency Hopping* systems, are frequency diversity, widely-used *Code Division Multiplexing Access* (CDMA) spread spectrum system is the most important implementation of time diversity (also known as *code diversity*).

- As it has been reported that the horizontal and vertical polarization paths between the transmitter and the receiver are uncorrelated [6], orthogonal polarization can be exploited to obtain *polarization diversity*.

- *Space diversity*, also known as *antenna diversity*, is one of the most popular forms of diversity used in wireless communication systems.

1.2.2 Space Diversity

The utilization of both time and frequency diversity incurs an expense to introduce redundancy - time in the case of time diversity and bandwidth in the case of frequency diversity. However, spatial diversity is an attractive alternative that does not cost additional time or bandwidth. This property of space diversity has sparked the interest in the implementation of space diversity in the 3G or beyond mobile communications system [5].

1.2.2.1 Receive Diversity

Traditionally, multiple antennas have been used at the receiver to combat channel fading. Each pair of Tx and Rx antennas provides a signal path from the transmitter to the receiver. By sending signals that carry the same information through different paths, multiple independently faded replicas of the data symbol can be obtained at the receiver end; hence, more reliable reception is achieved.

For example [2], in a slow Rayleigh-fading environment with one transmit and N receive antennas, the transmitted signal is passed through N different paths. It is well known that if the fading is independent across N antenna pairs, a maximal *diversity gain* of N can be achieved, i.e. an average error probability can be made to decay like the signal-to-noise ratio at the input of Rx array has been increased from SNR to SNR^N.

1.2.2.2 Transmit Diversity

Since 1990s, there has been an increasing interest in *transmit diversity* techniques. In *transmit diversity* there are multiple Tx antennas, among which the transmit power is distributed.

When the channel state information (CSI) is known to the transmitter, the

system is very similar to receive diversity. However, without CSI, transmit diversity technique requires a combination of space and time diversity via, for example, Alamouti scheme [7]. In Alamouti scheme, a space diversity order of 2 can be obtained by transmitting two different symbols s_1 and s_2 from antennas 1 and 2 respectively during the first symbol period, followed by signals $-s_2^*$ and s_1^* form antennas 1 and 2 respectively during the next symbol period. Extension of Alamouti scheme in systems with more than two Tx antennas results in *space-time block coding* (STBC) [8] [9].

1.2.2.3 Array Diversity

Array techniques can be seen as the most sophisticated and advanced space diversity techniques. *Antenna array* (or *smart antennas*) system is formed by a number of antenna elements with a given geometry with measurements taken with respect to the array reference point. Throughout the thesis, without loss of generality, all antennas considered are assumed to be isotropic and within the local area[1] of the array's reference point.

A typical structure of array system - (space-only) beamformer that exploits the space diversity at the receiver is depicted in Figure 1.2. It is a *narrowband* beamformer which assumes that the bandwidth of the signal is narrow enough that the baseband signal waveform stays almost constant at each array element. The beamformer operates by adjusting the phase and amplitude of the signals induced on each element of the antenna array using the weights $\{w_1, w_2, \ldots, w_N\}$ and combining to form the beamformer output, thus a beam has been formed towards the direction where maximum gain is obtained.

[1] Local area is the largest volume of free-space about a specific point $\underline{r} = [r_x, r_y, r_z]^T$ in which the wireless channel can be modelled as the summation of homogeneous plane waves.

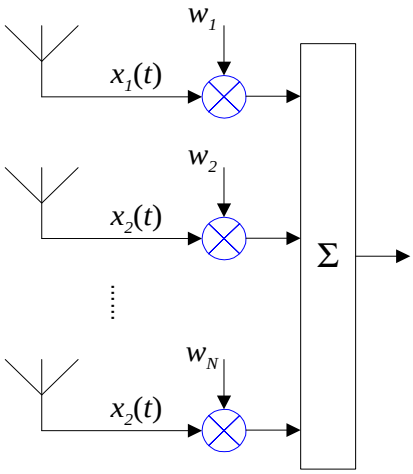


Figure 1.2: Structure of a space-only beamformer.

The *array gain* (diversity gain of array system) can be defined by [1]

$$G \triangleq \frac{\text{SNR}_{out}}{\text{SNR}_{in}} \tag{1.1}$$

where SNR_{in} and SNR_{out} refer respectively to the signal-to-noise ratio at the input and output of the beamformer. As shown by Figure 1.3 (a) and (b), for a 5-element uniform linear array (ULA) beamformer with half wavelength inter-element spacing, if simply adding up received signals of all antennas, i.e. $w_i = 1$ for all $i = 1, \cdots, N$, the SNR_{out} of the signal impinging from direction 90° and 270° will be increased 5 fold. By applying proper spatial array processing techniques steering the beam towards another direction, say, 120°, the SNR_{out} of the signal impinging from direction 120° and 240° will get the maximum array gain, as shown in (c) and (d) of Figure 1.3.

Different weight-vectors create different beamformers. The simplest weight-vector is formed using diversity combining rule. This is used to overcome the problem of fading in radio channels and utilizes the fact that the signals arriving at different locations fade differently. The combining techniques that are currently used in various space diversity systems are *selection combining*, *threshold*

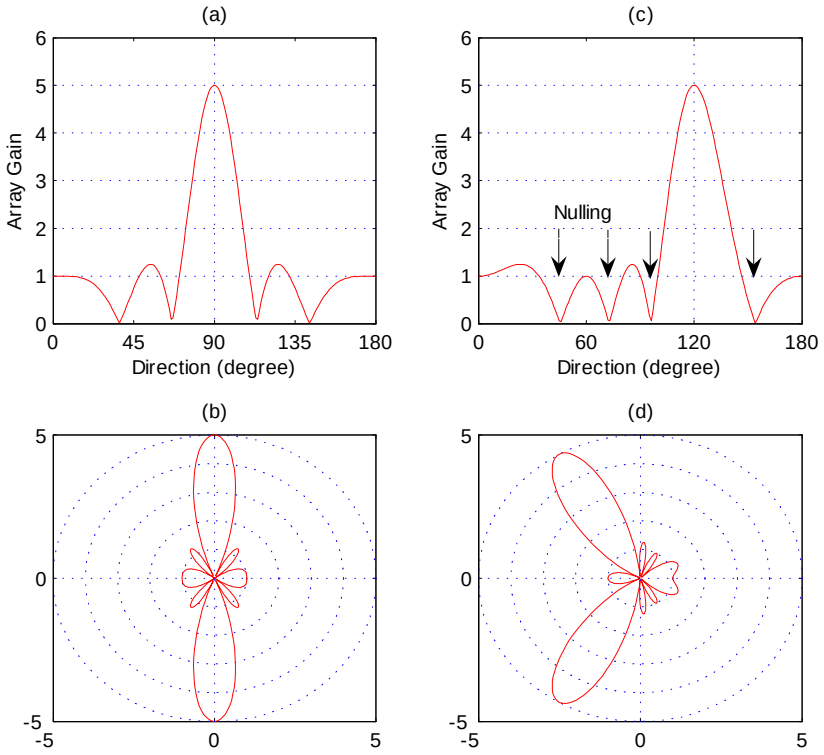


Figure 1.3: Array Patterns of a 5 element Uniform Linear Array.

combining (switch and stay combining), *equal gain combining* (EGC) and *maximal ratio combining* (MRC) [5].

Furthermore, as indicated in (c) of Figure 1.3, with beamformer, a number of *nulling directions* are created, which enable the receiver diminishes the interference from these directions. The beam pattern of the array depends on the geometry, the amplitude and phase excitation of the elements, and also the radiation pattern of individual elements.

With the effort of the community of array processing on wireless communications, integration of array processing and communication techniques has moved from the conventional direction nulling and phase-arrays to advanced superresolution arrays, e.g. multiple signal classification (MUSIC) method [10], direction finding and superresolution adaptive beamformers.

1.3 Space-Time Arrayed Communications

1.3.1 Space-Time Array Processing

At the multiple-antenna receiver, *space-time* and not just information associated with the time communication signals can be utilized to provide more sophisticated and powerful wireless communication systems. A typical structure of space-time beamformer that exploits both the space and the time diversity at the receiver is depicted in Figure 1.4.

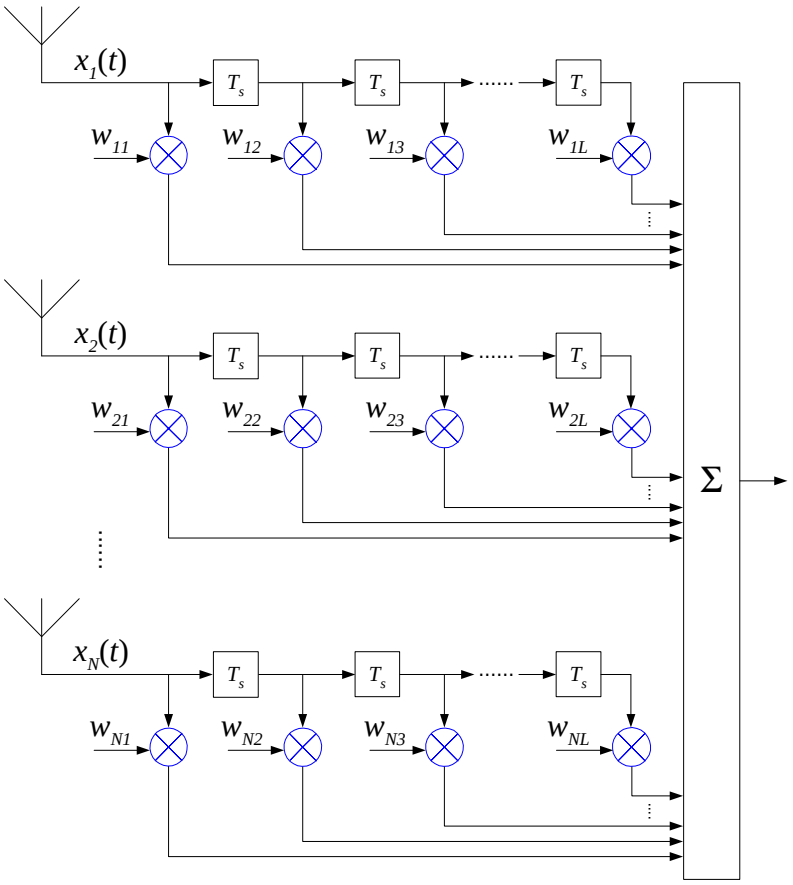


Figure 1.4: Structure of space-time beamformer using tapped delay lines.

Space-time beamformer is often employed in frequency selective channel where the transmitted signal bandwidth is much greater than the coherence bandwidth of the channel, e.g. in CDMA spread spectrum system. A bank of N tapped delay lines (TDL), each of length L, are concatenated to cope with the time dispersion caused by frequency selective fading. Again, the beamformer operates by adjusting the phase and amplitude of the signals induced on each tap of each element of the antenna array using the weights $\{w_{ik},\ i = 1, ..., N;\ k = 1, ...L\}$ and combining to form the space-time beamformer output, thus a beam has been formed towards the TOA as well as the DOA where maximum gain is required as shown in Figure 1.5. The space-time array processing techniques is capable of achieving space and time diversity simultaneously.

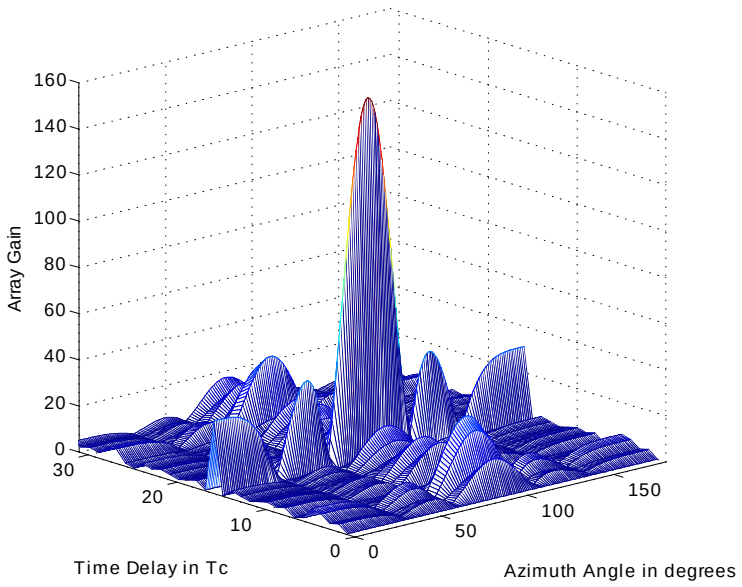


Figure 1.5: Array Pattern of a space-time beamformer using a 5 element Uniform Linear Array and tapped delay lines with 31 taps.

1.3.2 Classification of Space-Time Wireless Channels

From the viewpoint of array processing, space-time wireless channels can be classified, based on the number of inputs and outputs, into four main categories using the terms

- Scalar input/output to indicate a single input/output and
- Vector input/output to indicate a set of more than one input/output.

In a similar fashion the terms scalar-signal and vector-signal indicate a single signal or a set of more than one signal respectively. Using the above terms and with reference to Figure 1.6, the space-time communication channels can be classified into four basic types as follows:

- *Scalar-Input Scalar-Output (SISO)* channel: in point-to-point transmission, the single antenna element is employed at both ends of the transmission link.
- *Scalar-Input Vector-Output (SIVO)* channel: in point-to-point transmission, the system employs a single antenna transmitter and an antenna array receiver; in the multiple access system, (i) *SIVO MA-1* channel is formed with the single antenna element is employed at both the transmitter and the receivers of multiple users; (ii) *SIVO MA-2* channel is formed with the employment of antenna arrays at the receivers of multiple users and a single antenna element at the transmitter.
- *Vector-Input Scalar-Output (VISO)* channel: in the case of point-to-point transmission, *VISO* channel is formed when an antenna array is employed at the transmitter and a single antenna is used at the receiver; in the multiple access system, (i) *VISO MA-1* channel is formed with the single antenna element is employed at both the receiver and the transmitters of multiple

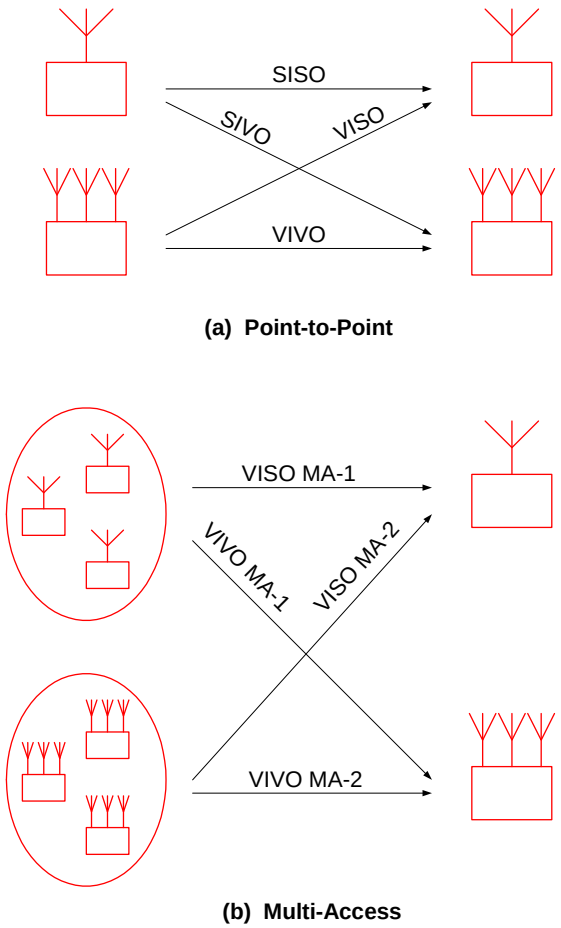


Figure 1.6: Classification of space-time channels.

users; (ii) *VISO MA-2* channel is formed with the employment of antenna arrays at the transmitters of multiple users and a single antenna element at the receiver.

- *Vector-Input Vector-Output (VIVO)* channel: Similar to the classification of VISO channel, there are different types of *VIVO* channels depending on how vector-signals are formed at the transmitter and receiver. In point-to-point transmission, the VIVO channel is formed with the employment of antenna arrays at both transmitter and receiver. In the case of a multiple access system, there are (i) *VIVO MA-1* where the system employs single

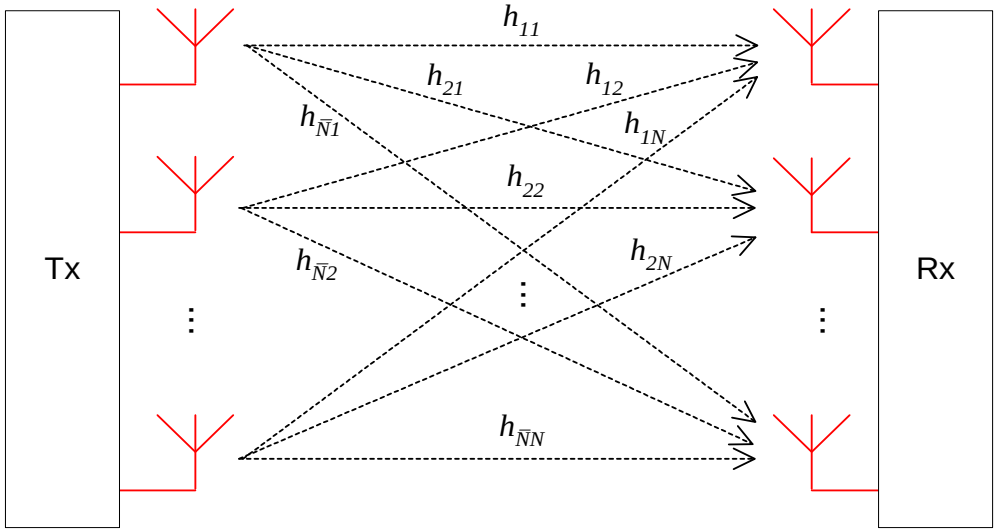


Figure 1.7: MIMO Channel

antenna transmitters and an antenna array receiver; and (ii) *VIVO MA-2* where antenna arrays are used at both the transmitters and the receiver in the system.

Please note that what is defined here as VIVO channel is similar with the definition of multiple-input multiple-output (MIMO) channel and, by using the former, the correlation of the multiple channels is highlighted.

1.4 Motivation and Organization of the research

In later 1990's, Telatar [11], Fochini and Gans [12] found that, by using Multiple antennas at both transmitter and receiver (as depicted in Figure 1.7), MIMO system can provide N^*-fold capacity increase compared with Single-Input Single-Output (SISO) systems, where $N^* = \min\left(\overline{N}, N\right)$, with $\overline{N}$ and N denotes the number of the antenna elements at the transmitter and the receiver[2].

[2]Note that, throughout this thesis, a symbol with a 'bar' at the top will denote a transmitter's parameter.

To illustrate the insight of conventional MIMO, consider a single-user (point-to-point), single polarization, narrowband MIMO system depicted in Figure 1.7 with $\overline{N}$ antenna elements at the transmitter, and N antenna elements at the receiver, referred to as $(\overline{N}, N)$-MIMO. The N dimensional received signal vector $\underline{x}(t)$ can then be modelled as

$$\underline{x}(t) = \mathbb{H}\underline{m}(t-\tau) + \underline{\mathrm{n}}(t) \tag{1.2}$$

where $\underline{m}(t)$ is a $\overline{N} \times 1$ transmitted signal vector, and $\underline{\mathrm{n}}(t)$ a $N \times 1$ circularly symmetric complex Additive White Gaussian Noise (AWGN) vector with zero mean and variance σ_n^2, i.e.,

$$\underline{\mathrm{n}}(t) \sim \mathcal{CN}\left(\underline{0}_N, \sigma_n^2 \mathbb{I}_N\right). \tag{1.3}$$

The $N \times \overline{N}$ channel matrix

$$\mathbb{H} = \begin{bmatrix} h_{1,1}, & h_{1,2}, & \cdots & h_{1,\overline{N}} \\ h_{2,1}, & h_{2,2}, & \cdots, & h_{2,\overline{N}} \\ \vdots & \vdots & \ddots & \vdots \\ h_{N,1}, & h_{N,2}, & \cdots & h_{N,\overline{N}} \end{bmatrix} \tag{1.4}$$

is called the MIMO channel matrix, where $h_{i,j}$ denotes the channel connecting the j^{th} transmitter antenna to i^{th} receiver antenna.

If the Channel State Information (CSI) is unknown to the transmitter and $\mathbb{R}_{mm} \triangleq \mathcal{E}\left\{\underline{m}(t)\,\underline{m}(t)^H\right\} = \mathbb{I}_{\overline{N}}$ (where $\mathcal{E}\{\cdot\}$ is the expectation operator), the capacity of the MIMO channel is [2]

$$C = B\log_2 \det\left(\mathbb{I}_N + \frac{\overline{P}}{\overline{N}\sigma_n^2}\mathbb{H}\mathbb{H}^H\right) \quad \text{bits/s} \tag{1.5}$$

For fixed $\overline{P}/\sigma_n^2$, if $\mathbb{H}$ is a random matrix with all elements to be independent, it has been proven that [12]

$$C(N^*) \to \text{constant} \cdot N^* \tag{1.6}$$

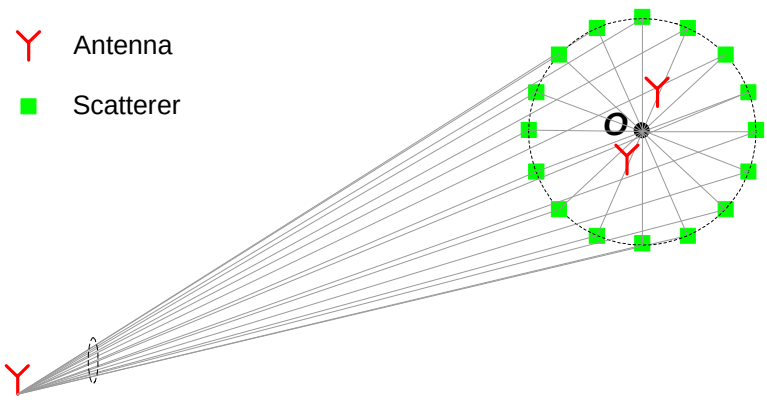


Figure 1.8: Illustration of Jakes' One-Ring Scattering Model

for high SNR scenarios and N^* being large. This means, asymptotically, the capacity increase is proportional to the increase of the number of the antenna elements at transmitter and receiver [11] [12] [13].

Since $\mathbb{H}$ is time-variant, the MIMO capacity C in Eqn. (1.5) is then a statistic variable relying heavily on the correlation matrix,

$$\mathbb{R}_H \triangleq \mathcal{E}\left\{\mathrm{vec}\left(\mathbb{H}\right)\mathrm{vec}^H\left(\mathbb{H}\right)\right\} \tag{1.7}$$

When the idea of MIMO systems was firstly brought out, i.i.d. condition

$$\boxed{\text{i.i.d. Assumption:} \quad \mathbb{R}_H = \mathbb{I}_{N\overline{N}}} \tag{1.8}$$

was its fundamental presumption(see [12]), i.e. all channel coefficients $h_{i,j}\left(t\right)$ in the channel matrix $\mathbb{H}$ are identical independent distributed (i.i.d.).

The widely-accepted i.i.d. assumption (1.8) originates from Jakes' one ring propagation model. As depicted in Figure 1.8, consider a system with single transmit antenna and the receiver employs two antennas with local scatterers uniformly distributed on a ring in the vicinity. When the distance between the transmitter and the receiver is much greater than the radii of the scattering ring and the number of the scatterers is large, the spatial correlation coefficient of two

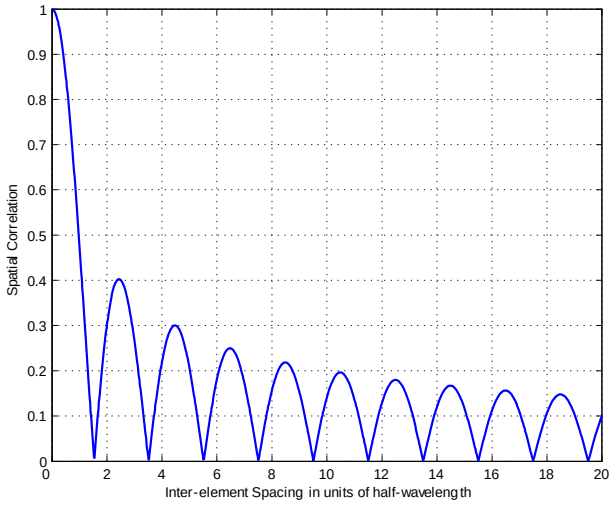


Figure 1.9: Spatial correlation changes with inter-element spacing in Jake's one-ring propagation model.

spatial channels can be expressed as

$$\rho \approx J_0\left(\frac{2\pi\, d}{\lambda_c}\right) \tag{1.9}$$

where $J_0(x)$ is the Bessel function of the first kind of zero order, d the inter-element spacing and λ_c the carrier's wavelength [14]. As shown in Figure 1.9, by increasing element spacing, the spatial correlation can be arbitrarily small.

Practical propagation greatly differed from Jake's one-ring model. Some practical limitations are:

- physical size of the *user equipment* (UE) limits the inter-element spacing;
- the scattering effect in the vicinity of the base station is very small, since they are always elevated and unobstructed by local scatterers.
- recent research has unveiled that, even at the vicinity of UE, the one-ring model is too idealized. The scattering environment around UE is more likely to be characterized by a number of dominant clusters, each with a

impinging direction and angular spread [15]. This will be elaborated in Chapter 2.

Dramatic deviation of, for example, the calculation of the capacity and STBC design will be caused if spatial correlation is taken into account in the investigation of MIMO. As a result, in recent years, attention has been paid to correlated MIMO system. However, existing researches on this topic are all statistical approaches. They model the overall stochastic channel as a random matrix conformed to certain distributions without characterizing individually the radio channel parameters. As stated by Ernst et. al.: "*Radio propagation forms the basis for any radio channel including MIMO systems ... popular mathematical models and commonly applied statistical assumptions sometimes turn out to neglect important properties of MIMO radio channels.*"

The whole work conducted in this thesis is motivated by investigating the correlation properties of MIMO channels from the radio propagation point of view. Thus, by exploiting antenna arrays in wireless channel, the research is based on parametric physical models which are more accurate descriptions of the actual propagation environment whose parameters represent physically meaningful quantities, such as path delay, direction and complex path gains. In this thesis, parametric channel models will be developed using the array manifold concept, which is a natural representation and thus a perfect abstraction of the channel propagation characteristics.

The rest of the thesis is structured as follows:

- In Chapter 2, MIMO system is investigated as an array-to-array communication system from the array processing viewpoint. By exploiting the propagation characteristics of multipaths for a single-user point-to-point communication, a novel arrayed MIMO model is derived using the concept

of the 'array manifold' associated with both Rx and Tx arrays. With the proposed model, spatial correlation, capacity and degree of freedom of the correlated MIMO system are extensively studied.

- In Chapter 3, the proposed correlated MIMO channel model of Chapter 2 has been used in a multi-user space-time CDMA environment. With the introduction of MIMO Spatial Temporal ARray (STAR) manifold, the uplink of the arrayed multi-user MIMO-CDMA system simultaneously transmitting multiple signal streams is studied. Based on the subspace techniques, the algorithms of channel parameters estimation as well as space-time receivers are proposed.

- In downlink of the arrayed multi-user MIMO-CDMA infrastructure, the powerful computational ability of base station makes the transmit side preprocessing possible. So, in Chapter 4, with the similar framework used in the chapter 3, the Tx-Rx joint optimization problem is addressed. Under different criterions, such as minimizing the mean-square-error (MSE) or received signal-to-noise-plus-interference ratio (SNIR), optimization and sub-optimization schemes with different computational cost are derived and compared.

- The work described in this thesis is concluded in Chapter 5. Furthermore, some future directions such as the robust arrayed MIMO, antenna selection, Space-Time Block Coding (STBC) in correlated MIMO systems and game theory based ad-hoc Tx-Rx optimization are presented in this chapter.

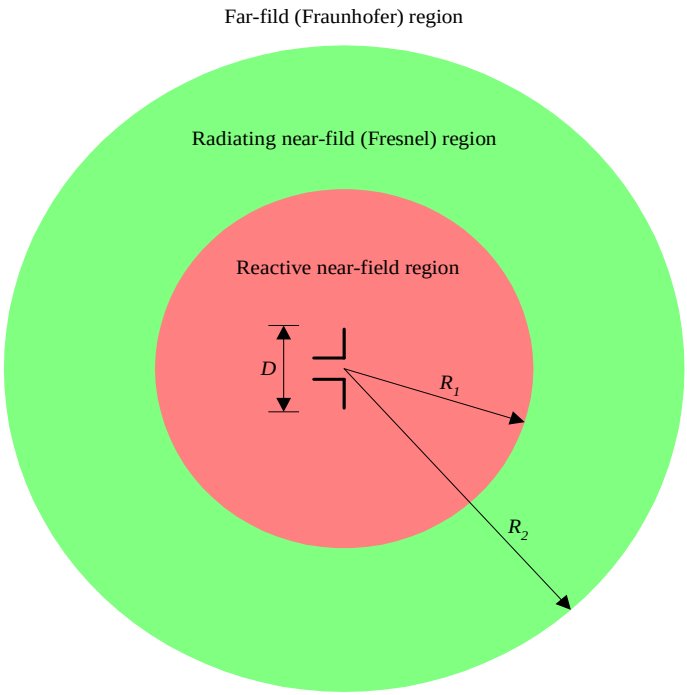


Figure 1.10: Field regions of an antenna.

Appendix 1.A Field Regions of Antenna

As shown in Figure 1.10, the space surrounding an antenna is usually subdivided into three regions: reactive near-field, radiating near-field (Fresnel) and far-field (Fraunhofer) regions [1].

Reactive near-field region is defined as "that region of the field immediately surrounding the antenna wherein the reactive field predominates."[3] For most antennas, the outer boundary of this region, R_1, is taken at

$$R_1 = 0.62\sqrt{\frac{D^3}{\lambda}} \tag{1.10}$$

where D is the largest dimension of the antenna and λ is the wavelength.

Far-field (Fraunhofer) region is defined as "that region of the field of an antenna where the angular field distribution is essentially independent of the dis-

[3]In this section, those in quotation marks is from the IEEE *Standard Definitions of Terms for Antennas* (IEEE Std 145-1973)

tance from the antenna." The inner boundary of this region, R_2, is taken at

$$R_2 = \frac{2D^2}{\lambda} \tag{1.11}$$

and the outer one at infinity.

Radiating near-field (Fresnel) region is the region of the field between the reactive near-field region and the far-field region wherein radiation fields predominate and the angular field distribution is dependent upon the distance from the antenna.

Appendix 1.B Selectivity and Coherence of Wireless Channels

- *Delay spread* T_{spread} is caused by multipath arrival with different time delays. It can be defined as the maximum excess delay between the first and last arrived path components, during which the received signal power falls below some threshold level. Typical values of delay spread are on the order of nanoseconds in indoor radio channel [15] and on the order of microseconds in the outdoor radio channels [16]. Additionally, the time dispersion of the fading channels can also be characterized by *coherence bandwidth* B_{coh}, which is defined as the frequency range over which the signals have a strong potential for amplitude correlation. Delay spread (T_{spread}) and coherence bandwidth (B_{coh}) are inversely proportional to one another, i.e.

$$B_{\text{coh}} \simeq \frac{1}{T_{\text{spread}}} \tag{1.12}$$

In a wireless communication system, if the symbol period of transmitting symbol T_s is much greater than delay spread, the effects of time dispersion are negligible at the receiver and multipath fading is frequency flat. Therefore, the channel is known as the *flat fading* channel if

$$T_s \gg T_{\text{spread}} \tag{1.13}$$

As the signal bandwidth B_s is inversely proportional to symbol period T_s, condition (1.13) is equivalent to

$$B_s \ll B_{\text{coh}} \tag{1.14}$$

Otherwise Inter-symbol-interference (ISI) arises and the multipath fading is frequency selective, resulting in *frequency selective* channel.

- The time variations of the channel which arise from the motion of transmitter/receiver antennas cause a *Doppler shift* in the received signal. *Doppler Spread* B_{Dop} is a measure of the spectral broadening caused by the time rate of the change of the wireless channel and is defined as the range of frequencies over which the received Doppler spectrum is essentially nonzero. The space-time correlation function is the Fourier transform of the Doppler power spectrum with T_{coh} defined as the channel coherence time over which the channel's response to a transmitted signal has a correlation greater than some threshold. *Doppler spread* and *coherence time* are parameters that describe the time varying nature of the channel. Analogous to the delay spread and coherence bandwidth, the approximate relationship between the two parameters is given as

$$T_{\mathrm{coh}} \simeq \frac{1}{B_{\mathrm{Dop}}} \tag{1.15}$$

If the baseband signal bandwidth B_s is much greater than the Doppler spread, the channel impulse response changes at a rate much slower than the transmitted baseband signal and the effects of Doppler spread are negligible. Thus the fading channel can be categorized as the *slow fading* (or time flat) channel. Therefore, a signal undergoes slow fading if

$$B_s \gg B_{\mathrm{Dop}} \tag{1.16}$$

or equivalently

$$T_s \ll T_{\mathrm{coh}} \tag{1.17}$$

Otherwise, in a *fast fading* (or time selective) channel, the channel impulse response changes rapidly within the symbol period. In practice, fast fading only occurs for relatively very low data rates.

- *Angle spread* at the receiver (θ_{spread}) refers to the spread in the Direction Of Arrival (DOA) of the multipath components at the receive; Similarly, *angle spread* ($\overline{\theta}_{\text{spread}}$) at the transmitter refers to the spread in the Direction of Departure (DOD) of the multipath components which finally reach the receiver. *Coherence distance* at the receiver (D_{coh}) and at the transmitter (D_{coh}) are the maximum spatial separations over which the channel response can be assumed constant. The coherence distance is inversely proportional to the angle spread - the larger the angle spread, the shorter the coherence distance, i.e.

$$D_{\text{coh}} \propto \frac{1}{\theta_{\text{spread}}} \tag{1.18}$$

and

$$\overline{D}_{\text{coh}} \propto \frac{1}{\overline{\theta}_{\text{spread}}} \tag{1.19}$$

The channel is said to be *space selective* between two antennas if their separation is larger than the coherence distance. Otherwise the channel is *space flat*.

Chapter 2

Arrayed MIMO Modelling

2.1 Introduction

A primary assumption made about MIMO was that the signals propagating between different elements of Tx and Rx array endured independent identical distributed (i.i.d.) Rayleigh fading [12]. This assumption has been widely used in capacity calculations and space-time coding. However, it has been reported recently [17][18] that this assumption does not hold in the majority (if not all) of practical scenarios.

As has been stated in [19], spatial correlation exists in practice and it is a function of scattering environment, antenna response, array aperture and array geometry. Under one-ring modelling of rich scattering propagation, the envelop of the spatial correlation between two channels connecting a Tx/Rx element and two Rx/Tx elements is a zero-order Bessel function of the receiver element spacing [14] (see Eqn. 1.9). With the increase of element spacing, the spatial correlation converges to zero rapidly. However, in commercial mobile communication systems, the inter-element spacing in a User Equipment (UE) will be limited by its actual size. Moreover, many field experimental measurements have found that the plane

wave propagation in MIMO communications is more likely to be characterized by a number of dominant clusters [15], instead of one-ring model. Researches (e.g. in [20]) have unveiled that capacity results taking into account spatial correlated fades will significantly deviate from results based on i.i.d. assumption. Therefore, analyzing and modeling of correlated MIMO channels become a vital task before realizing the promising bandwidth utility efficiency of MIMO systems.

2.1.1 Kronecker-based Model

One of the most popular models existing for spatial correlated MIMO systems is the so-called Kronecker-based model [2] [21] [22]. With reference to Figure 2.1, the essential assumptions made by this model are

- The spatial correlation[1] between the fading from two Tx antennas to one Rx antenna, known as Tx correlation, does not depend on the choice of the Rx antenna. That is

$$\rho\left(h_{11}, h_{12}\right) = \rho\left(h_{21}, h_{22}\right) \triangleq \rho_t \tag{2.1}$$

- The spatial correlation between the fading from one Tx antenna to two Rx antennas, known as Rx correlation, does not depend on the choice of Tx antenna. That is

$$\rho\left(h_{11}, h_{21}\right) = \rho\left(h_{12}, h_{22}\right) \triangleq \rho_r \tag{2.2}$$

- The spatial correlation of the fading channels between two pair of Tx and Rx antennas is the product of the corresponding transmitter and receiver correlation. That is

$$\rho\left(h_{12}, h_{21}\right) = \rho_t \rho_r \tag{2.3}$$

[1] For two random variables a and b, their correlation coefficient $\rho\left(a, b\right) \triangleq \frac{\mathcal{E}\{ab^*\}}{\sqrt{\mathcal{E}\{|a|^2\}\mathcal{E}\{|b|^2\}}}$

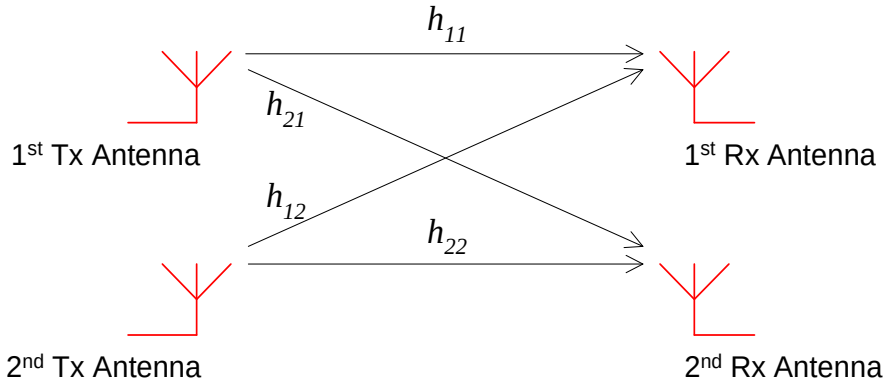


Figure 2.1: A schematic example of (2,2)-MIMO.

Based on the above three assumptions, it can be proved (see Appendix of [21]) that the spatial correlation matrix

$$\mathbb{R}_H \triangleq \mathcal{E}\left\{\mathrm{vec}\left(\mathbb{H}\right)\mathrm{vec}\left(\mathbb{H}\right)^H\right\} \quad \in \mathcal{C}^{\overline{N}N\times\overline{N}N} \tag{2.4}$$

can be represented as a Kronecker product of the Tx and Rx spatial correlation matrices $\overline{\mathbb{R}}$ and $\mathbb{R}$, i.e.

$$\mathbb{R}_H{=}\overline{\mathbb{R}}^T \otimes \mathbb{R} \tag{2.5}$$

where $\overline{\mathbb{R}}$ and $\mathbb{R}$ are defined by

$$\overline{\mathbb{R}} \triangleq \frac{1}{N}\mathcal{E}\left\{\mathbb{H}^H\mathbb{H}\right\} \quad \in \mathcal{C}^{\overline{N}\times\overline{N}} \tag{2.6}$$

$$\mathbb{R} \triangleq \frac{1}{\overline{N}}\mathcal{E}\left\{\mathbb{H}\mathbb{H}^H\right\} \quad \in \mathcal{C}^{N\times N} \tag{2.7}$$

Equivalently, the correlated MIMO channel corresponding to Kronecker correlation model (2.5) can be expressed [2] as

$$\mathbb{H} = \mathbb{R}^{1/2}\mathbb{H}_w\overline{\mathbb{R}}^{1/2} \tag{2.8}$$

where $\mathbb{H}_w$ refers to the spatially 'white' (i.i.d.) MIMO channel.

For instance, with reference to Figure 2.1, if

$$\overline{\mathbb{R}}{=}\begin{bmatrix} 1 & \rho_t \\ \rho_t^* & 1 \end{bmatrix} \tag{2.9}$$

$$\mathbb{R} = \begin{bmatrix} 1 & \rho_r \\ \rho_r^* & 1 \end{bmatrix} \tag{2.10}$$

then following the Kronecker-based model, the spatial correlation matrix is

$$\mathbb{R}_H = \begin{bmatrix} 1 & \rho_r & \rho_t^* & \rho_t^*\rho_r \\ \rho_r^* & 1 & \rho_t^*\rho_r^* & \rho_t^* \\ \rho_t & \rho_t\rho_r & 1 & \rho_r \\ \rho_t\rho_r^* & \rho_t & \rho_r^* & 1 \end{bmatrix} \tag{2.11}$$

Although the Kronecker-based correlated MIMO model provides a simple mean to characterize the correlated fading in MIMO channel, its accuracy has been questioned by a number of incompatible results reported recently (e.g. [17] and [18]). For instance, Svantesson et al. [18], via statistical tests, indicated that larger MIMO systems showed strong non-normality and could not be well modelled by Kronecker product. Measurements of an $(8, 8)$-MIMO system carried out by Bonek et al. [17] indicated that while the i.i.d. model largely overestimated the MIMO capacity, the Kronecker-based model underestimated the capacity systematically.

A perceivable explanation to the discrepancy of Kronecker-based model is that the assumption Eqn. (2.3) is derived from the rich scattering scenario, which is exactly assumed by i.i.d. Rayleigh propagation. The fact that the practical scattering scenario is not rich enough invalidates the independency of Tx/Rx correlation.

2.1.2 Weichselberger's Model

It is evident that properly dealing with the coupling of the transmitter and receiver spatial correlation is a key factor when modelling the correlated MIMO. To achieve this, Weichselberger et al. [23] have proposed a statistical model as

follows

$$\mathbb{H} = \mathbb{U}\left(\mathbb{G} \odot \mathbb{H}_w\right)\overline{\mathbb{U}}^T \tag{2.12}$$

where $\mathbb{U}$ and $\overline{\mathbb{U}}$ are respective the eigenvectors of the Rx and the Tx correlation matrices, i.e. $\mathbb{R} = \mathbb{U}\mathbb{D}\mathbb{U}^H \in \mathcal{C}^{N\times N}$ and $\overline{\mathbb{R}} = \overline{\mathbb{U}}\ \overline{\mathbb{D}}\ \overline{\mathbb{U}}^H \in \mathcal{C}^{\overline{N}\times\overline{N}}$. The so-called 'coupling matrix' $\mathbb{G}$ specifies how the mean amount of energy is coupled from the Rx's eigenvectors to the Tx's eigenvectors, reflecting the spatial arrangement of scattering objects. Some typical radio propagation environments and the corresponding coupling matrices are shown in Figure 2.2.

Simulations in [23] have shown that a MIMO channel, synthesized using Weichselberger's model, approximates a practical measured channel better than using the Kronecker-based model. Nevertheless, space information of MIMO systems, such as the geometry of the antenna arrays, is neglected by Weicheslberger's model.

2.1.3 Sayeed's Model

Sayeed [24] represented the MIMO channel with a virtual spatial channel matrix $\mathbb{H}_V \in \mathcal{C}^{N\times N}$:

$$\mathbb{H} = \mathbb{F}\mathbb{H}_V\overline{\mathbb{F}}^H \tag{2.13}$$

where $\mathbb{F} \in \mathcal{C}^{N\times N}$ and $\overline{\mathbb{F}} \in \mathcal{C}^{\overline{N}\times\overline{N}}$ are channel independent Discrete Fourier Transform (DFT) matrices. By DFT, the direction of departure (DOD) and the direction of Arrival (DOA) were artificially divided into $\overline{N}$ and N discrete beams, respectively. The propagation between the Tx and the Rx is partitioned into these $\overline{N} \times N$ virtual DOD-DOA bins, and the fading coefficients associated with the virtual bins are assumed to be independent.

With mathematical tractability, Sayeed's virtual representation is a good approach for modelling of correlated MIMO channel, although it suffers from some

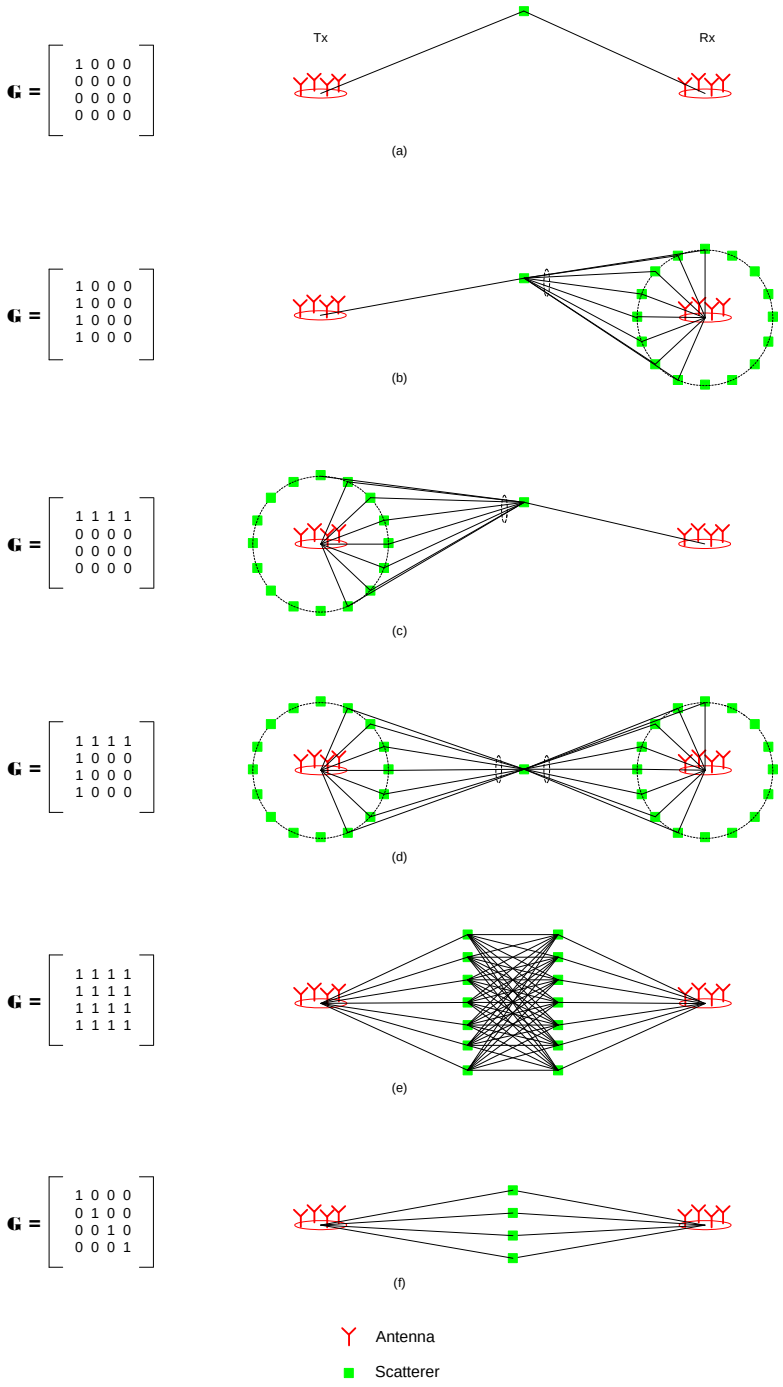


Figure 2.2: Some idealized radio propagation environments and their corresponding coupling matrice $\mathbb{G}$ for Weichselberger model.

principle limitations:

1. The independency of the fading coefficients of the virtual bins assumed by Sayeed is an asymptotic approximation, i.e. only stands when the number of Tx/Rx array elements increases to infinity. In the case of limited number of the array elements, it is plausible to imply the uncorrelated virtual fading coefficients from the well-accepted uncorrelated scattering assumption.

2. When determining the virtual directions with the steering vector of Uniform Linear Array (ULA), the sidelobes introduced by the steering vector is neglected by Sayeed.

3. As pointed out in [24], this model is restricted to uniform linear array and is not valid for any arbitrary array geometry.

2.1.4 Müller's Models

Another modelling approach made by Müller [25] expresses the MIMO channel as

$$\mathbb{H} = \mathbb{A}^H \begin{bmatrix} \beta_1 & 0 & \cdots & 0 \\ 0 & \beta_2 & \ddots & \vdots \\ \vdots & \ddots & \ddots & 0 \\ 0 & \cdots & 0 & \beta_K \end{bmatrix} \mathbb{B} \qquad \in \mathcal{C}^{N \times \overline{N}} \tag{2.14}$$

where K denotes the number of scattering objects, β_k the attenuation of the k^{th} path. The matrix $\mathbb{A} \in \mathcal{C}^{K \times \overline{N}}$ describes the propagation from the Tx array to the scattering objects, while $\mathbb{B} \in \mathcal{C}^{K \times N}$ describes the propagation from the scattering objects to the Rx array. The entries of $\mathbb{A}$ and $\mathbb{B}$ are assumed to be the i.i.d. random variables with zero mean and unit variance. Müller's model challenged the principle of the array processing theories that the propagation

between a scattering object and the different elements of an array are correlated in most circumstance. Furthermore, it requires each signal travelling from the transmitter to the receiver bounced off a scattering object exactly once.

Debbah and Müller, in [26], extends Eqn. (2.14) to

$$\mathbb{H} = \frac{1}{\sqrt{K\overline{K}}} \mathbb{A}^H \mathbb{P}^{1/2} \mathbb{X} \overline{\mathbb{P}}^{1/2} \mathbb{B} \qquad \in \mathcal{C}^{N \times \overline{N}} \tag{2.15}$$

where K and $\overline{K}$ refer respectively to the number of scattering objects at the receiver side and the transmitter side, matrix $\mathbb{X} \in \mathcal{C}^{K \times \overline{K}}$ describes the propagation from transmitter-side scattering objects to the receiver-side scattering objects with i.i.d. Gaussian random entries with zero-mean and unit variance. Matrix $\mathbb{A} \in \mathcal{C}^{\overline{K} \times \overline{N}}$ represents the DOA from receiver-side scattering objects to the receiver and matrix $\mathbb{B} \in \mathcal{C}^{K \times N}$ the DOD from the transmitter to the transmitter-side scattering objects. Diagonal matrices $\mathbb{P}$ and $\overline{\mathbb{P}}$ denote the power of the propagation of the DOA and DOD, respectively.

To exploit antenna arrays in wireless communications, it is necessary to obtain an accurate and tractable model of the channel via parametric physical modelling approach, which is more explicit description of the actual propagation environment whose parameters represent physically meaningful quantities such as path delays, directions, and complex path gains, etc.

Based on the concept of array manifold, a novel model is proposed in Section 2.2, connecting the $\overline{N} \times N$ statistical MIMO channel to an arbitrary number of multipaths. To represent the double direction nature of the propagation link, the array manifold used in this work associates with both the Rx and the Tx arrays. Without any presumptions about the coupling of the transmitter and receiver correlation, an expression of the spatial correlation matrix of the MIMO channel is then derived in Section 2.3. In the Section 2.4, the geometrical analysis about MIMO capacity is conducted, and is evaluated using computer simulation study.

Then, based on the new model, the spatial degree of freedom of correlated MIMO channel is investigated in Section 2.5. Finally, the chapter is concluded in Section 2.6.

2.2 System Modelling

Consider a single-user point-to-point, single polarization MIMO system with an array of $\overline{N}$ antennas at the transmitter[2], and an array of N antennas at the receiver, referred to as $(\overline{N}, N)$-MIMO. The transmitter and receiver arrays have geometries that can be described by a $\overline{N} \times 3$ matrix $[\underline{\overline{r}}_x, \underline{\overline{r}}_y, \underline{\overline{r}}_z]$ and $N \times 3$ matrix $[\underline{r}_x, \underline{r}_y, \underline{r}_z]$, respectively. For simplicity, all the antennas considered in this thesis are assumed to be isotropic.

Suppose the communication bandwidth is much smaller than the channel's coherent bandwidth, and channel matrix $\mathbb{H} \in \mathcal{C}^{N \times \overline{N}}$ can be treated as frequency-flat. From results of a 1.5 GHz multipath propagation measurements conducted by Saleh and Valenzuela [15], the maximum observed delay spread was $100 \sim 200$ ns within rooms, which means that to hold the flat-fading assumption, the communication bandwidth need be much less than 5 MHz. This condition is achievable in wideband communication, as by using orthogonal multi-carrier technique, a wideband communication channel can be partitioned into a number of narrowband subchannels. Throughout this chapter, the communication channel is assumed to be quasi-static, which means during a burst, the channel impulse response is approximately constant, i.e. $\mathbb{H} \in \mathcal{C}^{N \times \overline{N}}$ is time-invariant during a burst transmission.

The discrete-time version of the received signal of the MIMO system, corre-

[2]Note that a symbol with a bar on the top denotes a transmitter's parameter.

sponding to Eqn. (1.2), is

$$\underline{x}\,[n] = \mathbb{H}\underline{m}\,[n] + \underline{\mathrm{n}}\,[n] \tag{2.16}$$

where $\underline{m}\,[n] \in \mathcal{C}^{\overline{N}}$ denotes the baseband signal-vector and $\underline{\mathrm{n}}\,[n] \sim \mathcal{CN}\left(\underline{0}_N, \sigma_n^2 \mathbb{I}_N\right)$ is the discrete noise vector with complex normal distribution.

2.2.1 Propagation with DOD and DOA

The various popular radio propagation models, such as single-bounce model (one-ring model described in Section 1.4, elliptical model, etc.) used by Molisch [27] and Da Shan et al. [20], two-bounce model used by Molisch [27] and Thushara et al.[28] have been reviewed in [19]. However, the main assumption of rich scattering in all these propagation models neglects important properties contributing to the spatial correlation of MIMO channels. For instance, measurement results have demonstrated that in practical radio propagation a considerable amount of power is carried via multiply reflected components [29] [30], and the so-called double-directional evaluation provides accurate separation of the channels multi-path components.

Between the reference points of transmitter and receiver, a frequency-flat double-directional channel can be modelled as [29]

$$h\left(\underline{u}, \overline{\underline{u}}\right) = \sum_{k=1}^{K} \beta_k \delta\left(\underline{u} - \underline{u}_k\right) \delta\left(\overline{\underline{u}} - \overline{\underline{u}}_k\right) \tag{2.17}$$

where K is the number of resolvable paths, β_k is the complex amplitude of k^{th} path, $\underline{u}_k$ and $\overline{\underline{u}}_k$ denote the unit-norm vectors pointing towards the direction of arrival (DOA) and the direction of departure (DOD) of the k^{th} path, respectively:

$$\underline{u}_k = \begin{bmatrix} \cos\theta_k \cos\phi_k, & \sin\theta_k \cos\phi_k, & \sin\phi_k \end{bmatrix}^T \quad \in \mathcal{R}^3 \tag{2.18}$$

$$\overline{\underline{u}}_k = \begin{bmatrix} \cos\overline{\theta}_k \cos\overline{\phi}_k, & \sin\overline{\theta}_k \cos\overline{\phi}_k, & \sin\overline{\phi}_k \end{bmatrix}^T \quad \in \mathcal{R}^3 \tag{2.19}$$

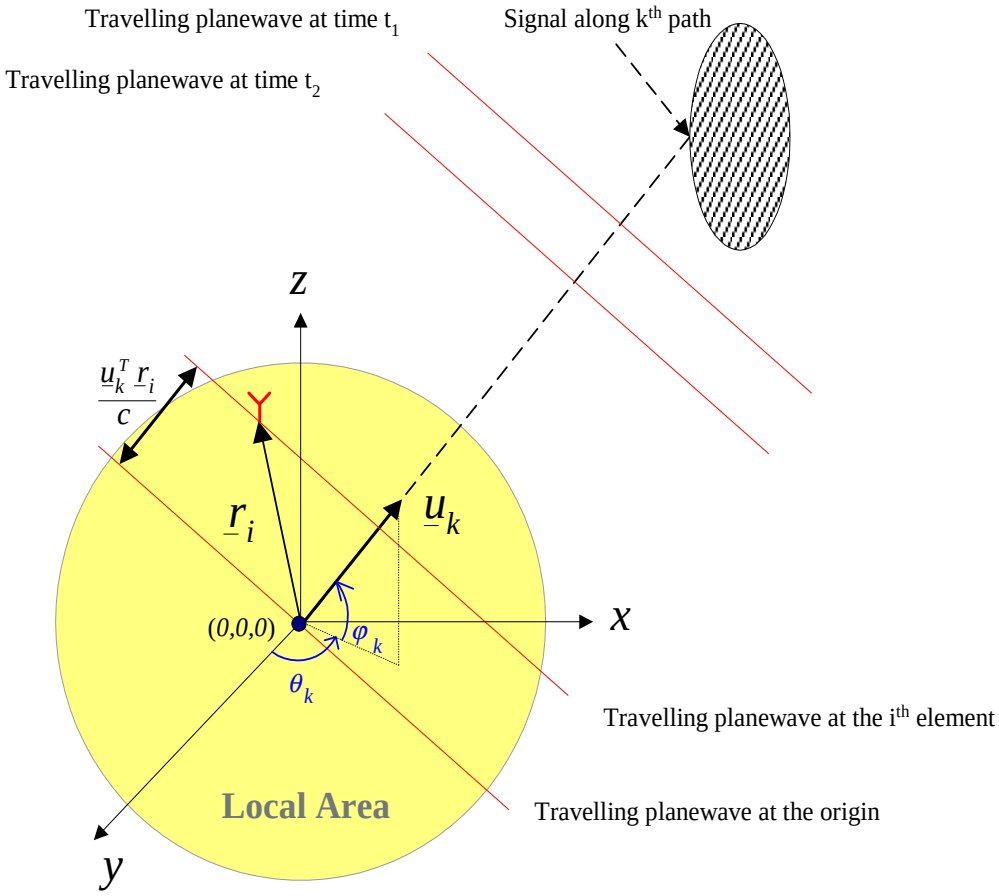


Figure 2.3: "Local area" and array manifold.

where (θ_k, ϕ_k) and $(\overline{\theta}_k, \overline{\phi}_k)$ are respectively the (azimuth, elevation) angles of DOA and DOD of the k^{th} multipath.

An array of antennas recalling its geometrical characteristics turns out to be a promising candidate to deal with the directional property of a practical MIMO channel.

In Figure 2.3, with "local area" assumption[3], the Rx array manifold vector

[3]For definition of local area, see page 21 Chapter 1.

$\underline{S}_k$ of the k^{th} path can be formulated as

$$\underline{S}_k \triangleq \exp\left(-\mathrm{j}\ [\underline{r}_x, \underline{r}_y, \underline{r}_z]\ \underline{\mathrm{k}}_k\right) \quad \in \mathcal{C}^N \tag{2.20}$$

where

$$\underline{\mathrm{k}}_k = \frac{2\pi F_c}{c}\underline{u}_k = \frac{2\pi F_c}{c}[\cos\theta_k \cos\varphi_k, \sin\theta_k \cos\varphi_k, \sin\varphi_k]^T \tag{2.21}$$

is the wavenumber vector pointing towards the DOA of the k^{th} path. Without loss of generality, all signals are assumed to propagate on x-y plane, i.e. $\forall k$, $\overline{\varphi}_k = \varphi_k = 0$, then

$$\underline{S}_k = \exp\left(-j\left(\underline{r}_x \cos\theta_k + \underline{r}_y \sin\theta_k\right)\right) \tag{2.22}$$

Note that, by using array manifold vector, the real spatial parameter $\underline{u}\,(\theta_k, \phi_k)$ is mapped to an N-dimensional complex vector $\underline{S}\,(\theta_k, \phi_k)$, denoted as

$$\underline{u}\,(\theta_k, \phi_k) \in \mathcal{R}^3 \longmapsto \underline{S}\,(\theta_k, \phi_k) \in \mathcal{C}^N \tag{2.23}$$

This enables the new model avoiding the multi-mapping defect incurred in the Sayeed's Model. In the rest of this thesis, the mapping of Eqn. (2.23) will be considered as 'one-to-one' mapping, ignoring the ambiguity problem [31].

The Tx array manifold vector, denoted as $\overline{\underline{S}}_k$, for the k^{th} path can be defined in a similar fashion to Eqn. (2.20) but with the parameters associated with the Tx. That is

$$\overline{\underline{S}}_k = \exp\left(-j\left(\overline{\underline{r}}_x \cos\overline{\theta}_k + \overline{\underline{r}}_y \sin\overline{\theta}_k\right)\right) \tag{2.24}$$

Using Tx and Rx array manifold vectors defined above, the received signal-vector $\underline{x}\,[n]$ in Eqn. (2.16) can be decomposed to a sum of signals of multipaths that emitted from the transmitter via different DOD and impinging at the receiver via different direction (DOA), i.e.

$$\underline{x}\,[n] = \underbrace{\sum_{k=1}^{K} \beta_k \underline{S}_k \overline{\underline{S}}_k^H}_{=\mathbb{H}} \underline{m}\,[n] + \underline{\mathrm{n}}\,[n] \tag{2.25}$$

However, Eqn. (2.25) is based on the point-like source assumption. Diffused propagation of the wireless signals [32] requires extension of the above model.

2.2.2 Cluster Model

In [33] - [36], indoor and outdoor multipath propagation models have been presented based on measurements, showing that the received signal rays arrive at Rx antennas in a number of clusters. Each cluster is composed of a large number of rays, diffused over a range of directions, referred to as *cluster angular spread*. Although during a long observation period, the mean angle of each cluster has been found to be uniformly distributed over all directions, as its variation is much slower than the change of path coefficient [36], the mean angles can be regarded as constants over a given observation interval. The *power azimuth spectrum* of each cluster is found to closely match a Laplacian distribution with respect to the cluster mean. Thus, it is clear that two clusters can be effectively separated by proper array processing techniques in a similar fashion to point sources.

In order to implement this double-directional (i.e. DOD & DOA) cluster propagation to MIMO system modelling, the following two definitions are necessary:

Definition 2.1 *Rx Scattering Point*

Rx Scattering Point is defined as a diffused source of the signals impinging on the Rx array.

Definition 2.2 *Tx Scattering Point*

Transmit Scattering Point is defined as a diffused sink of the signals emitted from the Tx array.

There are several assumptions about the scattering point to be made in this chapter:

- Quasi-static assumption: the cluster mean angles and the Rx/Tx scattering points are assumed to be quasi-stationary during the time of interest.

- Far field assumption: in comparison with the size of Tx/Rx arrays, the locations of the Rx/Tx scattering points are sufficiently far from the Rx/Tx (e.g. in the Fraunhofer region of the antenna). This enables the plane wave propagation [1] and make it possible to use the definition of array manifold introduced from Eqn. (2.37) to (2.23).

- One-to-one mapping scenario where one DOA corresponds to one and only one DOD. As measured in [35], a Rx scattering point may correspond to several Tx scattering point, and vice verse. In practice, the number of Rx/Tx scattering points mapping (i.e., multipath) is determined by the scattering environment and the receiver's spatial resolution[4].

Figure 2.4 illustrates a multi-cluster arrayed-MIMO channel based on both DOD and DOA clustering concepts. As shown in this figure, there are K resolvable clusters. For the k^{th} $(k = 1, \cdots K)$ cluster, there are L_k unresolved rays, each with fading coefficient β_{kl} , DOA θ_{kl} and DOD $\overline{\theta}_{kl}$, where

$$\overline{\theta}_{kl} = \overline{\theta}_k + \Delta\overline{\theta}_{kl}, \quad \Delta\overline{\theta}_{kl} \in \left[-\frac{\overline{\Delta}_k}{2}, \frac{\overline{\Delta}_k}{2}\right] \tag{2.26}$$

$$\theta_{kl} = \theta_k + \Delta\theta_{kl}, \quad \Delta\theta_{kl} \in \left[-\frac{\Delta_k}{2}, \frac{\Delta_k}{2}\right] \tag{2.27}$$

where $\overline{\Delta}_k$ and Δ_k are respective Tx/Rx angular spread of the k^{th} diffused cluster, $\overline{\theta}_k$ and θ_k are respectively DOD and DOA mean of the k^{th} diffused cluster, and $\Delta\overline{\theta}_{kl}$ and $\Delta\theta_{kl}$ the angular perturbation of the l^{th} path about the DOD and DOA mean of the k^{th} cluster. Note that in this chapter, with narrow-band assumption, the difference of the delay of multipaths within the same cluster is neglected.

[4] According to [35], in indoor MIMO propagation, the number of the multipaths is found to be 24 or 25, among which 7 of them (so-called dominant paths) occupy the majority of the power.

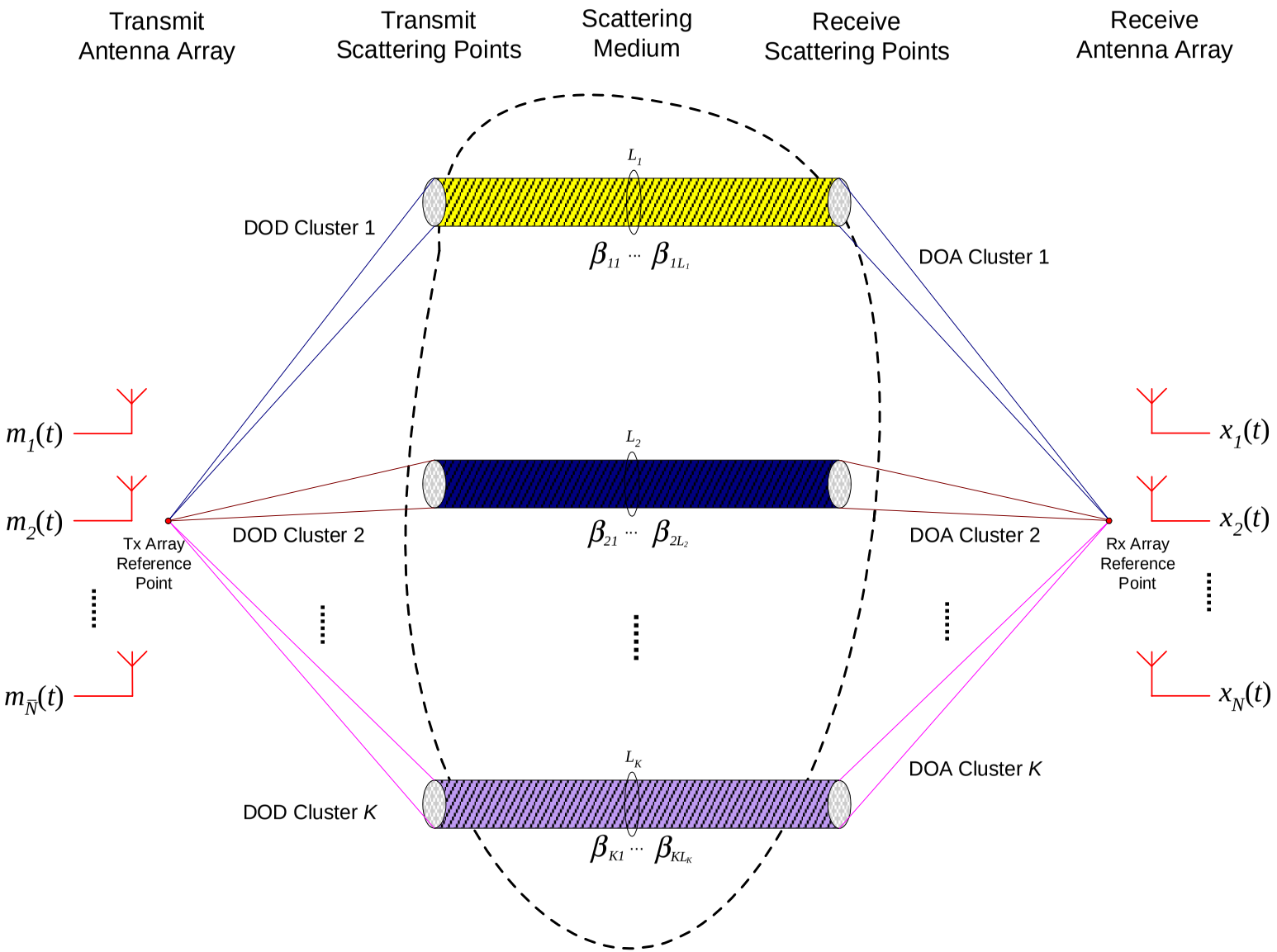


Figure 2.4: Schematic interpretation of the arrayed MIMO channel.

The system diagram corresponding to Figure 2.4 is depicted in Figure 2.5, and the received signal-vector at the output of receive array (2.25) is as follows:

$$\underline{x}(t) = \sum_{k=1}^{K}\sum_{l=1}^{L_k} \beta_{kl}\underline{S}(\theta_k + \Delta\theta_{kl})\,\underline{\bar{S}}^H\left(\overline{\theta}_k + \Delta\overline{\theta}_{kl}\right)\underline{m}(t-\tau_k) + \underline{\mathrm{n}}(t) \tag{2.28}$$

Assumed that Tx/Rx angular spread $\overline{\Delta}_k$ and Δ_k are small (e.g. $5^\circ \sim 10^\circ$), by implementing the first-order Taylor approximation, Eqn. (2.28) can be approximated as

$$\begin{aligned}\underline{x}(t) \;\approx\; & \sum_{k=1}^{K}\sum_{l=1}^{L_k} \beta_{kl}\left[\underline{S}(\theta_k) + \Delta\theta_{kl}\left.\frac{\partial \underline{S}}{\partial\theta}\right|_{\theta=\theta_k}\right]\left[\underline{\bar{S}}\left(\overline{\theta}_k\right) + \Delta\overline{\theta}_{kl}\left.\frac{\partial\overline{\underline{S}}}{\partial\overline{\theta}}\right|_{\overline{\theta}=\overline{\theta}_k}\right]^H \underline{m}(t-\tau_k) \\ & + \underline{\mathrm{n}}(t)\end{aligned} \tag{2.29}$$

where $\frac{\partial \underline{S}}{\partial\theta}$ is the first derivative of Rx array manifold vector $\underline{S}$ with respect to DOA θ , and $\frac{\partial\overline{\underline{S}}}{\partial\overline{\theta}}$ is the first derivative of Tx array manifold vector $\overline{\underline{S}}$ with respect to DOD $\overline{\theta}$. As $|\Delta\theta_{kl}| \le \frac{\Delta_k}{90}\pi \ll 1$ and $\left|\Delta\overline{\theta}_{kl}\right| \le \frac{\overline{\Delta}_k}{90}\pi \ll 1$, the higher-order cross-over terms are very small,

$$\begin{aligned}\underline{x}(t) \;\approx\; & \sum_{k=1}^{K} \beta_k\left[\underline{S}(\theta_k) + \varphi_k\left.\frac{\partial \underline{S}}{\partial\theta}\right|_{\theta=\theta_k}\right]\left[\underline{\bar{S}}\left(\overline{\theta}_k\right) + \overline{\varphi}_k\left.\frac{\partial\overline{\underline{S}}}{\partial\overline{\theta}}\right|_{\overline{\theta}=\overline{\theta}_k}\right]^H \underline{m}(t-\tau_k) \\ & + \underline{\mathrm{n}}(t)\end{aligned} \tag{2.30}$$

if

$$\beta_k \triangleq \sum_{l=1}^{L_k}\beta_{kl} \tag{2.31}$$

$$\varphi_k \triangleq \frac{\sum_{l=1}^{L_k}\beta_{kl}\Delta\theta_{kl}}{\beta_k} \tag{2.32}$$

$$\overline{\varphi}_k \triangleq \frac{\sum_{l=1}^{L_k}\beta_{kl}\Delta\overline{\theta}_{kl}}{\beta_k} \tag{2.33}$$

Here β_k, φ_k and $\overline{\varphi}_k$ are all random variables. As in [37] and [38], since β_k is the aggregate fading coefficient of the large number of the paths within one cluster, it can be well modelled by the complex normal distribution, i.e.,

$$\beta_k \sim \mathcal{CN}\left(0, \sigma_k^2\right) \tag{2.34}$$

and β_k of different clusters can be assumed uncorrelated, i.e.

$$\mathcal{E}\left\{\beta_k \beta_u^*\right\} = 0, \text{ for any } k \neq u \tag{2.35}$$

For normalization reason, it is assumed $\sum_{k=1}^{K} \sigma_k^2 = 1$.

For small angular spread Δ_k and $\Delta\theta_{kl}$ (see [38]) uniformly distributed between $-\frac{\Delta_k}{2}$ and $\frac{\Delta_k}{2}$, φ_k is very small and equal to $\frac{\Delta_k}{\sqrt{12}}$. However, in practice (see [34]), $\Delta\theta_{kl}$ follows a Laplacian distribution which means that φ_k is even smaller than $\frac{\Delta_k}{\sqrt{12}}$, i.e. $\varphi_k \ll \frac{\Delta_k}{\sqrt{12}}$. Thus, φ_k and $\overline{\varphi}_k$ in Eqn. (2.32) and Eqn. (2.33) are very small and can be neglected. Therefore, Eqn. (2.30) can be rewritten as

$$\underline{x}\,(t) = \sum_{k=1}^{K} \beta_k \underline{S}\,(\theta_k)\, \underline{\bar{S}}^H \left(\overline{\theta}_k\right) \underline{m}\,(t - \tau_k) + \underline{\mathrm{n}}\,(t) \tag{2.36}$$

which is similar the point-source version Eqn. (2.25) except that in Eqn. (2.25), β_k is deterministic whereas in Eqn. (2.36), β_k is random variable with

$$\underline{\beta} \sim \mathcal{CN}\left(\underbrace{\begin{bmatrix} 0 \\ 0 \\ \vdots \\ 0 \end{bmatrix}}_{\triangleq\ \underline{0}_K}, \underbrace{\begin{bmatrix} \sigma_1^2 & 0 & \cdots & 0 \\ 0 & \sigma_2^2 & \ddots & \vdots \\ \vdots & \ddots & \ddots & 0 \\ 0 & \cdots & 0 & \sigma_K^2 \end{bmatrix}}_{\triangleq\ \mathrm{diag}(\underline{\sigma}^2)} \right) \tag{2.37}$$

where

$$\underline{\beta} \triangleq [\beta_1,\, \beta_2,\, \cdots,\, \beta_K]^T \tag{2.38}$$

Based on the above, Figure 2.5 is simplified to Figure 2.6, where β_k is given by Eqn. (2.34). Thus the received baseband signal-vector $\underline{x}\,(t)$ is as follows

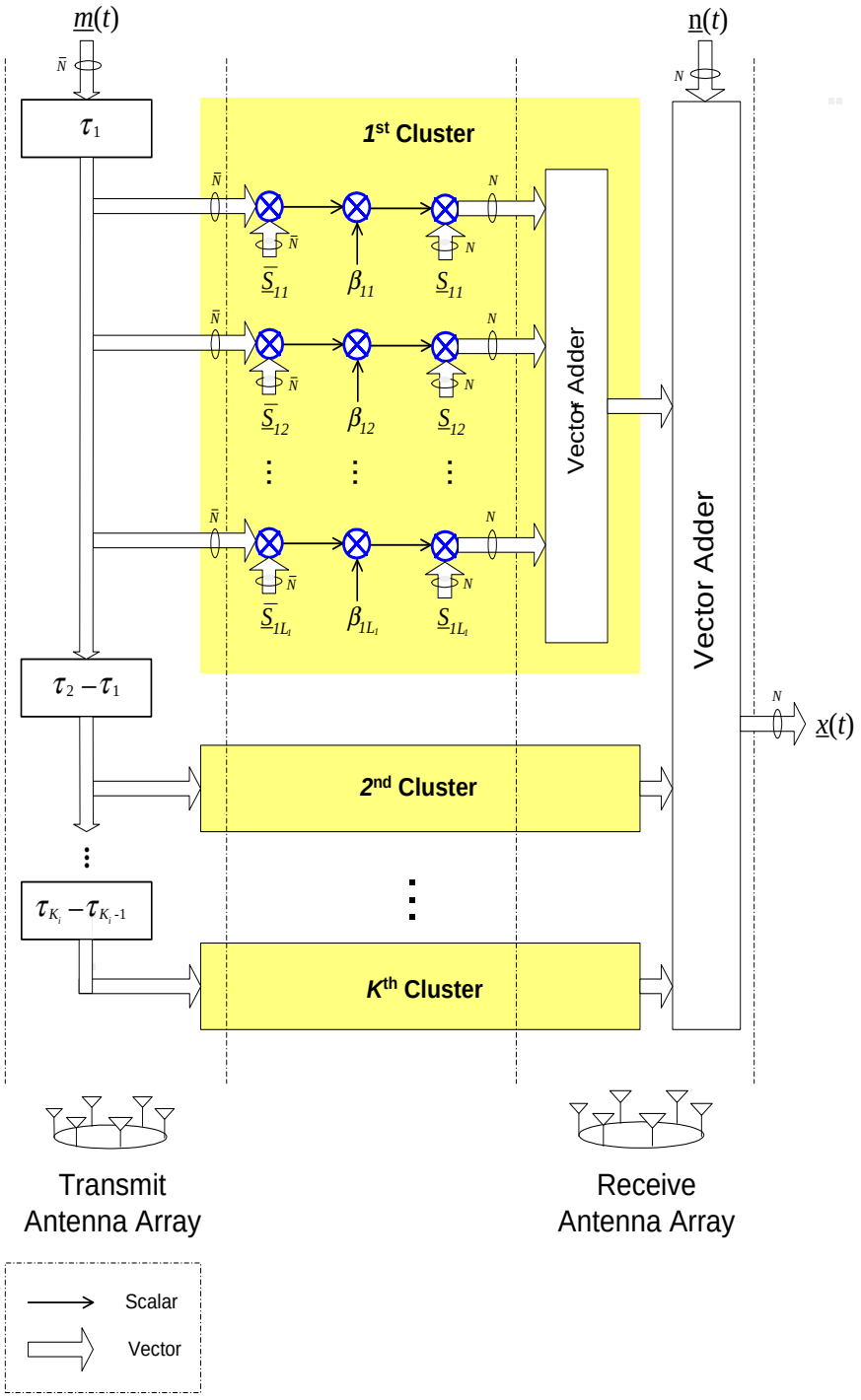


Figure 2.5: Modelling of diffused MIMO channel.

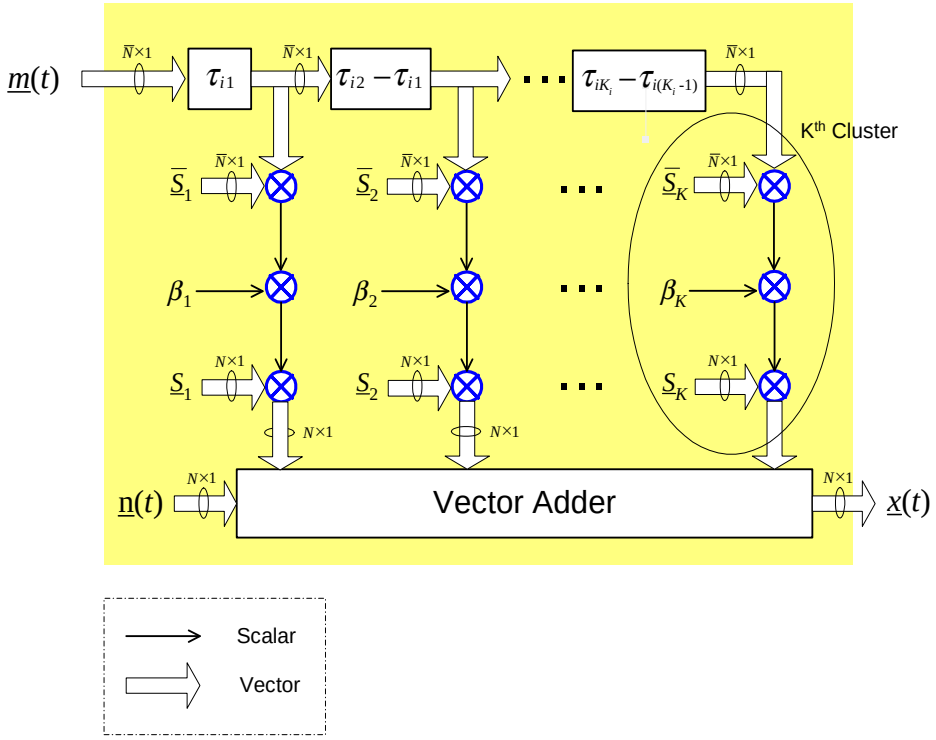


Figure 2.6: Modelling of arrayed MIMO Channel.

$$\underline{x}(t) = \left[\begin{array}{cccc} \underline{S}_1, & \underline{S}_2, & \cdots, & \underline{S}_K \end{array}\right] \left[\begin{array}{cccc} \beta_1 & 0 & \cdots & 0 \\ 0 & \beta_2 & \ddots & \vdots \\ \vdots & \ddots & \ddots & 0 \\ 0 & \cdots & 0 & \beta_K \end{array}\right] \left[\begin{array}{c} \overline{\underline{S}}_1^H \\ \overline{\underline{S}}_2^H \\ \vdots \\ \overline{\underline{S}}_K^H \end{array}\right] \underline{m}(t) + \underline{\mathrm{n}}(t)$$

$$= \underbrace{\mathbb{S}\,\mathrm{diag}(\underline{\beta})\overline{\mathbb{S}}^H}_{\mathbb{H}} \underline{m}(t) + \underline{\mathrm{n}}(t) \tag{2.39}$$

i.e.

$$\boxed{\mathbb{H} = \mathbb{S}\,\mathrm{diag}\left(\underline{\beta}\right)\overline{\mathbb{S}}^H \quad \in \mathcal{C}^{N\times\overline{N}}} \tag{2.40}$$

where matrices $\overline{\mathbb{S}}$ and $\mathbb{S}$ have columns the transmitter and receiver array manifold vectors corresponding to K DOD/DOA means. That is

$$\overline{\mathbb{S}} = \left[\begin{array}{cccc} \overline{\underline{S}}_1, & \overline{\underline{S}}_2, & \cdots, & \overline{\underline{S}}_K \end{array}\right] \quad \in \mathcal{C}^{\overline{N}\times K} \tag{2.41}$$

$$\mathbb{S} = \left[\begin{array}{cccc} \underline{S}_1, & \underline{S}_2, & \cdots, & \underline{S}_K \end{array}\right] \quad \in \mathcal{C}^{N\times K} \tag{2.42}$$

2.3 Spatial Correlation Studies

Substituting the arrayed MIMO channel model of Eqn. (2.40) into the definition of correlation matrix Eqn. (2.4) and using Eqn. (2.35), it can be derived that

$$\begin{aligned}
\mathbb{R}_H &= \mathcal{E}\left\{\mathrm{vec}\left(\mathbb{H}\right)\mathrm{vec}\left(\mathbb{H}\right)^H\right\} && (2.43)\\
&= \mathcal{E}\left\{\mathrm{vec}\left(\sum_{k=1}^{K}\beta_k\,\underline{S}_k\overline{\underline{S}}_k^H\right)\,\mathrm{vec}\left(\sum_{u=1}^{K}\beta_u\,\underline{S}_u\overline{\underline{S}}_u^H\right)^H\right\} && (2.44)\\
&= \mathcal{E}\left\{\sum_{k=1}^{K}\sum_{u=1}^{K}\beta_k\beta_u^*\,\mathrm{vec}\left(\underline{S}_k\overline{\underline{S}}_k^H\right)\,\mathrm{vec}\left(\underline{S}_u\overline{\underline{S}}_u^H\right)^H\right\} && (2.45)\\
&= \sum_{k=1}^{K}\sum_{u=1}^{K}\mathcal{E}\left\{\beta_k\beta_u^*\right\}\mathrm{vec}\left(\underline{S}_k\overline{\underline{S}}_k^H\right)\,\mathrm{vec}\left(\underline{S}_u\overline{\underline{S}}_u^H\right)^H && (2.46)\\
&= \sum_{k=1}^{K}\sigma_k^2\,\mathrm{vec}\left(\underline{S}_k\overline{\underline{S}}_k^H\right)\,\mathrm{vec}\left(\underline{S}_k\overline{\underline{S}}_k^H\right)^H && (2.47)
\end{aligned}$$

Applying the properties of Kronecker product[5] [65]

$$\mathrm{vec}(\underline{a}\underline{b}^T) = \underline{b}\otimes\underline{a} \tag{2.48}$$

$$\left(\mathbb{B}\otimes\mathbb{A}\right)^H = \mathbb{B}^H\otimes\mathbb{A}^H \tag{2.49}$$

$$\left(\mathbb{B}\otimes\mathbb{A}\right)^T = \mathbb{B}^T\otimes\mathbb{A}^T \tag{2.50}$$

$$\left(\underline{b}\otimes\underline{a}\right)\left(\underline{d}\otimes\underline{c}\right)^H = \left(\underline{b}\;\underline{d}^H\right)\otimes\left(\underline{a}\;\underline{c}^H\right) \tag{2.51}$$

Eqn. (2.47) can be further rewritten as

$$\begin{aligned}
\mathbb{R}_H &= \sum_{k=1}^{K}\sigma_k^2\,\left(\overline{\underline{S}}_k^*\otimes\underline{S}_k\right)\,\left(\overline{\underline{S}}_k^*\otimes\underline{S}_k\right)^H && (2.52)\\
&= \sum_{k=1}^{K}\sigma_k^2\,\left(\overline{\underline{S}}_k^*\overline{\underline{S}}_k^T\right)\otimes\left(\underline{S}_k\underline{S}_k^H\right) && (2.53)
\end{aligned}$$

Note that,

$$\overline{\underline{S}}_k^*\overline{\underline{S}}_k^T = \left(\overline{\underline{S}}_k\overline{\underline{S}}_k^H\right)^* = \left(\overline{\underline{S}}_k\overline{\underline{S}}_k^H\right)^T \tag{2.54}$$

[5] The proof of some properties of Kronecker product can be found in Appendix 2.A.

thus the spatial correlation matrix of the proposed model is

$$\boxed{\mathbb{R}_H = \sum_{k=1}^{K} \sigma_k^2 \, \overline{\mathbb{R}}_k^T \otimes \mathbb{R}_k} \tag{2.55}$$

in which $\overline{\mathbb{R}}_k$ and $\mathbb{R}_k$ are defined as the Tx/Rx correlation matrix regarding to k^{th} cluster, i.e.

$$\overline{\mathbb{R}}_k \triangleq \underline{\overline{S}}_k \underline{\overline{S}}_k^H \quad \in \mathcal{C}^{\overline{N}\times\overline{N}} \tag{2.56}$$

and

$$\mathbb{R}_k \triangleq \underline{S}_k \underline{S}_k^H \quad \in \mathcal{C}^{N\times N} \tag{2.57}$$

So, the full correlation matrix of the arrayed MIMO channel can be expressed as a weighted sum of the Kronecker products of the Tx/Rx correlation matrices with respect to all clusters.

Furthermore, substituting (2.40) into the definition of Rx correlation matrix Eqn. (2.7), it can be derived that

$$\begin{aligned}
\mathbb{R} &= \frac{1}{\overline{N}} \mathcal{E}\{\mathbb{H}\mathbb{H}^H\} && (2.58)\\
&= \frac{1}{\overline{N}} \mathcal{E}\left\{ \left(\sum_{k=1}^{K} \beta_k \, \underline{S}_k \underline{\overline{S}}_k^H \right) \left(\sum_{u=1}^{K} \beta_u \, \underline{S}_u \underline{\overline{S}}_u^H \right)^H \right\} && (2.59)\\
&= \frac{1}{\overline{N}} \mathcal{E}\left\{ \sum_{k=1}^{K} \sum_{u=1}^{K} \beta_k \beta_u^* \, \underline{S}_k \underline{\overline{S}}_k^H \underline{\overline{S}}_u \underline{S}_u^H \right\} && (2.60)\\
&= \frac{1}{\overline{N}} \sum_{k=1}^{K} \sum_{u=1}^{K} \mathcal{E}\left\{\beta_k \beta_u^*\right\} \, \underline{S}_k \, \underline{\overline{S}}_k^H \, \underline{\overline{S}}_u \underline{S}_u^H && (2.61)\\
&= \frac{1}{\overline{N}} \sum_{k=1}^{K} \sigma_k^2 \, \underline{S}_k \, \underline{\overline{S}}_k^H \, \underline{\overline{S}}_k \, \underline{S}_k^H && (2.62)
\end{aligned}$$

However, using Eqn. (2.24),

$$\underline{\overline{S}}_k^H \underline{\overline{S}}_k = \overline{N}, \ \ \forall k \tag{2.63}$$

so

$$\mathbb{R} = \sum_{k=1}^{K} \sigma_k^2 \underbrace{\underline{S}_k \underline{S}_k^H}_{\triangleq\ \mathbb{R}_k} \tag{2.64}$$

$$= \sum_{k=1}^{K} \sigma_k^2 \, \mathbb{R}_k \tag{2.65}$$

Note that similar expression of the Rx correlation matrix to Eqn. (2.64) can found in [19] where all σ_k are assumed identical.

Following the same procedure, the Tx correlation matrix can be written with a similar fashion.

$$\overline{\mathbb{R}} = \sum_{k=1}^{K} \sigma_k^2 \underbrace{\overline{\underline{S}}_k \overline{\underline{S}}_k^H}_{\triangleq\ \overline{\mathbb{R}}_k} \tag{2.66}$$

$$= \sum_{k=1}^{K} \sigma_k^2 \, \overline{\mathbb{R}}_k \tag{2.67}$$

The next two subsections compare the spatial correlation expression derived above with two existing spatial correlation models.

2.3.1 Comparison with Kronecker-based model

As matrix norms can be used to represent the 'distance' between two matrices, to quantify the discrepancy between the spatial correlation obtained using the proposed model, Eqn. (2.55), and the Kronecker-based model, Eqn. (2.5), the model discrepancy factor κ based on Frobenius-norm will be employed in a similar fashion as in [39]:

$$\kappa \triangleq \frac{||\mathbb{R}_H - \overline{\mathbb{R}}^T \otimes \mathbb{R}||_{\mathcal{F}}}{||\mathbb{R}_H||_{\mathcal{F}}} \tag{2.68}$$

Consider a simple example of $(\overline{N}, N)$ MIMO system with $\overline{N} = N$ exploiting Uniform Linear Array (ULA) for both transmitter and receiver array[6], and the

[6] This kind of MIMO system will be used frequently in the rest of the thesis, for convenience, it will be called Symmetrical ULA MIMO.

transmitter uniformly allocates the transmitting power among $\overline{N}$ Tx antennas. For simplicity, suppose all the clusters have the same path attenuation (σ_k^2 in Eqn. (2.34)), and the DOD and DOA of K clusters are evenly distributed in $[30°, 75°]$ and $[72°, 108°]$, respectively. Using Monte Carlo method, with 10000 channel realizations, numerical comparison of the model discrepancy factor κ between proposed and Kronecker-based model has been depicted in Figure 2.7 as a function of the number of array size N. Simulation is conducted with different number of clusters K.

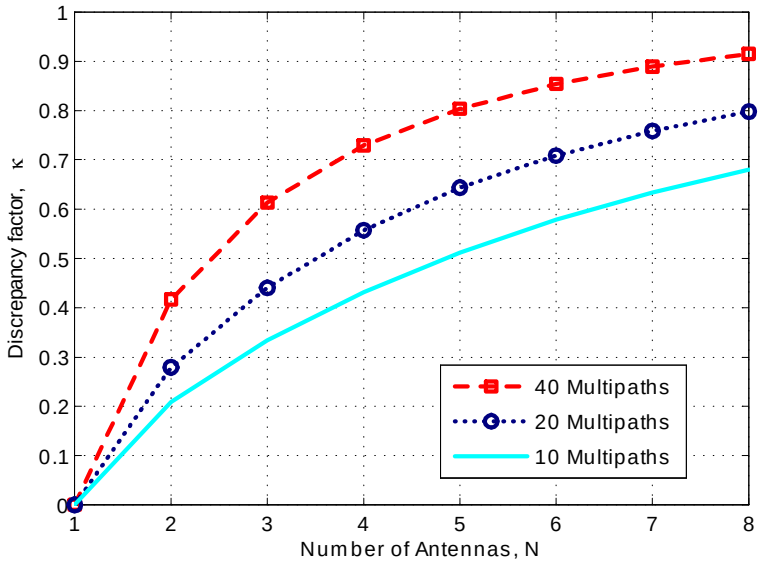


Figure 2.7: Model descrepancy factor κ as a function of the array size N for three different multipath cases.

The simulation results unveil that the estimating error introduced by the Kronecker-based model deteriorates with the increase of the *array size* (the number of antennas of the array), which is consistent with the conclusion of [39] and [18].

Figure 2.7 emphasizes the effect of scattering environment on the error introduced by Kronecker model. In richer scattering environment, the error gets worse. In [40], similar results have been observed using real measurements.

In a SIMO/MISO channel, the proposed model and the Kronecker-based model becomes equivalent, i.e.

$$\text{SIMO:} \quad \mathbb{R}_{\text{Kron}} = \mathbb{R}_H = \mathbb{R} \tag{2.69}$$

Similarly, for MISO channel

$$\text{MISO:} \quad \mathbb{R}_{\text{Kron}} = \mathbb{R}_H = \overline{\mathbb{R}} \tag{2.70}$$

2.3.2 Comparison with Weichselberger's model

Consider the singular value decomposition (SVD) of Tx/Rx array manifold matrices $\overline{\mathbb{S}} \in \mathcal{C}^{\overline{N}\times K}$ and $\mathbb{S} \in \mathcal{C}^{N\times K}$ i.e.

$$\overline{\mathbb{S}} = \overline{\mathbb{U}}\ \overline{\mathbb{D}}\ \overline{\mathbb{V}}^H \tag{2.71}$$

$$\mathbb{S} = \mathbb{U}\mathbb{D}\mathbb{V}^H \tag{2.72}$$

where $\mathbb{U} = [\underline{u}_1,\ \cdots,\ \underline{u}_N] \in \mathcal{C}^{N\times N}$, $\overline{\mathbb{U}} \in \mathcal{C}^{\overline{N}\times\overline{N}}$ and $\mathbb{V}$, $\overline{\mathbb{V}} \in \mathcal{C}^{K\times K}$ are unitary matrices and $\mathbb{D}$ and $\overline{\mathbb{D}}$ are matrices with non-zeros only on the diagonal. Thus by Eqn. (2.64) and Eqn. (2.66), $\mathbb{U}$ and $\overline{\mathbb{U}}$ are respectively unitary matrices of $\mathbb{R}$ and $\overline{\mathbb{R}}$.

Lemma 2.1 *Let $\mathbb{H}_w$ be an $N\times\overline{N}$ random matrix whose entries are i.i.d. $\mathcal{CN}(0,1)$, then probability distribution functions* $\text{pdf}(\mathbb{U}\mathbb{H}_w) = \text{pdf}(\mathbb{H}_w\mathbb{V}) = \text{pdf}(\mathbb{H}_w)$ *for any unitary matrices $\mathbb{U}$ and $\mathbb{V}$.*

Proof. *The proof of this Lemma can be found in [41].* ■

Substitute Eqn. (2.71) and (2.72) into arrayed MIMO channel model Eqn. (2.40),

$$\mathbb{H} = \mathbb{U}\mathbb{D}\mathbb{V}^H\ \text{diag}(\underline{\beta})\ \overline{\mathbb{V}}\ \overline{\mathbb{D}}^H\overline{\mathbb{U}}^H \tag{2.73}$$

From Lemma 2.1, if substituting $\mathrm{diag}(\underline{\beta})$ with $\widehat{\mathbb{H}}_{\mathrm{w}} \in \mathcal{C}^{K\times K}$,

$$\mathbb{H} = \mathbb{U}\mathbb{D}\widehat{\mathbb{H}}_{\mathrm{w}}\overline{\mathbb{D}}^{H}\overline{\mathbb{U}}^{H} \tag{2.74}$$

$$= \mathbb{U}\left(\left(\underline{\lambda}\,\overline{\underline{\lambda}}^{T}\right)\odot\widehat{\mathbb{H}}_{\mathrm{w}}\right)\overline{\mathbb{U}}^{H} \tag{2.75}$$

where $\underline{\lambda} = (\lambda_1, \cdots, \lambda_K)^T$ are the diagonal elements of $\mathbb{D}$ (if $K < N$, λ_{K+1},$\cdots$, $\lambda_N = 0$) and $\overline{\underline{\lambda}} = \left(\overline{\lambda}_1, \cdots, \overline{\lambda}_K\right)^T$ are the diagonal elements of $\overline{\mathbb{D}}$ (if $K < \overline{N}$, $\overline{\lambda}_{K+1}$,$\cdots$, $\overline{\lambda}_N = 0$). Eqn. (2.75) is a channel format proposed by Weichselberger model (2.12). By substituting $\mathrm{diag}(\underline{\beta})$ with $\widehat{\mathbb{H}}_{\mathrm{w}}$, it has been assumed that between every DOD and DOA, there exists a cluster. That is to say that totally K^2 clusters can be found in the channel.

From the above, it can be concluded that the Weichselberger's model is a special case of the proposed arrayed model. Furthermore, from Eqn. (2.75), the coupling matrix is determined by not only the scattering environment (propagation coefficients, DOD, DOA), but also the transmitter and receiver array configuration, the information that can only be represented by the proposed model.

2.4 Capacity and Array Geometry

In this section, the capacity of MIMO systems is investigated using the proposed array model, i.e. as a function of the array manifold vectors associated with both transmitter and receiver. A number of physical factors that influence the capacity of the system are examined and discussed.

Modelled by Eqn. (2.16), the capacity of the MIMO channel, normalized with respect to bandwidth (i.e. $\frac{C}{B}$ in bits/s/Hz), is [12]

$$C_{\mathbb{H}} = \log_2 \det\left[\mathbb{I}_N + \frac{\overline{P}}{\sigma_n^2\overline{N}}\mathbb{H}\mathbb{R}_{mm}\mathbb{H}^H\right] \qquad \text{bits/s/Hz} \tag{2.76}$$

where $\overline{P}$ denotes the total transmitted power and σ_n^2 the power of noise. Matrix $\mathbb{R}_{mm}$ is the correlation matrix of the transmitted signal-vector $\underline{m}(n)$, with

independent signal assumption, which can be idealized as $\mathbb{R}_{mm} = \mathbb{I}_{\overline{N}}$.

Using proposed arrayed-MIMO model (2.40), Eqn. (2.76) can be connected to array geometry. That is

$$C_{\mathbb{H}} = \log_2 \det \left[\mathbb{I}_N + \frac{\overline{P}}{\sigma_n^2 \overline{N}} \mathbb{S}\, \mathrm{diag}\left(\underline{\beta}\right) \overline{\mathbb{S}}^H \overline{\mathbb{S}}\, \mathrm{diag}\left(\underline{\beta}^*\right) \mathbb{S}^H \right] \qquad \text{bits/s/Hz} \qquad (2.77)$$

As the elements of $\mathbb{H}$ are random variables, $C_{\mathbb{H}}$ is also random and thus the *ergodic capacity* C_{ergodic} can be defined as follows:

$$C_{\text{ergodic}} = \mathcal{E}_{\mathbb{H}} \{C_{\mathbb{H}}\} \qquad \text{bits/s/Hz} \qquad (2.78)$$

where $\mathcal{E}_{\mathbb{H}} \{\cdot\}$ means the expectation taken on all $\mathbb{H}$ realizations. Alternatively, the cumulative distribution function (CDF) of the capacity $C_{\mathbb{H}}$ can be used to describe the maximum date rate the system can support with a certain outage probability.

To investigate the effect of the number of clusters (resolvable paths) on the arrayed-MIMO capacity in a frequency flat channel, consider a $(8, 8)$-MIMO system employing ULA with $0.5\lambda_c$ spacing at both the Tx and the Rx. For the sake of simplicity, assume identical path loss for all paths, with DODs and DOAs uniformly distributed on $[0°, 360°)$. In particular, in the simulations, the number of the paths K takes values 1, 8, 16, 32, 64 and 80, and each case uses 10000 channel realizations with $\overline{P}/\sigma_n^2 = 15$ dB. The resulting CDF of the capacity $C_{\mathbb{H}}$ (by Eqn. 2.77) is depicted in Figure 2.8. If K increases, then the outage capacity curve is shifted to the right - up to $K = 64$. When K is bigger than 64, increase of K hardly increases the capacity. When $K = 1$, the MIMO system degenerates to a SISO system because of the full correlation between the pair-wise channels.

If the inter-antenna spacing increases from $0.5\lambda_c$ to $5\lambda_c$ then, as shown in Figure 2.9, the curves for $K = 8$, 16 and 32 are shifted towards the 'upper' bound. This is intuitively understandable since the increased spacing diminishes

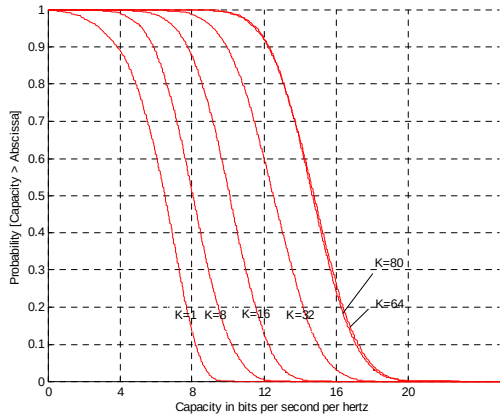


Figure 2.8: The complementary $\mathrm{CDF}_{\mathrm{capacity}}$ of a $(8,8)$-MIMO system employing ULA with $0.5\lambda_c$ spacing at both the Tx and the Rx. The number of resolvable multipaths $K = 1$, 8, 16, 32, 64 and 80, $\overline{\theta}_k$ and θ_k randomly distributed on $[0, 2\pi]$, and $\overline{P}/\sigma_n^2 = 15$ dB.

the effect of spatial correlation. However, increasing array aperture, on the other hand, introduces more ambiguity, which will decrease the number of resolvable paths.

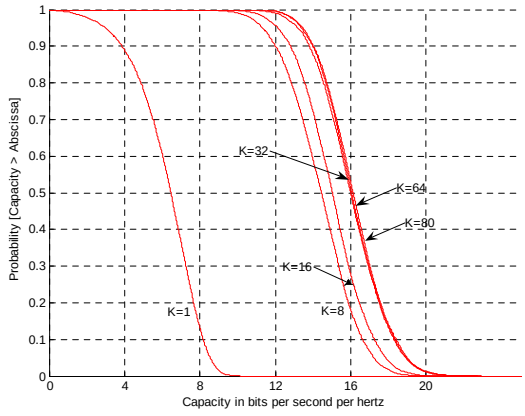


Figure 2.9: The same as Figure 2.8 except that the inter-element spacing of Tx and Rx array is increased to $5\lambda_c$.

Furthermore, consider a $(8,8)$-MIMO system employing Uniform Linear Arrays (ULA) with $0.5\lambda_c$ inter-element spacing at both transmitter and receiver. Arbitrarily assume there are 7 resolvable paths with identical path gain (i.e. σ_k

Path	$k=1$	$k=2$	$k=3$	$k=4$	$k=5$	$k=6$	$k=7$
θ_k	25°	80°	100°	55°	10°	25°	30°
$\overline{\theta}_k$	41°	62°	88°	119°	24°	160°	67°

Table 2.1: DOA and DOD parameters for capacity studying example.

in Eqn. 2.37). The DOD and DOA of the multipaths are set in Table 2.1.

Simulation is carried out with 10000 channel realizations using respectively ULA and Uniform Circular Array (UCA) at both Tx and Rx (see Figure 2.11). Figure 2.10 compares the ergodic capacity of the MIMO channel using the i.i.d. model, the Kronecker model and the proposed arrayed model. The MIMO system It can be observed that, as expected, the capacity obtained by proposed model is smaller than capacity of i.i.d. model which neglects spatial correlation. Furthermore, the capacity obtained by the proposed model is larger than that obtained by Kronecker model. This fits the fact discovered by measurements conducted in [17], where the i.i.d. model ignores the spatial correlation while the Kronecker model overestimates the spatial correlation.

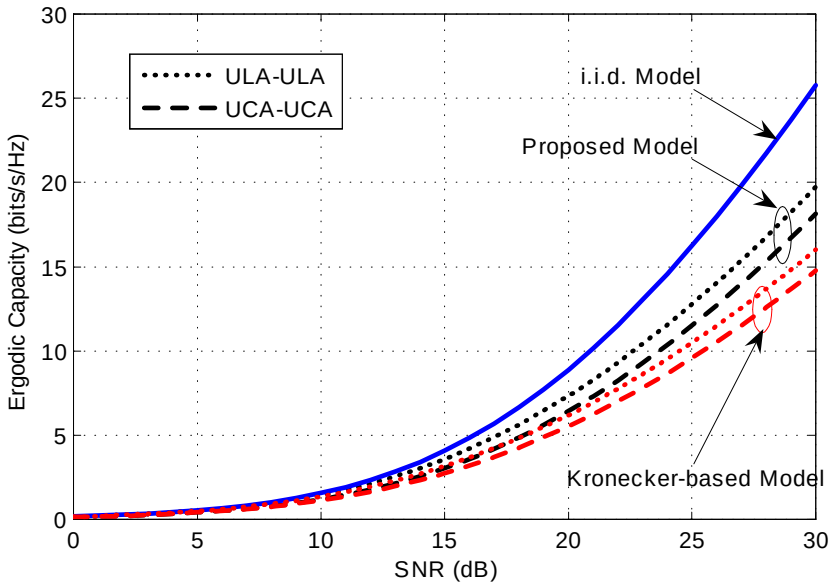


Figure 2.10: Ergodic Capacities of a (8,8)-MIMO system employing $0.5\lambda_c$ inter-antenna spacing ULA and UCA (shown in Figure 2.11) at both Tx and Rx, simulated using i.i.d. model, Kronecker-based model and proposed model.

Another significance brought by arrayed correlated MIMO model is that it enables the study of the relationship between the MIMO capacity and the geometry of the multiple antenna array.

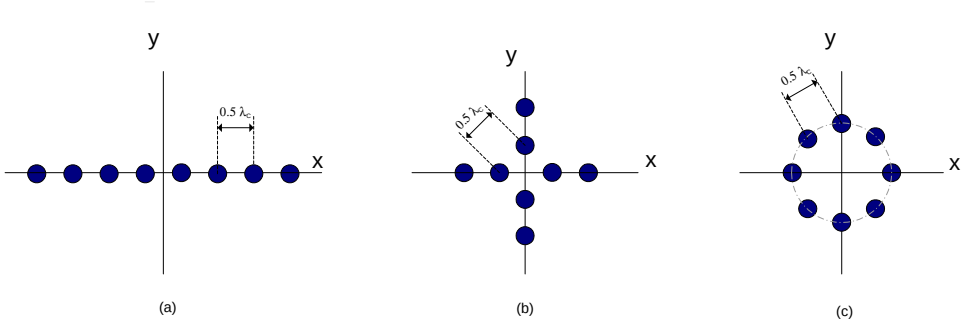


Figure 2.11: Array geometries investigated in the simulation: (a) Uniform Linear Array; (b) Cross Array; (c) Uniform Circle Array, all with fixed spacing.

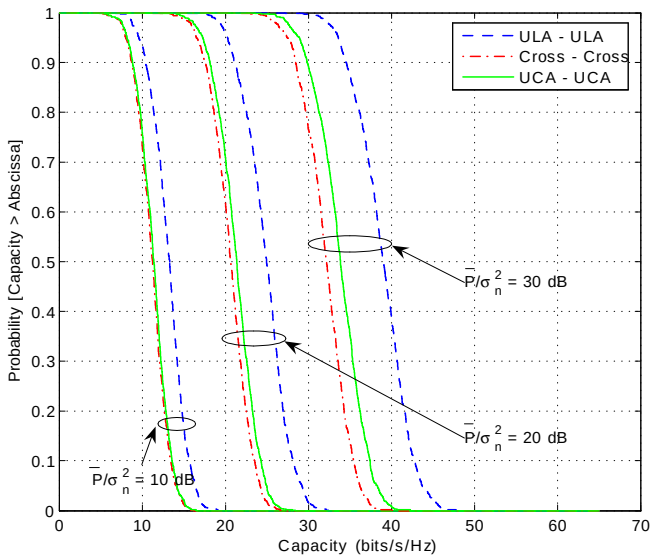


Figure 2.12: $\text{CDF}_{\text{capacity}}$ of $(8, 8)$-MIMO system employing different array geometries with fixed inter-antenna spacing $0.5\lambda_c$ and $\overline{P}/\sigma_n^2 = 10$ dB, 20 dB and 30 dB.

In order to explore the effect of array geometry to the capacity, three MIMO systems are considered, at both Tx and Rx, employing ULA, Cross Array and Uniform Circular Array (UCA) of 8 antennas (as shown in Figure 2.11). Assume

eight resolvable paths with DOA and DOD uniformly distributed at $[18°, 78°]$ and $[75°, 135°]$ respectively. Figure 2.12 depicts the estimated capacity CDF of the 3 systems while fixing the element-spacing at half wavelength. It shows that the ULA tends to provide the largest capacity while the Cross Array the smallest, and the capacity gap introduced by geometry enlarges with $\overline{P}/\sigma_n^2$. This result can be explained by the fact that with the identical inter-element spacing and the same number of antennas, the aperture of the ULA is the largest among the three geometries.

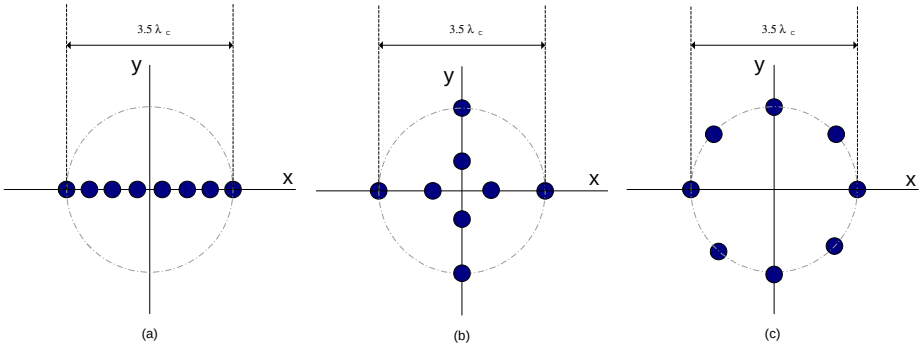


Figure 2.13: Array geometries investigated in the simulations: (a) Uniform Linear Array; (b) Cross Array; (c) Uniform Circle Array, all with fixed aperture.

Similarly, as shown in Figure 2.13, by fixing the aperture at 3.5 wavelength, the CDF of Capacity for different geometries are simulated and plotted in Figure 2.14. It suggests that for the fixed aperture, the Cross array outperforms other two. It is understandable that within the circle of a fix radius, Cross array distributes its elements apart as far as possible, and thus to the maximum extent weakens the spatial correlation. As expected, the ULA contributes the worst capacity because of its poor antenna arrangement. Again the capacity difference introduced by array geometry got greater in higher $\overline{P}/\sigma_n^2$ scenario.

Employing ULAs with $0.5\lambda_c$ spacing at both Tx and Rx, the ergodic capacity of a $(2, 2)$-MIMO system with 2 resolvable paths is simulated in Figure 2.15. The

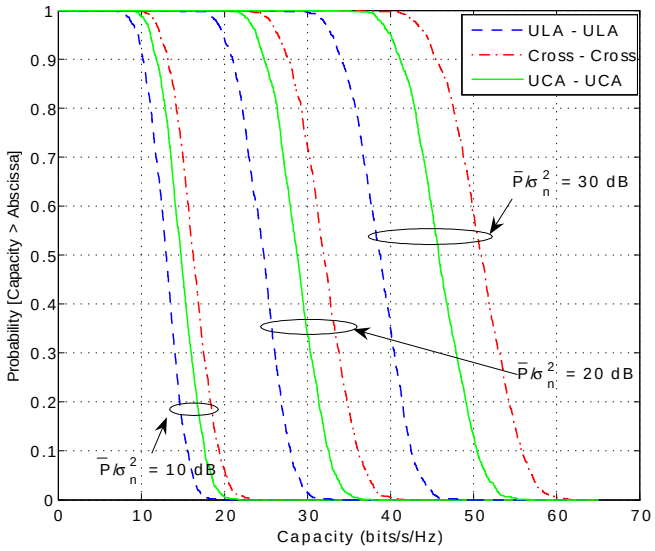


Figure 2.14: $\mathrm{CDF}_{\mathrm{capacity}}$ of $(8,8)$-MIMO employing different array geometries with fixed aperture $3.5\lambda_c$ and $\overline{P}/\sigma_n^2 = 10$ dB, 20 dB, and 30 dB.

direction of one path has been fixed at $(\mathrm{DOA}, \mathrm{DOD}) = (45°, 132°)$, while the DOA and DOD of another change among [0,180], with which the capacity varies accordingly. As expected, the two 'nulling' directions are located near the DOA and DOD of fixed path, i.e. $(45°, 132°)$, which indicates the area the two paths are not longer resolvable.

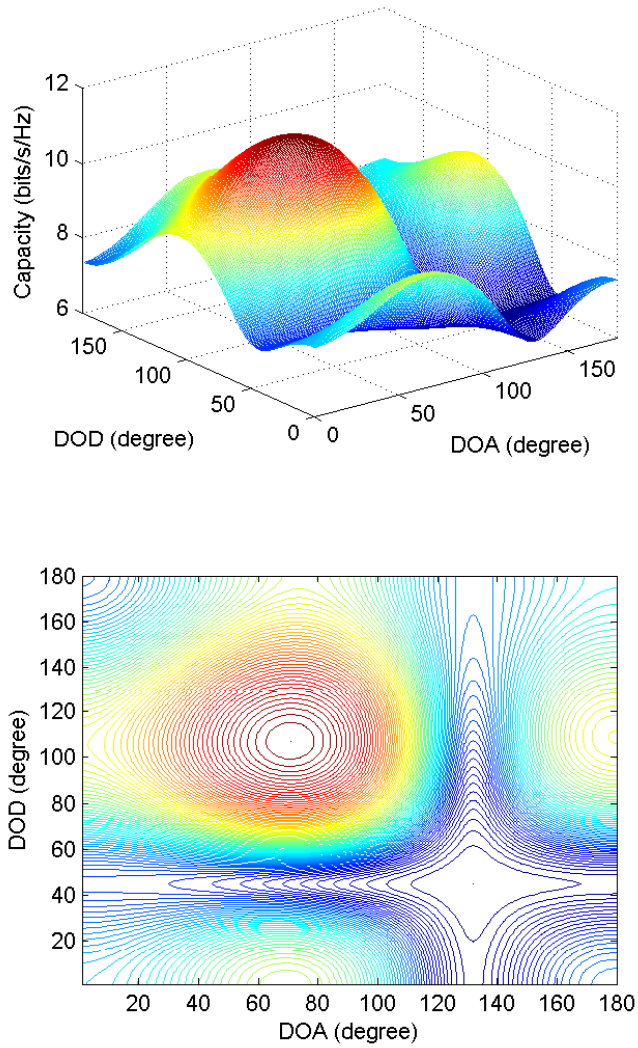


Figure 2.15: (a) Capacity of a (2,2)-MIMO system employing half wave spacing ULA at both Tx and Rx. There are two resolvable multipaths, one fixed at $(\mathrm{DOD}, \mathrm{DOA}) = (45°, 132°)$, another varies. (b) Contour figure of (a).

2.5 Number of Multipaths and Spatial Degree of Freedom

As shown in Appendix 2.B, in the high SNR regime, every G fold increase of SNR will result an increase of $\log_2 G$ bits/s/Hz for the capacity of SISO channel. However, for MIMO channel, every G fold increase of SNR will result in an increase of $N^* \log_2 G$ bits/s/Hz in the capacity, where N^* is known as *spatial degree of freedom* of the MIMO channel [12]. This is the significance of MIMO system's capacity multiplexing ability.

For i.i.d. MIMO channel, consider SVD of the channel matrix $\mathbb{H} = \mathbb{U}\mathbb{D}\mathbb{V}^H$, where $\mathbb{U}$ and $\mathbb{V}$ are unitary matrices, $\mathbb{D}$ is a diagonal matrix whose elements are the singular values of $\mathbb{H}$. The rank of $\mathbb{D}$ is the ideal *spatial degree of freedom* of the MIMO. It is well-known that $N^* = \min(\overline{N}, N)$. For instance, as shown in Figure 2.16, when the total transmitted power is increased by 3 dB, the $\mathrm{CDF}_{\mathrm{capacity}}$ curve of SISO right-shifts 1 bit/s/Hz accordingly, whereas for the $(8, 8)$-MIMO channel, the curve right-shifts about 8 bits/s/Hz.

In [20], Shiu et al. pointed out that the spatial degree of freedom N^* might decrease because of the spatial correlation. In [42] and [43], Poon et al. derived the limit to the *spatial degree of freedom* given the constraints of array aperture and array geometry but with infinite number of antennas in the array.

Based on the proposed arrayed MIMO model, the *spatial degree of freedom* is shown not only to be bounded by the number of antennas in Tx/Rx array, but also by the number of multipaths in the propagation environment.

Theorem 2.1 *Bound of Spatial Degree of Freedom*

For a $(\overline{N}, N)$-MIMO system operating in a scattering environment with K spa-

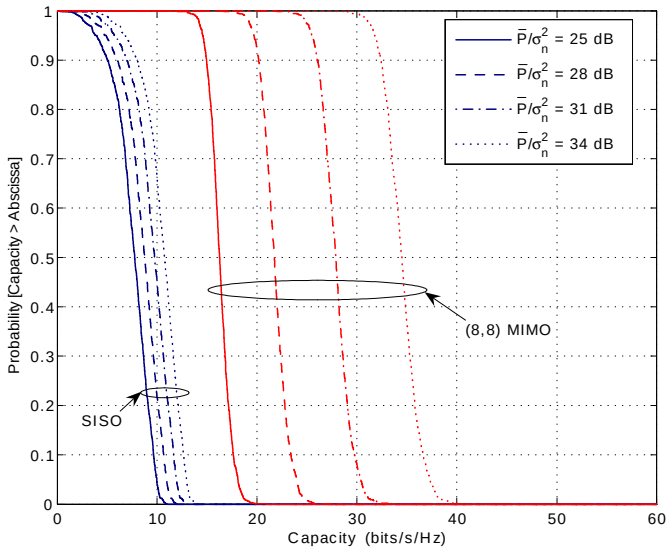


Figure 2.16: Cumulative distribution functions of capacity for a SISO and a (8,8) i.i.d. MIMO channels with $\overline{P}/\sigma_n^2 = 25$, 28, 31 and 34 dB.

tially resolvable paths, its spatial degree of freedom N^* is bounded as follows

$$\boxed{N^* \leq \min\left(K, \overline{N}, N\right)} \tag{2.79}$$

Proof. The proof is given in Appendix 2.B. ■

The immediate corollary of this theorem is that in particular scattering environment, the *spatial degree of freedom* of MIMO system cannot be increased infinitely by using more antennas at the transmitter and the receiver, since *spatial degree of freedom* is also up-bounded by the number of resolvable paths. To investigate the effect of the number of multipaths on the spatial degree of freedom, numerical simulations are conducted as follows.

Firstly, a symmetrical MIMO system with ULA at both transmitter and receiver is investigated based on 10000 channel realizations. As shown in Figure 2.17, given a certain number of resolvable paths, *spatial degree of freedom* does not change linearly with the increased with the number of antennas. When the array aperture is large, *spatial degree of freedom* is upper-bounded by the number

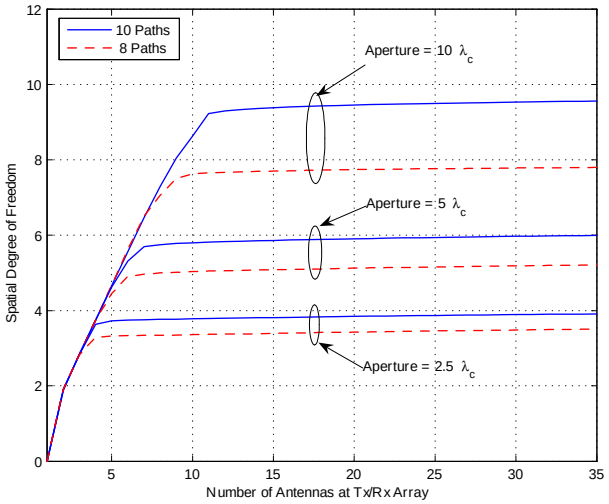


Figure 2.17: Relation of Spatial Degree of Freedom and the number of antennas in Tx/Rx arrays, with the array aperture fixed at $2.5\lambda_c$, $5\lambda_c$ and $10\lambda_c$, with $\overline{P}/\sigma_n^2 = 20$ dB.

of resolvable paths. When the aperture is small, the upper bound of the *spatial degree of freedom* is found even less than the number of resolvable paths. This is intuitive because spatial correlation will increase if more antenna elements are used for a given aperture.

Furthermore, to investigate how *spatial degree of freedom* changes with the scattering environment, simulations are conducted to compare the *spatial degree of freedom* of ULA MIMO under different number of paths, in the scenario of $(4,4)$-MIMO, $(3,3)$-MIMO, $(2,2)$-MIMO and SISO systems with inter-element spacing fixed at $0.5\lambda_c$. As shown in Figure 2.18, to achieve the upper-bound of the degree of freedom as specified in Theorem 2.1, the required number of paths of a $(\overline{N}, N)$-MIMO with $\overline{N} = N$ needs to be much more than N, even greater than N^2. The reason of this phenomena can be attributed to the dramatic effect of the spatial correlation between pair-wise channels.

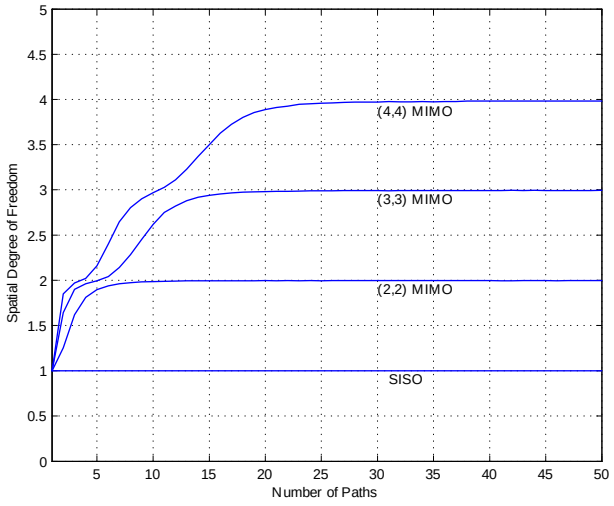


Figure 2.18: Relationship between Spatial Degree of Freedom.and the number of paths for SISO, (2,2)-MIMO, (3,3)-MIMO and (4,4)-MIMO.

2.6 Summary

In this chapter, from the viewpoint of array processing, a novel spatial discrete channel model for spatial correlated MIMO system is proposed using the concept of array manifold of both Tx and Rx arrays. By implementing the first-order Taylor approximation, the diffused MIMO channel is approximated by modified point-source channel and the MIMO channel matrix is expressed explicitly by its multipath characteristics, such as DODs, DOAs and complex path gains, and the geometry of both Tx and Rx arrays. The spatial correlation matrix is then derived, which provides more realistic results than the widely-used Kronecker model and recently-proposed Weichselberger's model. With the proposed arrayed model, the effect of Tx/Rx array geometry on the spatial correlation and then capacity of correlated MIMO has been investigated, which suggests that for the fixed aperture, for example, the cross array outperforms uniform linear array and uniform circle array. The capacity of correlated MIMO increases with the array aperture as well as the number of resolvable paths, until the theoretic capacity of

i.i.d. MIMO is achieved. In the arrayed MIMO system, the array aperture and the number of resolvable paths is found of great importance on bounding of the spatial degree of freedom of MIMO system. When the array aperture is large, spatial degree of freedom is upper-bounded by the number of resolvable paths. When the aperture is small, the upper bound of the spatial degree of freedom is found even less than the number of resolvable paths.

Appendix 2.A Kronecker Product

Definition

The Kronecker product of matrices $\mathbb{A} \in \mathcal{C}^{p\times q}$ and $\mathbb{B} \in \mathcal{C}^{u\times k}$ is defined as

$$\mathbb{A} \otimes \mathbb{B} = \begin{bmatrix} a_{1,1}\mathbb{B} & a_{1,2}\mathbb{B} & \cdots \\ a_{2,1}\mathbb{B} & a_{2,2}\mathbb{B} & \cdots \\ \cdots & \cdots & \cdots \end{bmatrix} \quad \in \mathcal{C}^{up\times kq} \tag{2.80}$$

Proof of Eqn. (2.48)

Proof. If $\underline{a} = [a_1,\, a_2,\, \cdots,\, a_m]^T$ and $\underline{b} = [b_1,\, b_2,\, \cdots,\, b_n]^T$, then

$$\begin{aligned} \mathrm{vec}(\underline{a}\underline{b}^T) &= \mathrm{vec}\left(\begin{bmatrix} a_1b_1 & a_1b_2 & \cdots & a_1b_n \\ a_2b_1 & a_2b_2 & \ddots & \vdots \\ \vdots & \ddots & \ddots & \vdots \\ a_mb_1 & \cdots & \cdots & a_mb_n \end{bmatrix}\right) && (2.81) \\ &= [a_1b_1,\, a_2b_1,\, \cdots,\, a_mb_1,\, a_1b_2 \cdots,\, a_mb_n]^T && (2.82) \\ &= \underline{b} \otimes \underline{a} && (2.83) \end{aligned}$$

■

Proof of Eqn. (2.48)

Proof. If $\underline{a} = [a_1,\, a_2,\, \cdots,\, a_m]^T$, $\underline{b} = [b_1,\, b_2,\, \cdots,\, b_n]^T$, $\underline{c} = [c_1,\, c_2,\, \cdots,\, c_m]^T$ and $\underline{d} = [d_1,\, d_2,\, \cdots,\, d_n]^T$,

$$(\underline{b} \otimes \underline{a})\,(\underline{d} \otimes \underline{c})^T \tag{2.84}$$

$$= [a_1 b_1,\, \cdots,\, a_m b_1,\, a_1 b_2 \cdots,\, a_m b_n]^T\,[c_1 d_1,\, \cdots,\, c_m d_1,\, c_1 d_2 \cdots,\, c_m d_n] \tag{2.85}$$

$$= \begin{bmatrix} a_1b_1c_1d_1 & a_1b_1c_2d_1 & \cdots & a_1b_1c_md_n \\ a_2b_1c_1d_1 & a_2b_1c_2d_1 & \ddots & \vdots \\ \vdots & \ddots & \ddots & \vdots \\ a_mb_nc_1d_1 & \cdots & \cdots & a_mb_nc_md_n \end{bmatrix} \in \mathcal{C}^{mn\times mn} \tag{2.86}$$

$$= \begin{bmatrix} b_1d_1 & b_1d_2 & \cdots & b_1d_n \\ b_2d_1 & b_2d_2 & \ddots & \vdots \\ \vdots & \ddots & \ddots & \vdots \\ b_nd_1 & \cdots & \cdots & b_nd_n \end{bmatrix} \otimes \begin{bmatrix} a_1c_1 & a_1c_2 & \cdots & a_1c_m \\ a_2c_1 & a_2c_2 & \ddots & \vdots \\ \vdots & \ddots & \ddots & \vdots \\ a_mc_1 & \cdots & \cdots & a_mc_m \end{bmatrix} \tag{2.87}$$

$$= \left(\underline{b}\;\underline{d}^T\right) \otimes \left(\underline{a}\;\underline{c}^T\right)$$

■

Appendix 2.B Degree of Freedom

In this Appendix, Degree of Freedom (DOF), defined in Section 2.5, will be used.

For SISO Channel

$$C_{\text{SISO}}\left(\text{SNR}=\gamma\right)=\log_2\left(1+\gamma\right) \qquad \text{bits/s/Hz} \tag{2.88}$$

If $\gamma \gg 1$, then

$$C_{\text{SISO}}\left(\text{SNR}=\gamma\right)\approx\log_2\left(\gamma\right) \qquad \text{bits/s/Hz} \tag{2.89}$$

and

$$\begin{aligned} C_{\text{SISO}}\left(\text{SNR}=2\gamma\right) &= \log_2\left(2\gamma\right) && (2.90)\\ &= C_{\text{SISO}}\left(\text{SNR}=\gamma\right)+\underbrace{1}_{\text{DOF}} \qquad \text{bits/s/Hz} && (2.91)\end{aligned}$$

i.e.

$$\boxed{\text{DOF}_{\text{SISO}}=1} \tag{2.92}$$

For Conventional MIMO

Recall the general channel model

$$\underline{x}\left(t\right)=\mathbb{H}\underline{m}\left(t\right)+\underline{n}\left(t\right) \tag{2.93}$$

so,

$$\mathbb{R}_{xx}=\mathbb{H}\mathbb{R}_{mm}\mathbb{H}^H+\mathbb{R}_{nn} \tag{2.94}$$

By definition of capacity [44],

$$\begin{aligned} C_{\text{MIMO}} &= \log_2\left(\frac{\det\left(\mathbb{R}_{xx}\right)}{\det\left(\mathbb{R}_{nn}\right)}\right) && (2.95)\\ &= \log_2\det\left(\mathbb{I}_N+\mathbb{H}\mathbb{R}_{mm}\mathbb{H}^H\right) && (2.96)\\ &= \log_2\det\left(\mathbb{I}_N+\frac{\gamma}{N}\underbrace{\mathbb{H}\mathbb{H}^H}_{=\mathbb{U}\mathbb{D}\mathbb{U}^H}\right) \qquad \text{bits/s/Hz} && (2.97)\end{aligned}$$

where $\mathbb{U}\mathbb{D}\mathbb{U}^H$ is the eigendecomposition of positive-definite matrix $\mathbb{H}\mathbb{H}^H$ and $\mathbb{D} = \begin{bmatrix} \lambda_1 & 0 & \cdots \\ 0 & \lambda_2 & \ddots \\ \vdots & \ddots & \ddots \end{bmatrix}$. By property of determinants:

$$\det(\mathbb{I} + \mathbb{A}\mathbb{B}) = \det(\mathbb{I} + \mathbb{B}\mathbb{A}) \tag{2.98}$$

The capacity of a MIMO channel can be rewritten as

$$C_{\text{MIMO}} = \log_2 \det\left(\mathbb{I}_N + \frac{\gamma}{\overline{N}}\mathbb{D}\right) \tag{2.99}$$

$$= \log_2 \prod_{i=1}^{N}\left(1 + \frac{\gamma}{\overline{N}}\lambda_i\right) \qquad \text{bits/s/Hz} \tag{2.100}$$

When $\frac{\gamma}{\overline{N}}\lambda_i \gg 1$ (which is only valid assumption for non-zero λ_i),

$$C_{\text{MIMO}} = \sum_{i=1}^{n^*} \log_2\left(\frac{\gamma}{\overline{N}}\lambda_i\right) \qquad \text{bits/s/Hz} \tag{2.101}$$

where $n^* = \min(N, \overline{N})$ is the number of non-zero eigenvalue of $\mathbb{H}\mathbb{H}^H$.

For i.i.d. MIMO model

Following [45] and [2], If $N < \overline{N}$, for fixed N, by the law of large numbers [46], the k^{th} diagonal element of $\frac{1}{\overline{N}}\mathbb{H}_{\text{w}}\mathbb{H}_{\text{w}}^H$ is

$$\lim_{\overline{N}\to\infty} \frac{1}{\overline{N}} \sum_{j=1}^{\overline{N}} |h_{kj}|^2 = 1, \text{ (variance of } h_{ij}) \tag{2.102}$$

and the (k, u) non-diagonal elements of $\frac{1}{\overline{N}}\mathbb{H}_{\text{w}}\mathbb{H}_{\text{w}}^H$ is

$$\lim_{\overline{N}\to\infty} \frac{1}{\overline{N}} \sum_{j=1}^{\overline{N}} h_{kj}h_{ju}^* = 0, \text{ (independency of } h_{ij}) \tag{2.103}$$

that is

$$\lim_{\overline{N}\to\infty} \frac{1}{\overline{N}}\mathbb{H}_{\text{w}}\mathbb{H}_{\text{w}}^H = \mathbb{I}_N \tag{2.104}$$

Similarly, If $N > \overline{N}$, for fixed $\overline{N}$,

$$\lim_{N\to\infty} \frac{1}{N}\mathbb{H}_{\text{w}}^H\mathbb{H}_{\text{w}} = \mathbb{I}_{\overline{N}} \tag{2.105}$$

Substitute (2.104) and (2.105) into (2.100)

$$C_{\text{MIMO}} \rightarrow \begin{cases} N \log_2 (1+\gamma) & \text{if } N \leq \overline{N} \\ \overline{N} \log_2 \left(1 + \frac{N}{\overline{N}} \gamma\right) & \text{else} \end{cases} \tag{2.106}$$

So if γ is large,

$$C_{\text{i.i.d.}} (\text{SNR} = 2\gamma) = \underbrace{n^*}_{\text{DOF}} + C_{\text{i.i.d.}} (\text{SNR} = \gamma) \tag{2.107}$$

For Rx Beamforming System

$$C_{\text{Rx}} (\text{SNR} = \gamma) = \log_2 (1 + N\gamma) \qquad \text{bits/s/Hz} \tag{2.108}$$

If γ is large,

$$\begin{aligned} C_{\text{Rx}} (\text{SNR} = 2\gamma) &= \log_2 (N 2\gamma) && (2.109) \\ &= C_{\text{Rx}} (\text{SNR} = \gamma) + \underbrace{1}_{\text{DOF}} \qquad \text{bits/s/Hz} && (2.110) \end{aligned}$$

For Tx-Rx beamforming system

$$C_{\text{Tx/Rx}} (\text{SNR} = \gamma) = \log_2 \left(1 + \overline{N} N \gamma\right) \qquad \text{bits/s/Hz} \tag{2.111}$$

If $\gamma \gg 1$,

$$\begin{aligned} C_{\text{Tx/Rx}} (\text{SNR} = 2\gamma) &= \log_2 \left(\overline{N} N 2\gamma\right) && (2.112) \\ &= C_{\text{Tx/Rx Beamforming}} (\text{SNR} = \gamma) + \underbrace{1}_{\text{DOF}} \qquad \text{bits/s/Hz} \\ & && (2.113) \end{aligned}$$

For Proposed Arrayed MIMO

Proof of Theorem 2.1

Proof. The received signal-vector:

$$\underline{x}(t) = \mathbb{S}\, \text{diag}\left(\underline{\beta}\right) \overline{\mathbb{S}}^H \underline{m}(t) + \underline{n}(t) \tag{2.114}$$

Thus

$$\mathbb{R}_{xx} = \mathbb{S}\,\mathrm{diag}\left(\underline{\beta}\right)\overline{\mathbb{S}}^{H}\mathbb{R}_{mm}\overline{\mathbb{S}}\,\mathrm{diag}\left(\underline{\beta^{*}}\right)\mathbb{S}^{H} + \mathbb{R}_{nn} \tag{2.115}$$

and

$$\begin{aligned} & C_{\mathrm{prop}}\left(\mathrm{SNR} = \gamma\right) && (2.116)\\ = \;& \log_2\left(\frac{\det\left(\mathbb{R}_{xx}\right)}{\det\left(\mathbb{R}_{nn}\right)}\right) && (2.117)\\ = \;& \log_2 \det\left(\mathbb{I}_N + \frac{\gamma}{\overline{N}}\mathbb{S}\,\mathrm{diag}\left(\underline{\beta}\right)\overline{\mathbb{S}}^{H}\overline{\mathbb{S}}\,\mathrm{diag}\left(\underline{\beta^{*}}\right)\mathbb{S}^{H}\right) && (2.118)\end{aligned}$$

If $\min\left(K, N, \overline{N}\right) = N$

$$\begin{aligned} & C_{\mathrm{prop}}\left(\mathrm{SNR} = \gamma\right) && (2.119)\\ = \;& \log_2 \det\left(\mathbb{I}_{\overline{N}} + \frac{\gamma}{\overline{N}}\underbrace{\mathbb{S}\,\mathrm{diag}\left(\underline{\beta}\right)\overline{\mathbb{S}}^{H}\overline{\mathbb{S}}\,\mathrm{diag}\left(\underline{\beta^{*}}\right)\mathbb{S}^{H}}_{N\times N \;\text{ non-singular}}\right) && (2.120)\end{aligned}$$

if γ is large,

$$\begin{aligned} & C_{\mathrm{prop}}\left(\mathrm{SNR} = \gamma\right) && (2.121)\\ \approx \;& \log_2\left[\det\left(\frac{\gamma}{\overline{N}}\mathbb{S}\,\mathrm{diag}\left(\underline{\beta}\right)\overline{\mathbb{S}}^{H}\overline{\mathbb{S}}\,\mathrm{diag}\left(\underline{\beta^{*}}\right)\mathbb{S}^{H}\right)\right] && (2.122)\end{aligned}$$

and by property $\det\left(a \underset{n\times n}{\mathbb{B}}\right) = a^{n}\det\left(\mathbb{B}\right)$,

$$\begin{aligned} & C_{\mathrm{prop}}\left(\mathrm{SNR} = \gamma\right) && (2.123)\\ = \;& \log_2\left[\left(\frac{\gamma}{\overline{N}}\right)^{N}\det\left(\mathbb{S}\,\mathrm{diag}\left(\underline{\beta}\right)\overline{\mathbb{S}}^{H}\overline{\mathbb{S}}\,\mathrm{diag}\left(\underline{\beta^{*}}\right)\mathbb{S}^{H}\right)\right] && (2.124)\\ = \;& N\log_2\left(\frac{\gamma}{\overline{N}}\right) + \log_2\det\left(\mathbb{S}\,\mathrm{diag}\left(\underline{\beta}\right)\overline{\mathbb{S}}^{H}\overline{\mathbb{S}}\,\mathrm{diag}\left(\underline{\beta^{*}}\right)\mathbb{S}^{H}\right) && (2.125)\end{aligned}$$

Then.

$$\begin{aligned} & C_{\mathrm{prop}}\left(\mathrm{SNR} = 2\gamma\right) && \\ = \;& N\log_2\left(\frac{2\gamma}{\overline{N}}\right) + \log_2\det\left(\mathbb{S}\,\mathrm{diag}\left(\underline{\beta}\right)\overline{\mathbb{S}}^{H}\overline{\mathbb{S}}\,\mathrm{diag}\left(\underline{\beta^{*}}\right)\mathbb{S}^{H}\right) && (2.126)\\ = \;& \underbrace{N}_{DOF} + C_{\mathrm{prop}}\left(\mathrm{SNR} = \gamma\right) && (2.127)\end{aligned}$$

If $\min\left(K, N, \overline{N}\right) = \overline{N}$ and γ is large,

$$
\begin{aligned}
& C_{\text{prop}}\left(\text{SNR} = \gamma\right) && (2.128)\\
= \; & \log_2 \det\left(\mathbb{I}_{\overline{N}} + \frac{\gamma}{\overline{N}} \underbrace{\overline{\mathbb{S}}\, \text{diag}\left(\underline{\beta^*}\right) \mathbb{S}^H \mathbb{S}\, \text{diag}\left(\underline{\beta}\right) \overline{\mathbb{S}}^H}_{\overline{N}\times\overline{N} \text{ non-singular}}\right) && (2.129)\\
= \; & \log_2 \left[\det\left(\frac{\gamma}{\overline{N}} \overline{\mathbb{S}}\, \text{diag}\left(\underline{\beta^*}\right) \mathbb{S}^H \mathbb{S}\, \text{diag}\left(\underline{\beta}\right) \overline{\mathbb{S}}^H\right)\right] && (2.130)
\end{aligned}
$$

As $\overline{\mathbb{S}} \in \mathcal{C}^{\overline{N}\times K}$, $\mathbb{S} \in \mathcal{C}^{N\times K}$ and $\text{diag}\left(\underline{\beta}\right) \in \mathcal{C}^{K\times K}$, and $\overline{N} < K$ and $\overline{N} < N$, the rank of $\overline{\mathbb{S}}\, \text{diag}\left(\underline{\beta^*}\right) \mathbb{S}^H \mathbb{S}\, \text{diag}\left(\underline{\beta}\right) \overline{\mathbb{S}}^H$ is $\overline{N}$,

$$
\begin{aligned}
& C_{\text{prop}}\left(\text{SNR} = \gamma\right) && (2.131)\\
= \; & \log_2 \left[\left(\frac{\gamma}{\overline{N}}\right)^{\overline{N}} \det\left(\overline{\mathbb{S}}\, \text{diag}\left(\underline{\beta^*}\right) \mathbb{S}^H \mathbb{S}\, \text{diag}\left(\underline{\beta}\right) \overline{\mathbb{S}}^H\right)\right] && (2.132)\\
= \; & \overline{N} \log_2\left(\frac{\gamma}{\overline{N}}\right) + \log_2 \det\left(\overline{\mathbb{S}}\, \text{diag}\left(\underline{\beta^*}\right) \mathbb{S}^H \mathbb{S}\, \text{diag}\left(\underline{\beta}\right) \overline{\mathbb{S}}^H\right) && (2.133)
\end{aligned}
$$

then

$$
\begin{aligned}
& C_{\text{prop}}\left(\text{SNR} = 2\gamma\right) && \\
= \; & \overline{N} \log_2\left(\frac{2\gamma}{\overline{N}}\right) + \log_2 \det\left(\overline{\mathbb{S}}\, \text{diag}\left(\underline{\beta^*}\right) \mathbb{S}^H \mathbb{S}\, \text{diag}\left(\underline{\beta}\right) \overline{\mathbb{S}}^H\right) && (2.134)\\
= \; & \underbrace{\overline{N}}_{DOF} + C_{\text{prop}}\left(\text{SNR} = \gamma\right) && (2.135)
\end{aligned}
$$

If $\min\left(K, N, \overline{N}\right) = K$ and γ is large

$$
\begin{aligned}
& C_{\text{prop}}\left(\text{SNR} = \gamma\right) && (2.136)\\
= \; & \log_2 \det\left(\mathbb{I}_{\overline{N}} + \frac{\gamma}{\overline{N}}\, \text{diag}\left(\underline{\beta}\right) \overline{\mathbb{S}}^H \overline{\mathbb{S}}\, \text{diag}\left(\underline{\beta^*}\right) \mathbb{S}^H \mathbb{S}\right) && (2.137)\\
= \; & \log_2 \left[\left(\frac{\gamma}{\overline{N}}\right)^{K} \det\left(\text{diag}\left(\underline{\beta}\right) \overline{\mathbb{S}}^H \overline{\mathbb{S}}\, \text{diag}\left(\underline{\beta^*}\right) \mathbb{S}^H \mathbb{S}\right)\right] && (2.138)\\
= \; & K \log_2\left(\frac{\gamma}{\overline{N}}\right) + \log_2 \det\left(\text{diag}\left(\underline{\beta}\right) \overline{\mathbb{S}}^H \overline{\mathbb{S}}\, \text{diag}\left(\underline{\beta^*}\right) \mathbb{S}^H \mathbb{S}\right) && (2.139)
\end{aligned}
$$

then

$$C_{\text{prop}}\left(\text{SNR} = 2\gamma\right) \tag{2.140}$$

$$= K \log_2\left(\frac{2\gamma}{\overline{\overline{N}}}\right) + \log_2 \det\left(\text{diag}\left(\underline{\beta}\right) \overline{\mathbb{S}}^H \overline{\mathbb{S}}\, \text{diag}\left(\underline{\beta^*}\right) \mathbb{S}^H \mathbb{S}\right) \tag{2.141}$$

$$= \underbrace{K}_{DOF} + C_{\text{prop}}\left(\text{SNR} = \gamma\right) \tag{2.142}$$

■

Chapter 3

Space-time Design in Arrayed MIMO-CDMA Uplink Systems

3.1 Introduction

CDMA technique will play a crucial role in the next generation mobile systems and, thus, the integration of MIMO with the infrastructure of the CDMA multi-user systems is a necessary condition for MIMO to be ultimately commercialized.

In order to accomplish this integration, the single-user narrow-band arrayed model developed in Chapter 2 needs to be extended to a multiuser form for frequency selective channels, in which

- time dispersion of multipath channel causes the received symbol overlapping with adjacent symbols, introducing *inter-symbol interference* (ISI);
- the multiple users transmit asynchronously, overlapping in both time and frequency resulting in *multiple access interference* (MAI);
- if all User Equipments (UE) transmit at similar power level, at the Base Station (BS), the power of the signals received from the nearby UEs will

be much stronger than those far away, introducing the so-called *near-far* problem.

To cope with all these issues, in this and next chapter, the MIMO-CDMA communication systems are investigated using spatial-temporal array processing concepts. By exploiting the array geometry and spatial-temporal information of the channel, e.g. direction and delay of multipath, an arrayed MIMO-CDMA system operating in a multiple-access environment provides a powerful solution using Tx beamforming based on subspace channel estimation and interference cancellation techniques.

This chapter, which is concerned with the uplink of the MIMO-CDMA system is organized as follows. In Section 3.2, the uplink of an asynchronous DS-CDMA channel, with multiple antennas deployed at both receiver and transmitter, is modelled. By using the MIMO-STAR manifold matrix, a composite *spatial-temporal array* (STAR) MIMO-CDMA channel matrix is expressed as a function of the antenna-array manifold vectors of both transmitter and receiver. In Section 3.3, the spatio-temporal (ST) types of single-user (SU) and multi-user (MU) linear receivers are proposed based on the MIMO-STAR manifold matrix concept. In Section 3.4, the subspace-based joint DOA/TOA estimation is developed and a DOD estimation scheme based on Tx beam rotation is proposed. The chapter is summarized in Section 3.5.

Please note that some material of this chapter has been published in [47].

3.2 Arrayed CDMA-MIMO System Modeling

Consider the uplink of an M-user asynchronous MIMO-CDMA wireless communication system operating in a multipath propagation environment. The BS's

receiver has an array of N antennas whereas each UE's transmitter is equipped with an array of $\overline{N}$ antennas.

At the transmitter of a CDMA-MIMO systems as depicted in Figure 3.1, the i^{th} user's BPSK (or QPSK) symbols are first demultiplexed into $\overline{N}$ multiple streams $\underline{b}_i[n]$ by a serial-to-parallel (S/P) convertor, then spread with the spreading signal

$$c_{PN,i}(t) = \sum_{k=0}^{N_c-1} \alpha_i[k]\, p(t - kT_c) \tag{3.1}$$

where T_c denotes the chip period, $\{\alpha_i[k] = \pm 1, k = 0, \ldots, N_c - 1\}$ is the i^{th} user's unique PN sequence of period $N_c = T_{cs}/T_c$, where T_{cs} is the data symbol period, $p(t)$ is the chip waveform. After beamforming (weight vector $\underline{\overline{w}}_i \in \mathcal{C}^{\overline{N}\times 1}$), the i^{th} user's baseband transmitted signal-vector (point E in Figure 3.1) is given by

$$\begin{aligned} \underline{m}_i(t) &= \sum_{n=-\infty}^{\infty} \underline{\overline{w}}_i \odot \underline{b}_i[n]\, c_{PN,i}(t - nT_{cs}) \\ & \quad nT_{cs} \le t \le (n+1)T_{cs} \end{aligned} \tag{3.2}$$

In this chapter, unless otherwise specified, the Tx beamforming weight vector $\underline{\overline{w}}_i = \underline{1}_{\overline{N}}$, which is the default beamformer (i.e. no weighs). Thus Eqn. (3.2) can be simplified as follows

$$\begin{aligned} \underline{m}_i(t) &= \sum_{n=-\infty}^{\infty} \underline{b}_i[n]\, c_{PN,i}(t - nT_{cs}) \\ & \quad nT_{cs} \le t \le (n+1)T_{cs} \end{aligned} \tag{3.3}$$

Let us assume plane-wave propagation with transmitted signals of the i^{th} user arriving at the receiver via K_i multipaths. Furthermore, consider that the j^{th} path of the i^{th} user's direction of departure (DOD) (azimuth, elevation) $= \left(\overline{\theta}_{ij}, \overline{\varphi}_{ij}\right)$ and direction of arrival (DOA) $\left(\theta_{ij}, \varphi_{ij}\right)$. The array manifold vector of the receiver $\underline{S}_{ij}$ of the j^{th} path of the i^{th} user can be formulated as

$$\underline{S}_{ij} = \exp(-\mathrm{j}\ [\underline{r}_x,\ \underline{r}_y,\ \underline{r}_z]\ \underline{\mathrm{k}}_{ij}) \tag{3.4}$$

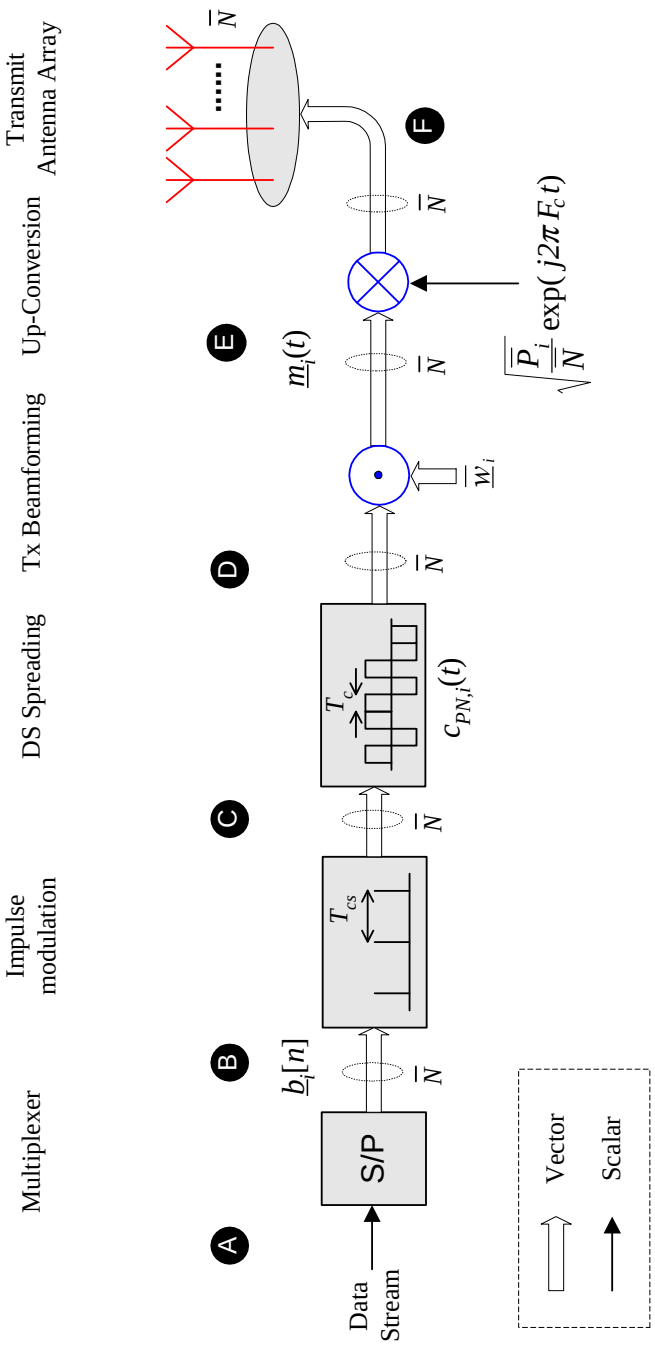


Figure 3.1: Diagram of uplink MIMO-CDMA transmitter.

where $[\underline{r}_x, \underline{r}_y, \underline{r}_z] = [\underline{r}_1, \underline{r}_2, \cdots, \underline{r}_N]^T \in \mathcal{R}^{N\times 3}$ with $\underline{r}_k$ denoting the Cartesian coordinates of the k^{th} antenna. The vector $\underline{\mathrm{k}}_{ij}$, defined as

$$\underline{\mathrm{k}}_{ij} = \frac{2\pi F_c}{c}[\cos\theta_{ij}\cos\phi_{ij}, \sin\theta_{ij}\cos\phi_{ij}, \sin\phi_{ij}]^T \tag{3.5}$$

is the wavenumber vector pointing towards the DOA of the j^{th} path of the i^{th} user. The Tx array manifold vector $\overline{\underline{S}}_{ij}$ of the j^{th} path of the i^{th} user can be defined in a similar fashion to Eqn. (3.4) but with the parameters associated with the transmitters. Without loss of generality, all the signals are assumed to propagate on x-y plane, i.e., $\overline{\phi}_{ij} = \phi_{ij} = 0$.

With reference to the channel model shown in Figure 3.2, the received complex baseband signal-vector at the input of the Rx antenna array (point I) can be expressed as

$$\underline{x}\,(t) = \sum_{i=1}^{M}\sum_{j=1}^{K_i} \beta_{ij}\underline{S}_{ij}\overline{\underline{S}}_{ij}^{H}\underline{m}_i\,(t-\tau_{ij}) + \underline{\mathrm{n}}\,(t) \tag{3.6}$$

where β_{ij} and τ_{ij} represent the fading coefficient and the delay of the j^{th} path of the i^{th} user, and $\underline{\mathrm{n}}\,(t)$ denotes the complex white Gaussian noise vector with zero mean and covariance matrix $\sigma_n^2\mathbb{I}_N$.

As it is shown in Figure 3.3, the baseband received signal-vector $\underline{x}\,(t)$ is initially sampled with a period $T_s = T_c$. The lack of synchronization is modelled as $(\tau_{ij} \mod T_{cs})$, which can be written as follows:

$$\tau_{ij} \mod T_{cs} = \left(l_{ij} + \rho_{ij}\right) T_c \tag{3.7}$$

where $\rho_{ij} \in [0, 1)$ is the fractional part and l_{ij} is the integer part,

$$l_{ij} = \left\lfloor \frac{\tau_{ij} \mod T_{cs}}{T_c} \right\rfloor \tag{3.8}$$

with $0 \le l_{ij} < N_c$. Note that the fractional delay provides the phase shift $\exp\left(-j2\pi F_c\rho_{ij}T_c\right)$ which can be absorbed by the complex fading coefficient β_{ij}.

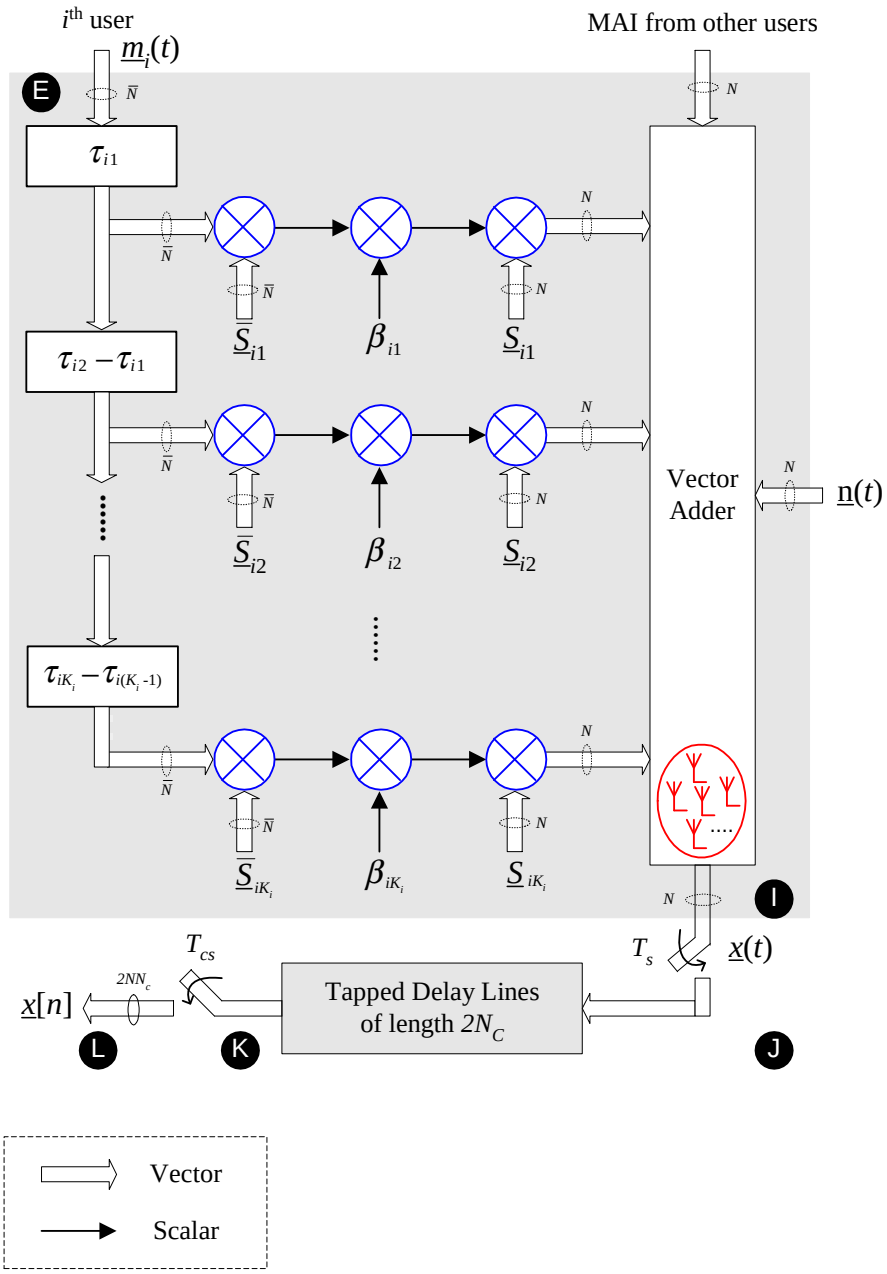


Figure 3.2: Uplink arrayed MIMO frequency selective channel of the i^{th} user.

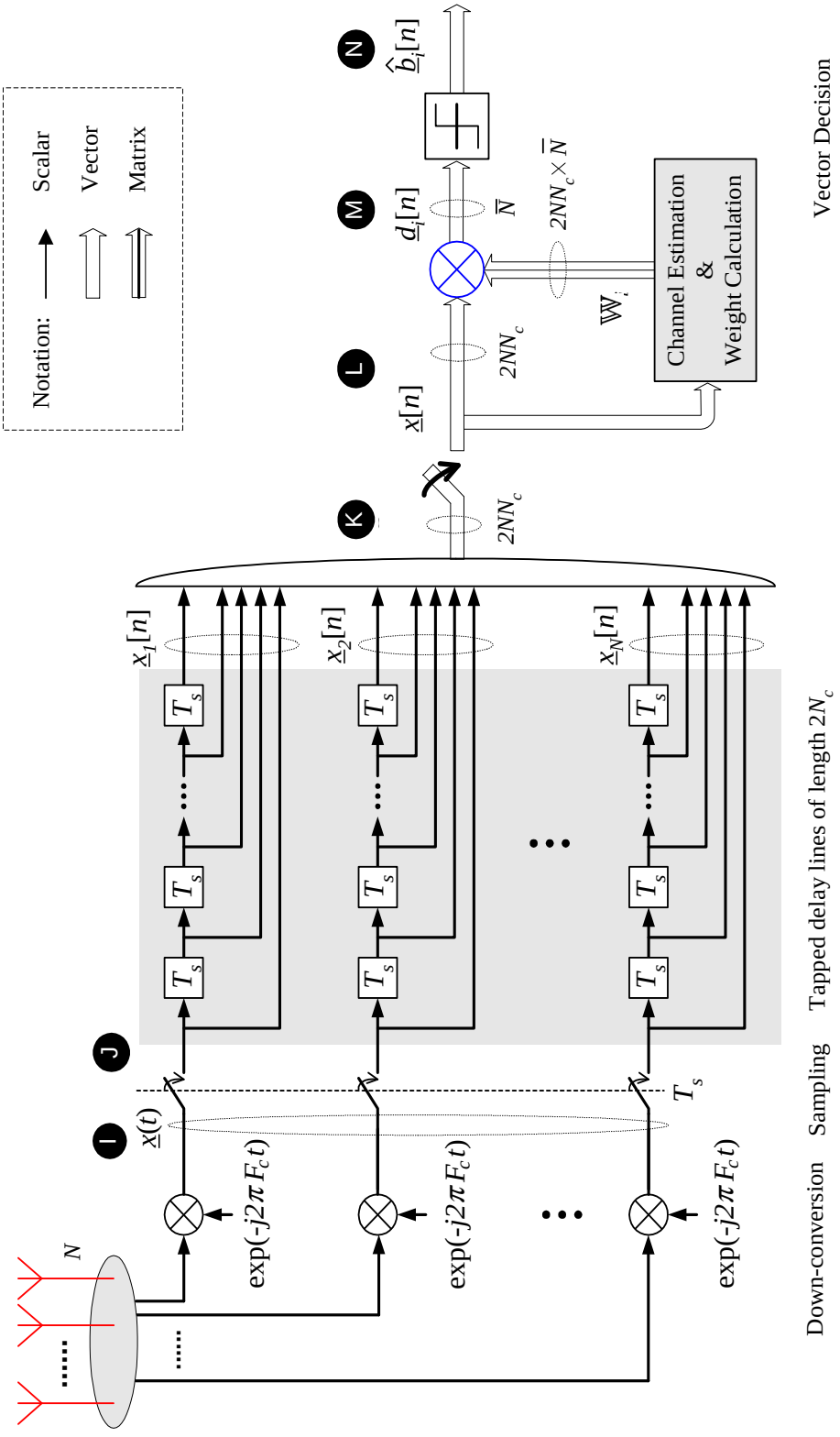


Figure 3.3: Diagram of uplink MIMO-CDMA Receiver

At point L in Figure 3.3, the contents of a bank of N tapped delay lines (TDL), each of length $2N_c$, are concatenated to obtain

$$\underline{x}[n] = \begin{bmatrix} \underline{x}_1[n] \\ \underline{x}_2[n] \\ \vdots \\ \underline{x}_N[n] \end{bmatrix} \in \mathcal{C}^{2NN_c \times 1} \tag{3.9}$$

where $\underline{x}_k[n] \in \mathcal{C}^{2N_c \times 1}$ represents the contents of the TDL at k^{th} receiver antenna associated with the n^{th} data-symbol period.

Note that because of the lack of symbol synchronization, $\underline{x}_k[n]$ contains contributions from not only the current (n^{th}) data-symbol, but also the $(n-1)^{\text{th}}$ (previous) and $(n+1)^{\text{th}}$ (next) data-symbol as shown in Figure 3.4.

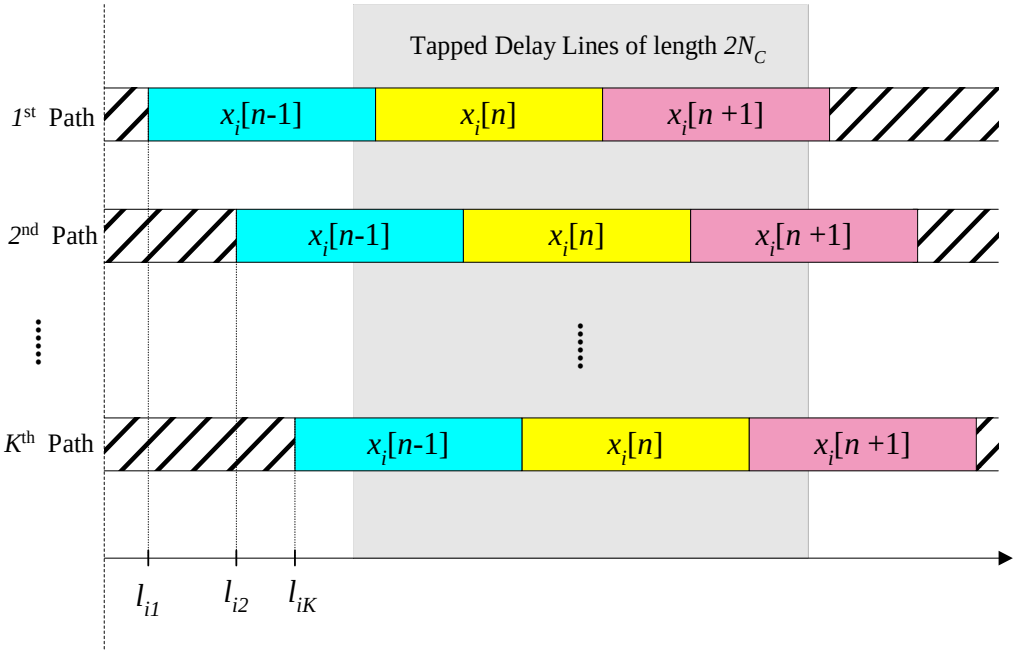


Figure 3.4: Inter-Symbol Interference (ISI) resulted from previous and next symbols.

In [48] the STAR manifold vector was defined for a CDMA system where only the receiver was equipped with an antenna array. Here, to model the above effects, the STAR manifold vector of the j^{th} path of i^{th} user is extended to a

MIMO-STAR manifold matrix as follows

$$\left(\underline{S}_{ij}\overline{\underline{S}}_{ij}^{H}\right)\otimes\left(\mathbb{J}^{l_{ij}}\underline{\mathfrak{c}}_{i}\right)\quad\in\mathcal{C}^{2NN_{c}\times\overline{N}}\tag{3.10}$$

which involves the PN-code of the user as well as the manifold vectors of both Tx and Rx. Note that to model the lack of synchronization, the $2N_c \times 2N_c$ matrix $\mathbb{J}$, known as time down-shift operator matrix, is used and defined[1] as follows

$$\mathbb{J}=\begin{bmatrix}0&0&\cdots&0&0\\1&0&\cdots&0&0\\0&1&\ddots&\vdots&\vdots\\\vdots&\ddots&1&0&0\\0&\cdots&0&1&0\end{bmatrix}=\begin{bmatrix}\underline{0}_{2N_c-1}^{T}&0\\\mathbb{I}_{2N_c-1}&\underline{0}_{2N_c-1}\end{bmatrix}\tag{3.11}$$

Furthermore, $\underline{\mathfrak{c}}_i$ is the i^{th} user's PN code $\underline{\alpha}_i$ padded with N_c zeros, i.e.

$$\underline{\mathfrak{c}}_{i}=\Big[\underbrace{\alpha_{i}\left[0\right],\alpha_{i}\left[1\right],\cdots,\alpha_{i}\left[N_{c}-1\right]}_{i^{\text{th}}\text{ user's PN code}},\underline{0}_{N_{c}}^{T}\Big]^{T}\quad\in\mathcal{C}^{2N_{c}\times1}\tag{3.12}$$

Using the MIMO-STAR manifold matrix defined by Eqn. (3.10), the sampled baseband signal-vector $\underline{x}\left[n\right]\in\mathcal{C}^{2NN_{c}}$ (see Eqn. 3.9) can be rewritten as

$$\underline{x}\left[n\right]=\sum_{i=1}^{M}\sum_{j=1}^{K_{i}}\beta_{ij}\left[\underline{S}_{ij}\overline{\underline{S}}_{ij}^{H}\otimes\left(\mathbb{J}^{l_{ij}}\underline{\mathfrak{c}}_{i}\right)\right]\underline{b}_{i}\left[n\right]+\text{ISI}\left[n\right]+\underline{\mathfrak{n}}\left[n\right]\tag{3.13}$$

or equivalently as

$$\underline{x}\left[n\right]=\sum_{i=1}^{M}\left(\begin{array}{l}\underbrace{\mathbb{H}_{i}\left(\underline{\beta}_{i}\otimes\mathbb{I}_{\overline{N}}\right)}_{\triangleq\ \mathbb{G}_{i}}\underline{b}_{i}\left[n\right]+\\\underbrace{\mathbb{H}_{i,\text{prev}}\left(\underline{\beta}_{i}\otimes\mathbb{I}_{\overline{N}}\right)}_{\triangleq\ \mathbb{G}_{i,\text{prev}}}\underline{b}_{i}\left[n-1\right]+\\\underbrace{\mathbb{H}_{i,\text{next}}\left(\underline{\beta}_{i}\otimes\mathbb{I}_{\overline{N}}\right)}_{\triangleq\ \mathbb{G}_{i,\text{next}}}\underline{b}_{i}\left[n+1\right]\end{array}\right)+\underline{\mathfrak{n}}\left[n\right]\tag{3.14}$$

[1] Note that $\mathbb{J}^T$ is a time up-shift operator matrix.

where $\underline{\mathrm{n}}\,[n] \in \mathcal{C}^{2NN_c}$ denotes the sampled noise vector during the n^{th} interval and

$$\mathbb{H}_i = \left[\underbrace{\left(\underline{S}_{i1}\overline{\underline{S}}_{i1}^{H}\right) \otimes \left(\mathbb{J}^{l_{i1}}\underline{\mathfrak{c}}_i\right)}_{\substack{\text{MIMO-STAR} \\ i^{\text{th}} \text{ user } 1^{\text{st}} \text{ path}}}, \quad \cdots, \quad \underbrace{\left(\underline{S}_{iK_i}\overline{\underline{S}}_{iK_i}^{H}\right) \otimes \left(\mathbb{J}^{l_{iK_i}}\underline{\mathfrak{c}}_i\right)}_{\substack{\text{MIMO-STAR} \\ i^{\text{th}} \text{ user } K_i^{\text{st}} \text{ path}}} \right] \quad \in \mathcal{C}^{2NN_c \times \overline{N}K_i} \tag{3.15}$$

Note that the vector $\underline{\beta}_i$ in Eqn. (3.14) is composed of the propagation coefficients of these K_i paths which model the effect of path loss, random phase shift due to reflection and Doppler phase shift due to the possible motion of scatterers, i.e.

$$\underline{\beta}_i = \left[\begin{array}{cccc} \beta_{i1}, & \beta_{i2}, & \cdots, & \beta_{iK_i} \end{array} \right]^T \quad \in \mathcal{C}^{K_i \times 1} \tag{3.16}$$

Furthermore, the matrices $\mathbb{H}_{i,\text{prev}}$ and $\mathbb{H}_{i,\text{next}}$ are used to incorporate the ISI effects. These matrices are defined as a function of $\mathbb{H}_i$ as

$$\mathbb{H}_{i,\text{prev}} = \left(\mathbb{I}_N \otimes \left(\mathbb{J}^T\right)^{N_c}\right) \mathbb{H}_i \quad \in \mathcal{C}^{2NN_c \times \overline{N}K_i} \tag{3.17}$$

$$\mathbb{H}_{i,\text{next}} = \left(\mathbb{I}_N \otimes \mathbb{J}^{N_c}\right) \mathbb{H}_i \quad \in \mathcal{C}^{2NN_c \times \overline{N}K_i} \tag{3.18}$$

Using matrices $\mathbb{G}_i$, $\mathbb{G}_{i,\text{prev}}$ and $\mathbb{G}_{i,\text{next}} \in \mathcal{C}^{2NN_c \times \overline{N}}$ defined in Eqn. (3.14), Eqn. (3.14) may be rewritten as

$$\underline{x}\,[n] = \sum_{i=1}^{M} \left[\mathbb{G}_{i,\text{prev}}, \mathbb{G}_i, \mathbb{G}_{i,\text{next}}\right] \left[\begin{array}{c} \underline{b}_i\,[n-1] \\ \underline{b}_i\,[n] \\ \underline{b}_i\,[n+1] \end{array} \right] + \underline{\mathrm{n}}\,[n] \tag{3.19}$$

$$= \underbrace{\mathbb{G}_i \underline{b}_i\,[n]}_{\text{Desired component}} + \underbrace{\left[\mathbb{G}_{i,\text{prev}}, \mathbb{G}_{i,\text{next}}\right] \left[\begin{array}{c} \underline{b}_i\,[n-1] \\ \underline{b}_i\,[n+1] \end{array} \right]}_{\text{ISI components}}$$

$$+ \underbrace{\sum_{\xi \neq i}^{M} \left[\mathbb{G}_{\xi,\text{prev}}, \mathbb{G}_\xi, \mathbb{G}_{\xi,\text{next}}\right] \left[\begin{array}{c} \underline{b}_\xi\,[n-1] \\ \underline{b}_\xi\,[n] \\ \underline{b}_\xi\,[n+1] \end{array} \right]}_{\text{MAI components}} + \underbrace{\underline{\mathrm{n}}\,[n]}_{\text{Noise}} \tag{3.20}$$

Hence, the discretized received signal-vector $\underline{x}[n] \in \mathcal{C}^{2NN_c}$ contains four components. That is the desired signal, ISI, MAI and noise as laid out in that order in Eqn. (3.20). The second order statistics $\mathbb{R}_{xx} \in \mathcal{C}^{2NN_c \times 2NN_c}$ of the received signal $\underline{x}[n]$ thus can be expressed as

$$\mathbb{R}_{xx} = \mathcal{E}\left\{\underline{x}[n]\,\underline{x}[n]^H\right\} \tag{3.21}$$

$$= \underbrace{\mathbb{G}_i\mathbb{G}_i^H}_{\mathbb{R}_{\text{desired}}} + \underbrace{\left[\mathbb{G}_{i,\text{prev}}, \mathbb{G}_{i,\text{next}}\right]\left[\mathbb{G}_{i,\text{prev}}, \mathbb{G}_{i,\text{next}}\right]^H}_{\mathbb{R}_{\text{ISI}}} + \underbrace{\sum_{\xi\neq i}^{M}\left[\mathbb{G}_{\xi,\text{prev}}, \mathbb{G}_{\xi}, \mathbb{G}_{\xi,\text{next}}\right]\left[\mathbb{G}_{\xi,\text{prev}}, \mathbb{G}_{\xi}, \mathbb{G}_{\xi,\text{next}}\right]^H}_{\mathbb{R}_{\text{MAI}}} + \underbrace{\sigma_{\text{n}}^2\mathbb{I}_{2NN_c}}_{\mathbb{R}_{\text{n}}} \tag{3.22}$$

where the multiple streams of the transmitted data signals are assumed to be independent, i.e.

$$\mathcal{E}\{\underline{b}_i[n]\ \underline{b}_i[n]^H\} = \mathbb{I}_{\overline{N}} \tag{3.23}$$

and strictly stationary, i.e.

$$\mathcal{E}\{\underline{b}_i[n]\ \underline{b}_i[n+n_\tau]^H\} = \mathbb{O}_{\overline{N}\times\overline{N}},\ \forall n_\tau \neq 0 \tag{3.24}$$

and the transmitted data signal of different users are also assumed to be independent, i.e.

$$\mathcal{E}\{\underline{b}_i[n]\ \underline{b}_j[n]^H\} = \mathbb{O}_{\overline{N}\times\overline{N}},\ \text{for } i \neq j, \tag{3.25}$$

3.3 MIMO-CDMA STAR Receivers

It is assumed the 1st user is the desired one[2]. At point M in Figure 3.3, the decision variable vector during the n^{th} symbol period (after the receiver beamforming $\mathbb{W}_1$)

[2]Throughout this thesis, unless otherwise stated, the 1st user is always assumed to be the desired user.

can be decoupled into four terms representing the desired, ISI, MAI and noise terms:

$$\underline{d}_1[n] = \underbrace{\mathbb{W}_1^H \mathbb{G}_1 \underline{b}_1[n]}_{\text{Desired component, } \underline{d}_{1,\text{desired}}[n]} + \underbrace{\mathbb{W}_1^H [\mathbb{G}_{1,\text{prev}}, \mathbb{G}_{1,\text{next}}] \begin{bmatrix} \underline{b}_1[n-1] \\ \underline{b}_1[n+1] \end{bmatrix}}_{\text{ISI components, } \underline{d}_{1,\text{isi}}[n]} + \underbrace{\mathbb{W}_1^H \sum_{\xi \neq 1}^{M} [\mathbb{G}_{\xi,\text{prev}}, \mathbb{G}_\xi, \mathbb{G}_{\xi,\text{next}}] \overline{\underline{b}}_\xi[n]}_{\text{MAI components, } \underline{d}_{1,\text{mai}}[n]} + \underbrace{\mathbb{W}_1^H \underline{\mathrm{n}}[n]}_{\text{Noise}} \tag{3.26}$$

Then at point N, the n^{th} data-symbol vector is detected by (for BPSK modulation)

$$\hat{\underline{b}}_1[n] = \text{sign}\left(\text{Re}\left\{\underline{d}_1[n]\right\}\right). \tag{3.27}$$

With the knowledge of the channel, space-time receivers can be devised to recover the transmitted information symbols. Linear receivers are considerably less complex to implement than many non-linear designs while producing satisfactory BER/SNIR performance. In the thesis both single-user (SU) and multi-user (MU) linear receivers are considered, where

- Single-user receivers require only the knowledge of the desired user's spreading sequence and its associated channel parameters, and
- Multi-user receivers require the spreading sequences and channel parameters of all the users (desired and unwanted).

In particular, the following receivers will be examined, by extending them to spatio-temporal (ST) type of receivers based on the MIMO-STAR manifold matrix concept.

1. ST-RAKE SU Receiver

   The space-time RAKE receiver is an optimum single user receiver under the

condition that all MAI as well as ISI are treated as additive white Gaussian noise. It is easy to prove that this receiver can be represented by matrix $\mathbb{W}_{\mathrm{RAKE}}$ for the above-proposed arrayed-MIMO channel as follows [48]

$$\mathbb{W}_{\mathrm{RAKE}} = \underset{\mathrm{Tr}\left(\mathbb{W}_1\mathbb{W}_1^H\right)=\text{constant}}{\arg\min} \mathrm{Tr}\left(\mathbb{W}_1^H\mathbb{G}_1\mathbb{G}_1^H\mathbb{W}_1\right) \tag{3.28}$$

$$= \mathbb{G}_1 \quad \in \mathcal{C}^{2NN_c\times\overline{N}} \tag{3.29}$$

Note that the derivation is based on Eqn. (3.14).

2. ST-MMSE SU Receiver

In MMSE reception, the weight matrix is constructed to minimize the mean squared error between the desired user's transmitted signal vector and the output of the beamformers, i.e.

$$\mathbb{W}_{\mathrm{MMSE}} = \underset{\mathrm{Tr}\left(\mathbb{W}_1\mathbb{W}_1^H\right)=\text{constant}}{\arg\min} \mathcal{E}\left\{\left\|\underline{b}_1 - \mathbb{W}_1^H\underline{x}\right\|\right\} \tag{3.30}$$

This provides the following solution [48]

$$\mathbb{W}_{\mathrm{MMSE}} = \mathbb{R}_{xx}^{-1}\mathbb{G}_1 \quad \in \mathcal{C}^{2NN_c\times\overline{N}} \tag{3.31}$$

where $\mathbb{R}_{xx}$ is defined in Eqn. (3.22).

3. ST MU Receiver

If all parameters for every user are known (or have been estimated), then Eqn. (3.19) can be rewritten as follows

$$\underline{x}[n] = \sum_{i=1}^{M}\left[\mathbb{G}_{i,\mathrm{prev}}, \mathbb{G}_i, \mathbb{G}_{i,\mathrm{next}}\right]\begin{bmatrix}\underline{b}_i[n-1]\\ \underline{b}_i[n]\\ \underline{b}_i[n+1]\end{bmatrix} + \underline{\mathrm{n}}[n] \tag{3.32}$$

$$= \mathbb{G}\underline{b}[n] + \underline{\mathrm{n}}[n] \quad \in \mathcal{C}^{2NN_c\times 1} \tag{3.33}$$

where

$$\mathbb{G} = \left[\mathbb{G}_{1,\mathrm{prev}}, \mathbb{G}_1, \mathbb{G}_{1,\mathrm{next}}, \cdots, \mathbb{G}_{M,\mathrm{prev}}, \mathbb{G}_M, \mathbb{G}_{M,\mathrm{next}}\right] \in \mathcal{C}^{2NN_c\times 3M\overline{N}} \tag{3.34}$$

$$\underline{b}\,[n] = \begin{bmatrix} \underline{b}_1\,[n-1] \\ \underline{b}_1\,[n] \\ \underline{b}_1\,[n+1] \\ \vdots \\ \underline{b}_M\,[n-1] \\ \underline{b}_M\,[n] \\ \underline{b}_M\,[n+1] \end{bmatrix} \in \mathcal{C}^{3M\overline{N}\times 1} \tag{3.35}$$

In this case, the ST weight matrix can be expressed as

$$\mathbb{W}_1 = \mathrm{col}_{\overline{N}+1:2\overline{N}} \left\{ \left[\mathbb{G}(\mathbb{G}^H\mathbb{G})^{-1} \right] \right\} \in \mathcal{C}^{2NN_c\times\overline{N}} \tag{3.36}$$

The formulation of the decorrelating receiver is to eliminate the MAI and ISI interferences, thus providing significant performance (e.g. SNIR and BER) improvement compared with SU receivers.

4. Subspace-based STAR Receivers

As discussed previously, the desired signal component, ISI and MAI components all lie in the same signal subspace. However, in order to suppress interferences from the received signals, the interference subspace spanned by ISI and MAI components should be identified and isolated from the overall signal subspace.

By applying $\mathbb{P}^{\perp}_{\text{unwanted}}$, the projection operator of the noise subspace, to $\underline{x}[n]$, the received vector-signal is projected on to the orthogonal complement subspace of unwanted signals. Thus based on Eqn. (3.20), it is clear that both MAI and ISI from the received signals can be successfully suppressed leaving only the transformed terms of desired signals and noise:

$$\mathbb{P}^{\perp}_{\text{unwanted}}\underline{x}[n] \approx \underbrace{\mathbb{P}^{\perp}_{\text{unwanted}}\mathbb{H}_1 \left(\underline{\beta}_1 \otimes \mathbb{I}_{\overline{N}} \right) \underline{b}_1\,[n]}_{\text{transformed desired signal}} + \underbrace{\mathbb{P}^{\perp}_{\text{unwanted}}\underline{\mathbf{n}}[n]}_{\text{transformed noise}} \tag{3.37}$$

Then, by pre-multiplying both sides of Eqn. (3.37) with

$$\left(\underline{\beta}_1^H \otimes \mathbb{I}_{\overline{N}}\right) \left(\mathbb{H}_1^H \mathbb{P}_{\text{unwanted}}^{\perp} \mathbb{H}_1\right)^{-1} \mathbb{H}_1^H \tag{3.38}$$

Eqn. (3.37) is further transformed to

$$\begin{aligned} & \left(\underline{\beta}_1^H \otimes \mathbb{I}_{\overline{N}}\right) \left(\mathbb{H}_1^H \mathbb{P}_{\text{unwanted}}^{\perp} \mathbb{H}_1\right)^{-1} \mathbb{H}_1^H \mathbb{P}_{\text{unwanted}}^{\perp} \underline{x}[n] && (3.39) \\ = & \left(\underline{\beta}_1^H \otimes \mathbb{I}_{\overline{N}}\right) \underbrace{\left(\mathbb{H}_1^H \mathbb{P}_{\text{unwanted}}^{\perp} \mathbb{H}_1\right)^{-1} \mathbb{H}_1^H \mathbb{P}_{\text{unwanted}}^{\perp} \mathbb{H}_1}_{=\mathbb{I}_{K_1}} \left(\underline{\beta}_1 \otimes \mathbb{I}_{\overline{N}}\right) \underline{b}_1[n] \\ & + \left(\underline{\beta}_1^H \otimes \mathbb{I}_{\overline{N}}\right) \left(\mathbb{H}_1^H \mathbb{P}_{\text{unwanted}}^{\perp} \mathbb{H}_1\right)^{-1} \mathbb{H}_1^H \mathbb{P}_{\text{unwanted}}^{\perp} \underline{\mathrm{n}}[n] && (3.40) \\ = & \left\|\underline{\beta}_1\right\|^2 \underline{b}_1[n] + \left(\underline{\beta}_1^H \otimes \mathbb{I}_{\overline{N}}\right) \left(\mathbb{H}_1^H \mathbb{P}_{\text{unwanted}}^{\perp} \mathbb{H}_1\right)^{-1} \mathbb{H}_1^H \mathbb{P}_{\text{unwanted}}^{\perp} \underline{\mathrm{n}}[n] \end{aligned}$$

$$(3.41)$$

Based on the above, the weight matrix $\mathbb{W}$ can be formed as follows[3]

$$\mathbb{W}_{\text{prop}} = \kappa_1 \mathbb{P}_{\text{unwanted}}^{\perp} \mathbb{H}_1 \left(\mathbb{H}_1^H \mathbb{P}_{\text{unwanted}}^{\perp} \mathbb{H}_1\right)^{-1} \left(\underline{\beta}_1 \otimes \mathbb{I}_{\overline{N}}\right) \tag{3.42}$$

where κ_i is the normalization factor.

Eqn. (3.42) assumes that $\mathbb{P}_{\text{unwanted}}^{\perp}$ can be formed/estimated. Here two approaches are presented for the estimation of $\mathbb{P}_{\text{unwanted}}^{\perp}$.

(a) If the receiver is capable of obtaining the channel parameters (including the spreading codes) of all the users, the multi-user (MU) complement projection operator $\mathbb{P}_{\text{unwanted}}^{\perp}$ can be constructed by

$$\mathbb{P}_{\text{unwanted}}^{\perp} = \mathbb{I}_{2NN_c} - \tilde{\mathbb{H}}_1 \left(\tilde{\mathbb{H}}_1^H \tilde{\mathbb{H}}_1\right)^{-1} \tilde{\mathbb{H}}_1^H \tag{3.43}$$

where

$$\tilde{\mathbb{H}}_1 = [\mathbb{H}_{1,\text{prev}}, \mathbb{H}_{1,\text{next}}, \mathbb{H}_{2,\text{prev}}, \mathbb{H}_2, \mathbb{H}_{2,\text{next}}, \cdots, \mathbb{H}_{M,\text{prev}}, \mathbb{H}_M, \mathbb{H}_{M,\text{next}}] \tag{3.44}$$

[3] This is a zero-forcing (ZF) type Receiver.

(b) If only the desired user's channel is known or has been estimated, then $\mathbb{R}_{\text{unwanted}}$ can be constructed by removing desired user's multipath component from $\mathbb{R}_{xx}$ as

$$\mathbb{R}_{\text{unwanted}} = \mathbb{R}_{\text{ISI}} + \mathbb{R}_{\text{MAI}} + \mathbb{R}_{\text{n}} \tag{3.45}$$

$$= \mathbb{R}_{xx} - \mathbb{H}_1 \left(\underline{\beta}_1 \otimes \mathbb{I}_{\overline{N}} \right) \left(\underline{\beta}_1^H \otimes \mathbb{I}_{\overline{N}} \right) \mathbb{H}_1^H \tag{3.46}$$

By performing the eigendecomposition of $\mathbb{R}_{\text{unwanted}}$, the matrix $\mathbb{E}_{\text{unwanted}}$ is formed, which has $(3M-1)\,\overline{N}$ signal eigenvectors as its columns, and is a basis for the unwanted signal subspace $\mathcal{L}[\mathbb{E}_{\text{unwanted}}]$. Having found the unwanted signal subspace, the single-user (SU) complement projection operator can be derived by

$$\mathbb{P}_{\text{unwanted}}^{\perp} = \mathbb{I}_{2NN_c} - \mathbb{E}_{\text{unwanted}} \left(\mathbb{E}_{\text{unwanted}}^H \mathbb{E}_{\text{unwanted}}^{-1} \right)^{-1} \mathbb{E}_{\text{unwanted}}^H \tag{3.47}$$

$$= \mathbb{I}_{2NN_c} - \mathbb{E}_{\text{unwanted}} \mathbb{E}_{\text{unwanted}}^H \tag{3.48}$$

In the following context of this thesis, the proposed space-time weight matrix (3.42) in connection with the MU complement projection operator Eqn. (3.43) will be called ST-1 receiver. The receiver based on (3.42) with the SU complement projection operator Eqn. (3.48) will be called ST-2 receiver. With these two proposed approaches, the weight matrix $\mathbb{W}_1$ is made orthogonal to the estimated unwanted-signal subspace containing the contributions of ISI and MAI. The power of the residual interference is determined by the angle between the estimated unwanted-signal subspace and the actual MAI+ISI subspaces.

If all required channel parameters have been successfully estimated (see Section 3.4 for detail), the MMSE, ST-1 and ST-2 weight matrices can be constructed with Eqn. (3.31) - (3.42). An example of the decision variables for one realization at the output of MMSE, ST-1 and ST-2 receivers is shown in Figure 3.5. Note

that to take into account the near-far problem of CDMA system, the Interference-to-Noise Ration (ISR) is assumed 20 dB, i.e.

$$\mathrm{ISR}_i \triangleq 10\log_{10}\left(\frac{\sum_{k=1}^{K_i}|\beta_{ik}|^2}{\sum_{k=1}^{K_1}|\beta_{1k}|^2}\right) = 20 \text{ dB}, \quad \text{for } \forall i \neq 1 \tag{3.49}$$

With the same setting but QPSK modulation, the decision variables at the output of MMSE, ST-1 and ST-2 receivers can be found in the Appendix 3.A.

In Figure 3.6 and 3.7, the Bit-Error-Rate (BER) performance of various receivers is evaluated for $\overline{N} = 2$ transmitter antennas and $N = 2$ and 4 receiver antennas. There are 10 users, each with 3 paths. The simulation is executed for 10000 bursts of 200 symbols each. The results demonstrate that the two proposed ST receivers outperform RAKE and MMSE receivers. The BER performance of all ST receivers improves as the number of receive antennas increases from 2 to 4. It is important to point out that because of near-far effect, the scenario considered here is MAI-dominant, which explains why the performance of MMSE or RAKE receivers do not improve by increasing the SNR.

The performance of the receivers is expected to decrease with the increase of the number of users in the CDMA system and simulation results presented in Figure 3.8 show such effect. For a (2,3) CDMA-MIMO channel with 2 multipaths per user. The performance improvement of the proposed ST receivers is clearly shown in Figure 3.8.

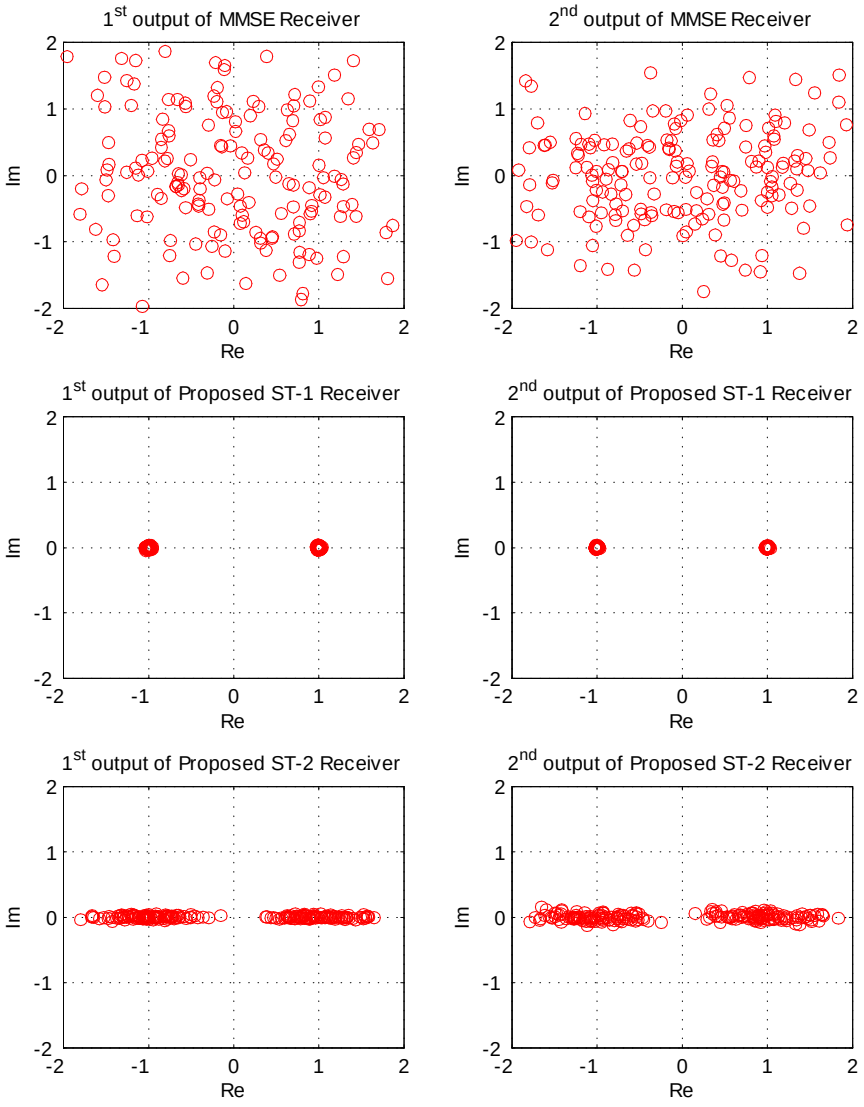


Figure 3.5: Diagram of decision variables at the output of different receivers of the MIMO-CDMA systems with BPSK modulation. for a single run of 200 data symbols. The subspace-based ST receivers show significant near-far resistant ability.

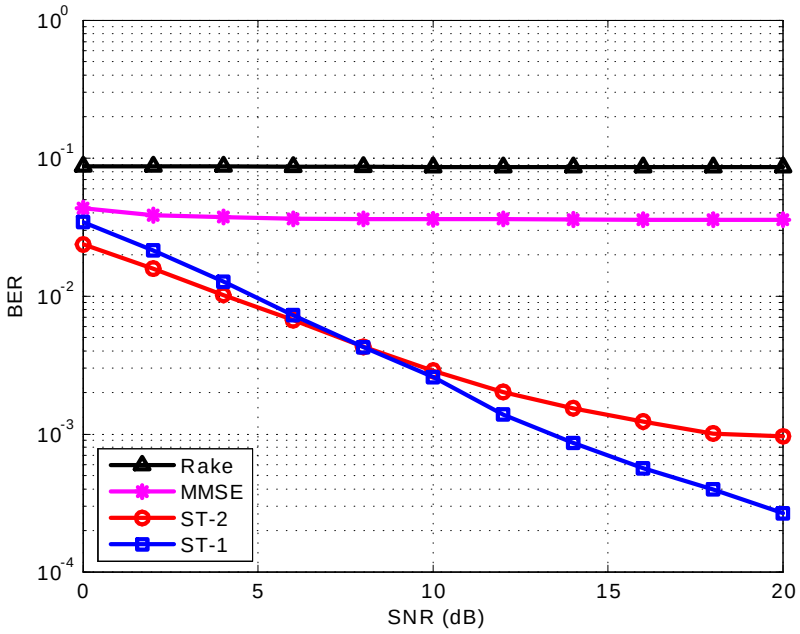


Figure 3.6: BER performance of different receivers in a MIMO-CDMA system with 10 users, each with 3 multipaths. $\overline{N} = 2$ and $N = 2$, with half-wavelength spacing.

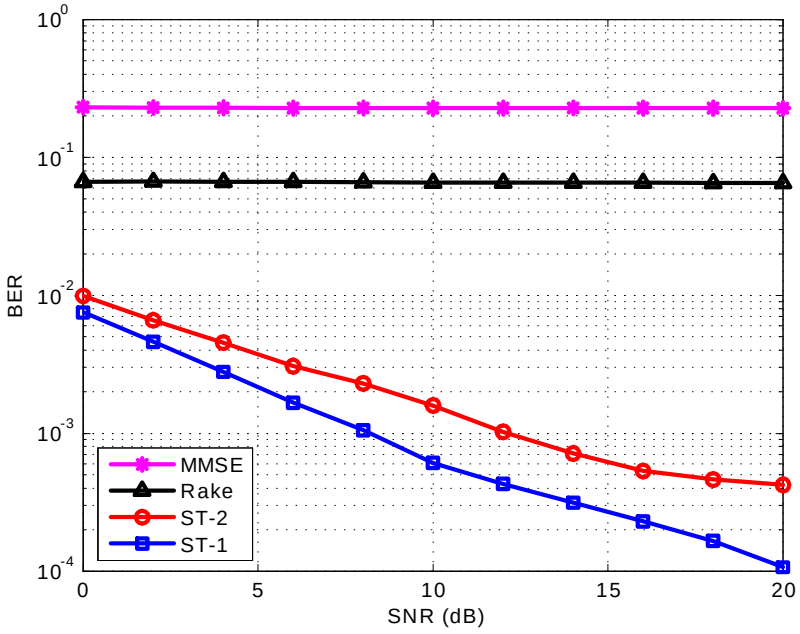


Figure 3.7: BER performance of different receivers in a MIMO-CDMA system with 10 users, each with 3 multipaths. $\overline{N} = 2$ and $N = 4$. All arrays are ULA with half-wavelength spacing.

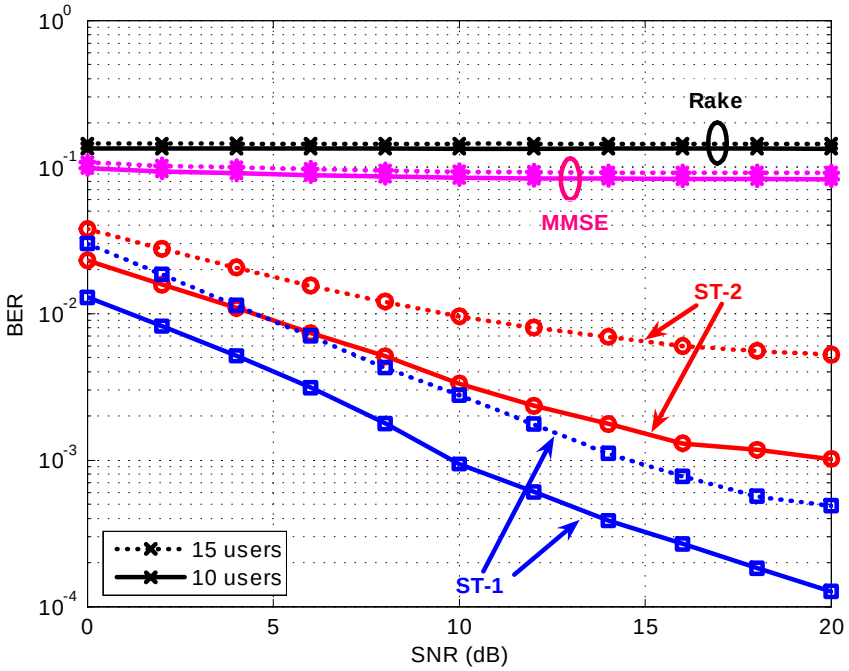


Figure 3.8: BER performance of MIMO-CDMA system of 10 and 15 users, using 2-element ULA (half-wavelength spacing) at transmitters, 3-element ULA (half-wavelength spacing) at receivers, and assuming perfect channel estimation.

3.4 Channel Estimation

So far, it is assumed that all required channel parameters have been successfully estimated. Recalling Eqn. (3.14), these parameters are DOA, TOA, DOD and path coefficients. In this section, the joint DOA-TOA estimation and the DOD estimation approaches are addressed. Once DOAs and TOAs of the channel have been identified, the path coefficient vector $\underline{\beta}_1 = \left[\beta_{11}, \beta_{12}, \cdots, \beta_{1K_1}\right]^T$ can be estimated using, for instance, the extension of [51] or [52].

3.4.1 Blind STAR Estimation of DOA and TOA

By observing the covariance matrix $\mathbb{R}_{xx}$ of the signals received by base station given in Eqn. (3.21), the observation complex space of dimensionality $2NN_c$ (dimensionality of $\mathbb{R}_{xx}$) can be partitioned into two complementary subspaces:

1. The "overall signal subspace" spanned by the invariant MIMO-STAR manifold matrices of the receive array associated with all the paths of all the users, which includes the effects of
   (a) the desired (1^{st}) user's signal (MIMO-STAR matrices of $\mathbb{H}_1$),
   (b) ISI (MIMO-STAR matrices of $\mathbb{H}_{1,\text{prev}}$ and $\mathbb{H}_{1,\text{next}}$) and
   (c) MAI (MIMO-STAR matrices of $\mathbb{H}_{\xi,\text{prev}}$, $\mathbb{H}_{\xi}$ and $\mathbb{H}_{\xi,\text{next}}$, $\forall \xi \neq 1$).
2. The "noise" subspace, which is orthogonal to the overall signal subspace.

This implies that for the estimation be validated, the dimensionality of this subspace (i.e. the total number of paths from all users)

$$\mathcal{K} = \sum_{i=1}^{M} K_i \tag{3.50}$$

need to be less than $2\mathcal{N}_c N$, the total dimensionality of $\mathbb{R}_{xx}$, i.e. $\mathcal{K} < 2\mathcal{N}_c N$.

However, the paths of the desired user, in addition to belonging to the overall signal subspace, also belong to another nonlinear subspace (manifold of all MIMO-STAR matrices) defined as follows

$$\mathcal{M} = \left\{ \left(\underline{S}(\theta)\overline{\underline{S}}^{H}(\overline{\theta}) \right) \otimes (\mathbb{J}^{l}\underline{\mathfrak{c}}_{1}) \in \mathcal{C}^{2\mathcal{N}_{c}N},\ \forall \overline{\theta} \in \Omega_{\overline{\theta}},\ \forall \theta \in \Omega_{\theta},\ l \in \Omega_{l} \right\} \tag{3.51}$$

where

$$\Omega_{\overline{\theta}} = [0, 180) \tag{3.52}$$

$$\Omega_{\theta} = [0, 180) \tag{3.53}$$

and

$$\Omega_{l} = [0, \mathcal{N}_{c} - 1] \tag{3.54}$$

are the parameter spaces of DOA θ and TOA l. Therefore, by searching this manifold for MIMO-STAR matrices that are orthogonal to the noise subspace, only the desired signal components are obtained.

The distance between a MIMO-STAR matrix $\left(\underline{S}(\theta)\overline{\underline{S}}^{H}(\overline{\theta}) \right) \otimes (\mathbb{J}^{l}\underline{\mathfrak{c}}_{1})$ and the noise subspace $\mathcal{L}[\mathbb{E}_{\mathrm{n}}]$ can be expressed as

$$\xi(\theta, \overline{\theta}, l) = \mathrm{Tr}\left\{ \left[\left(\underline{S}(\theta)\overline{\underline{S}}^{H}(\overline{\theta}) \right) \otimes \left(\mathbb{J}^{l}\underline{\mathfrak{c}}_{1} \right) \right]^{H} \mathbb{P}_{\mathbb{E}_{\mathrm{n}}} \left[\left(\underline{S}(\theta)\overline{\underline{S}}^{H}(\overline{\theta}) \right) \otimes \left(\mathbb{J}^{l}\underline{\mathfrak{c}}_{1} \right) \right] \right\} \tag{3.55}$$

where $\mathbb{P}_{\mathbb{E}_{\mathrm{n}}}$ is the projection operator of the noise subspace $\mathcal{L}[\mathbb{E}_{\mathrm{n}}]$ and can be obtained by the eigendecomposition of covariance matrix $\mathbb{R}_{xx}$ and

$$\mathbb{P}_{\mathbb{E}_{\mathrm{n}}} = \mathbb{E}_{\mathrm{n}}(\mathbb{E}_{\mathrm{n}}^{H}\mathbb{E}_{\mathrm{n}})^{-1}\mathbb{E}_{\mathrm{n}}^{H} = \mathbb{E}_{\mathrm{n}}\mathbb{E}_{\mathrm{n}}^{H}. \tag{3.56}$$

Theoretically, the dimension of the noise subspace $\mathbb{E}_{\mathrm{n}}$ is specified by the size of covariance matrix minus the number of DOA, which can be decided by counting the number of bigger eigenvalues of $\mathbb{R}_{xx}$. However, for a finite observation interval, direct counting may not be accurate and the number of DOA is estimated using Akaike Information Criterion (AIC), Minimum Description Length (MDL) (see [49] for detail).

Note that by property of trace $\mathrm{Tr}\left(\mathbb{AB}\right) = \mathrm{Tr}\left(\mathbb{BA}\right)$, Eqn. (3.55) can be rewritten as follows

$$\begin{aligned} & \xi(\theta, \overline{\theta}, l) \\ = \; & \mathrm{Tr}\left\{ \mathbb{E}_{\mathrm{n}}^{H} \left[\left(\underline{S}(\theta) \overline{\underline{S}}^{H}(\overline{\theta}) \right) \otimes \left(\mathbb{J}^{l} \underline{\mathfrak{c}}_1 \right) \right] \left[\left(\underline{S}(\theta) \overline{\underline{S}}^{H}(\overline{\theta}) \right) \otimes \left(\mathbb{J}^{l} \underline{\mathfrak{c}}_1 \right) \right]^{H} \mathbb{E}_{\mathrm{n}} \right\} \end{aligned} \tag{3.57}$$

Furthermore, using the property of Kronecker product

$$\left(\mathbb{AB}\right) \otimes \left(\mathbb{CD}\right) = \left(\mathbb{A} \otimes \mathbb{C}\right) \left(\mathbb{B} \otimes \mathbb{D}\right) \tag{3.58}$$

Eqn. (3.57) can further simplified as follows

$$\xi(\theta, \overline{\theta}, l) \tag{3.59}$$

$$= \mathrm{Tr}\left\{ \mathbb{E}_{\mathrm{n}}^{H} \left[\left(\underline{S}(\theta) \; \underbrace{\overline{\underline{S}}^{H}(\overline{\theta}) \overline{\underline{S}}(\overline{\theta})}_{= \overline{N} \text{ by Eqn. (2.24)}} \; \underline{S}^{H}(\theta) \right) \otimes \left(\left(\mathbb{J}^{l_{ij}} \underline{\mathfrak{c}}_i \right) \left(\mathbb{J}^{l_{ij}} \underline{\mathfrak{c}}_i \right)^{H} \right) \right] \mathbb{E}_{\mathrm{n}} \right\} \tag{3.60}$$

$$= \mathrm{constant} \underbrace{\left[\underline{S}(\theta) \otimes \left(\mathbb{J}^{l} \underline{\mathfrak{c}}_1 \right) \right]^{H} \mathbb{P}_{\mathbb{E}_{\mathrm{n}}} \left[\underline{S}(\theta) \otimes \left(\mathbb{J}^{l} \underline{\mathfrak{c}}_1 \right) \right]}_{\triangleq \; \xi'(\theta, l)} \tag{3.61}$$

where means $\xi(\theta, \overline{\theta}, l)$ is invariant for different $\overline{\theta}$. So, at the receiver, the intersection of the MIMO-STAR manifold $\mathcal{M}$ with the "overall signal subspace" will only provide the desired user's receiver-side parameters, DOA and TOA. This intersection can be found from the following MUSIC-type optimization problem

$$\left(\underline{\theta}_1, \underline{l}_1\right) = \arg \min_{\theta, l} \xi'(\theta, l) \tag{3.62}$$

Consider a 3-user MIMO-CDMA system with the transmitters and receiver employing respectively 5 and 3 element uniform linear array (ULA) of half-wavelength inter-element spacing. Each user is assigned an unique Gold sequence of length $\mathcal{N}_c = 31$ with rectangular chip pulse-shaping. The receivers operate in the presence of multipath effects from other users (MAI), as well as the ISI introduced in a frequency-selective fading channel.

Assume 10 multipaths for 1st (desired) user, 8 multipaths for 2nd user and 6 multipaths for 3rd user and that the desired user has an input signal-to-noise-ratio (SNR) of 20 dB. To take into account the near-far problem, the rest of the interferers are constituted with the Interference-to-Noise Ratio (ISR) of 20 dB. The multipath parameters of the 3 users are listed in Table 3.1.

By partitioning the 5-element Rx array into 2 overlapping 4-element subarrays for spatial smoothing, it is seen from Figure 3.9 that all the 10 multipaths, associated with the two transmitting elements of the desired user, can be identified/estimated successfully using the proposed algorithm. Notice that the algorithm can still operate even when the desired user's paths are arriving from the same direction (co-directional) or arriving at the same time (co-delay). The former case cannot be resolved for a general array geometry but for a uniform linear array where spatial smoothing can be overlaid on top of $\mathbb{R}_{xx}$ to form the smoothed covariance matrix $\mathbb{R}_{\text{smooth}}$ (see [50] for detail).

1st User (desired)					2nd User					3rd User				
Path	$\overline{\theta}_{1k}$	θ_{1k}	l_{1k}	β_{1k}	Path	$\overline{\theta}_{2k}$	θ_{2k}	l_{2k}	β_{2k}	Path	$\overline{\theta}_{3k}$	θ_{3k}	l_{3k}	β_{3k}
1	30°	50°	$2T_c$	$-0.081+0.197i$	1	12°	100°	$5T_c$	$-0.969+3.836i$	1	42°	50°	$3T_c$	$-1.362+5.21i$
2	38°	119°	$4T_c$	$-0.122+0.01i$	2	58°	60°	$6T_c$	$-1.187-2.945i$	2	13°	10°	$4T_c$	$-1.067+1.267i$
3	24°	100°	$5T_c$	$-0.009-0.184i$	3	84°	27°	$12T_c$	$3.799-0.501i$	3	55°	129°	$7T_c$	$-5.234+2.883i$
4	55°	20°	$10T_c$	$-0.043-0.022i$	4	45°	85°	$15T_c$	$0.189-0.467i$	4	84°	15°	$8T_c$	$-0.845+3.396i$
5	92°	65°	$10T_c$	$-0.234-0.489i$	5	32°	45°	$18T_c$	$-2.536+0.721i$	5	14°	25°	$11T_c$	$0.428+3.396i$
6	61°	20°	$15T_c$	$0.315+0.264i$	6	21°	30°	$24T_c$	$-2.638-1.343i$	6	39°	70°	$12T_c$	$1.136-3.580i$
7	20°	80°	$19T_c$	$0.107-0.239i$	7	28°	118°	$27T_c$	$4.072-2.293i$					
8	18°	90°	$23T_c$	$0.312-0.168i$	8	108°	105°	$29T_c$	$4.545-1.048i$					
9	36°	70°	$24T_c$	$-0.121-0.327i$										
10	10°	40°	$28T_c$	$-0.273-0.222i$										
Note: (1) The first user is assumed to be the desired user with $\mathrm{ISR}_2 = \mathrm{ISR}_3 = 20$ dB and SNR = 20 dB;														
(2) Path delays are assumed multiple of T_c. Delays in fractional T_c are absorbed by the fading coefficients.														

Table 3.1: User's parameters for DOA and TOA estimation example

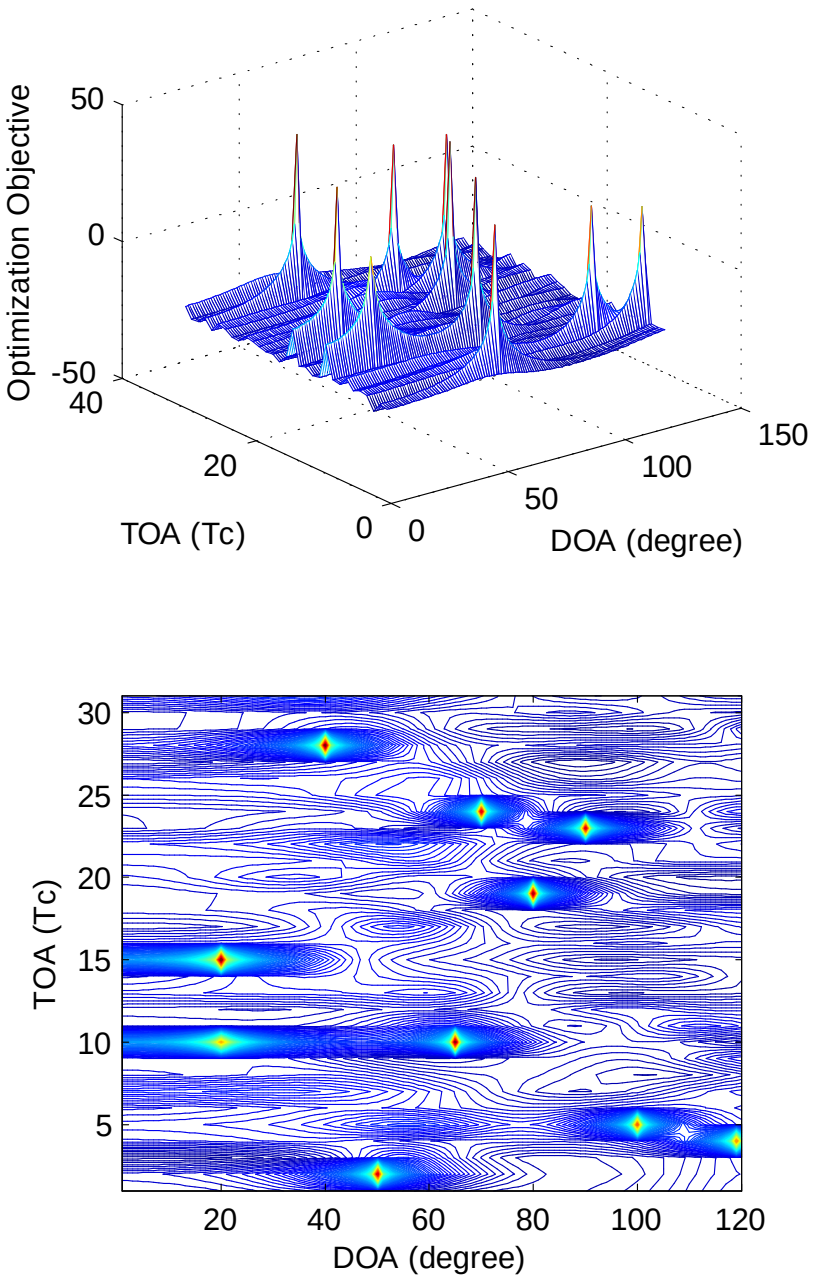


Figure 3.9: Joint angle (DOA) and delay (TOA) estimation of all the multipath components of the desired user based on Eqn. (3.62) as shown in (a) 3D surface plot and (b) 2D contour plot of (a).

3.4.2 Cooperative Beamforming: Estimation of DODs

In this subsection, assuming the existence of a feedback channel, the DODs are estimated by a cooperative beamforming approach which is illustrated by a representative example of 3-user system whose channel parameters are specified in Table 3.2. Each UE's Tx employs an antenna array of 3 elements and the Rx of the base station is equipped with an antenna array of 5 elements, as shown in Figure 3.10 (a).

Algorithm 3.1: Cooperative Beamforming

1. With default Tx beamforming vector $\underline{\overline{w}}_1 = \underline{1}_{\overline{N}}$, DOA/TOA of the various paths are estimated using an approach similar to sub-section 3.4.1.

2. The Rx steers one main lobe per estimated DOA. This is shown in Figure 3.10 (b).

3. The Tx, by using the transmit array manifold vector as the weight vector, i.e.

$$\underline{\overline{w}}_1\left(\overline{\theta}\right) = \underline{\overline{S}}_1\left(\overline{\theta}_{\text{rotate}}\right) \tag{3.63}$$

steers the main lobe towards direction $\overline{\theta}_{\text{rotate}}$ which changes with a predefined manner known to the Rx from 0° to 360° (as shown in Figure 3.10 (b)). The Rx using its knowledge of the rotation pattern of the Tx, estimates the DOD (as shown in Figure 3.11) for all paths. At the output of the receive beamformers, the gain patterns can be expressed as a function of the rotated direction of the transmit beam, $\overline{\theta}_{\text{rotate}}$, denoted as $\underline{G}(\overline{\theta}_{\text{rotate}})$. When $\overline{\theta}_{\text{rotate}}$ equals the DOD of, for instance, the j^{th} path, the j^{th} element in $\underline{G}(\overline{\theta}_{\text{rotate}})$ will get a maximum value. For the example specifies by Table 3.2, Figure 3.11 shows clearly that peaks can be found in rotating direction $\overline{\theta}_{\text{rotate}}$ where paths do exist (i.e. $\overline{\theta}_{11} = 60°$ and $\overline{\theta}_{12} = 105°$).

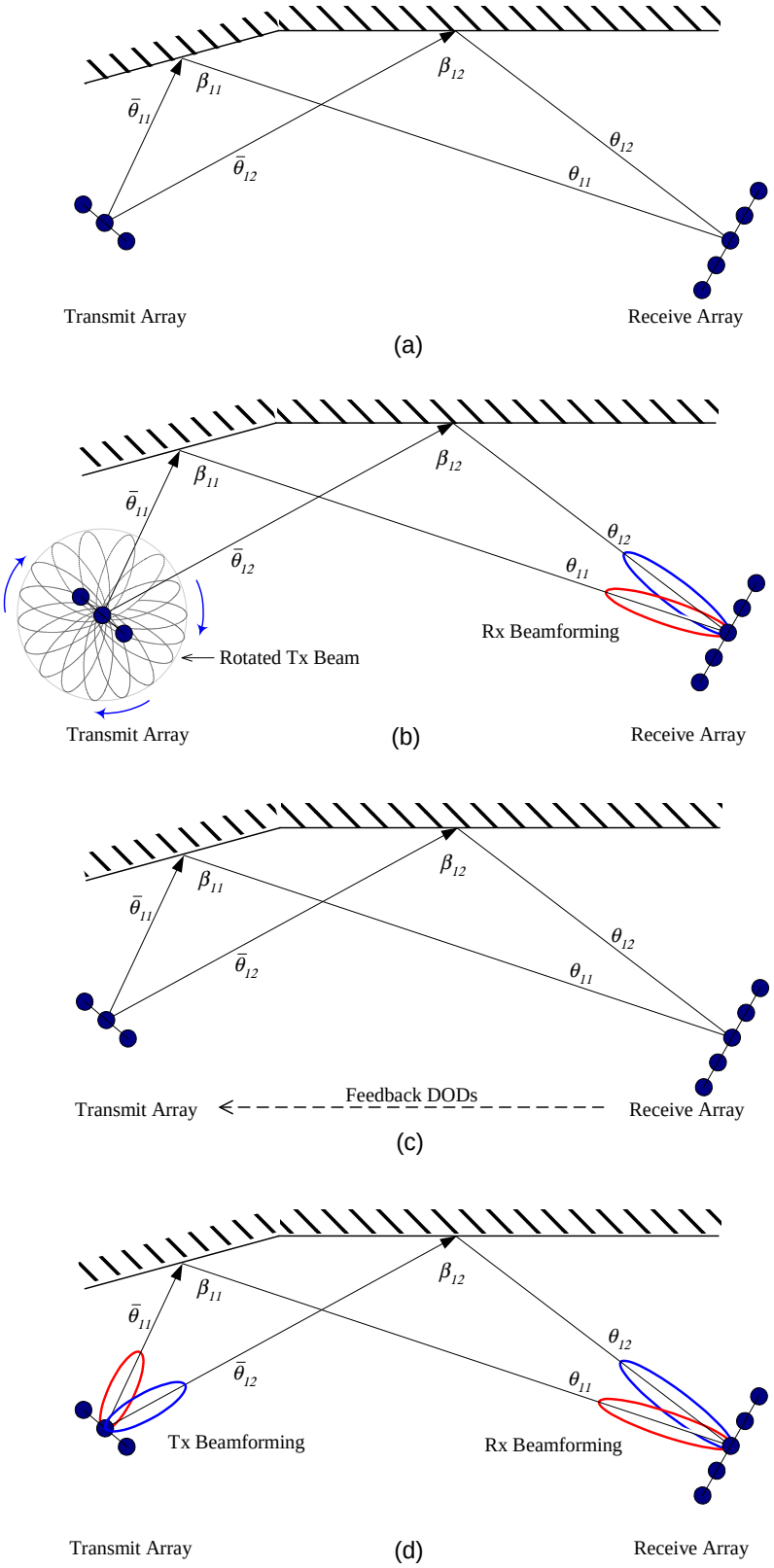


Figure 3.10: An example of cooperative beamforming approach: (a) DOA/TOA estimation; (b) rotated Tx beamforming while steering mainlobes towards DOA at Rx; (c) DOD information feedback; (d) Tx-Rx beamforming.

Table 3.2: Channel parameters for DOD estimation example.

User	Path	DOD	DOA	TOA (T_c)	Path Coefficient
1^{st}	1	60°	77°	8	$0.5798 - 0.0645i$
	2	105°	135°	12	$0.3883 - 0.7134i$
2^{nd}	1	55°	30°	10	$0.7100 + 0.2550i$
	2	97°	87°	25	$-0.12216 + 0.6449i$
3^{rd}	1	68°	34°	15	$0.6002 - 0.1237i$
	2	143°	73°	4	$0.5746 + 0.5425i$

4. The Rx sends the maximum points (estimates of DOD) to the Tx using a feedback channel.

5. Tx-Rx beamforming can be used to improve, for instance, the SNR of the received signal, as shown in Figure 3.10 (d).

Note that this algorithm is triggered when, for example, the received SNR is below a predefined threshold.

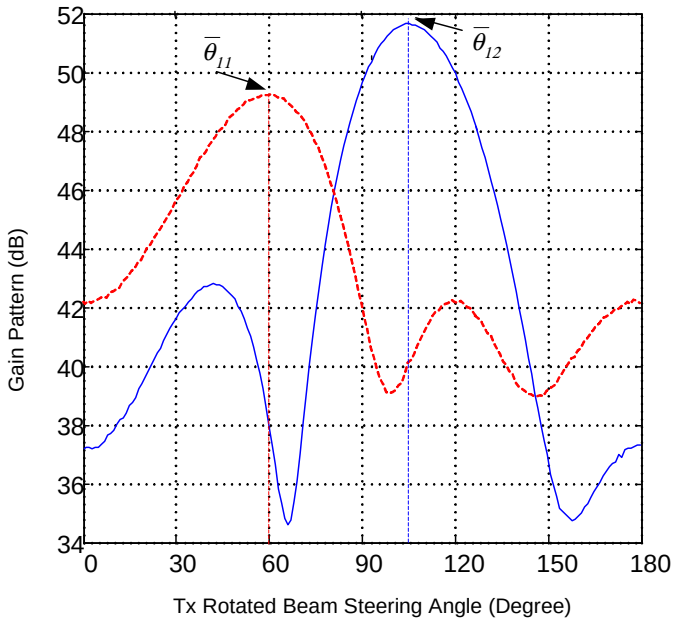


Figure 3.11: The gain pattern at the output of the receiver array beamformers as a function of the direction of the transmit rotating beam.

3.5 Summary

In this chapter, from the viewpoint of array processing, the uplink of a multiuser asynchronous MIMO-CDMA wireless communication system operating in frequency selective fading channel has been studied. The concept of STAR manifold vector associated with only the receiver of BS has been extended to MIMO-STAR manifold matrix associated with both the transmitter of UEs and the receiver of BS. Given the complete estimation of the multipath parameters, spatio-temporal type of conventional single-user and multi-user linear receivers have been developed. Furthermore, two linear subspace-based space-time receivers have been proposed, both single user ST-2 and multi-user ST-1, by transforming the received signal-vector using the complement projection operator of the noise subspace. Simulation results show that, the proposed subspace-based ST receivers have shown great advantage compared with MMSE or RAKE receivers, e.g., on handing near-far effect. In general, ST-2 receiver performs better than ST-1 receiver since the MU receiver is supported to know the spreading sequences and channel parameters of all the users while the SU receiver requires only that of the desired user. A blind subspace-based joint DOA-TOA estimation algorithm is proposed by searching the MIMO-STAR manifold matrices that are orthogonal to the noise subspace. Furthermore, with the cooperation of Tx and Rx, the Tx beam rotation based DOD estimation scheme have been developed. A transmit beamforming can then be implemented to increase the receiver-side signal-to-noise ratio.

Appendix 3.A Decision variables of different space-time receivers for MIMO-CDMA with QPSK modulation

Consider a 3-user MIMO-CDMA systems with the transmitters and receiver employing respectively 5 and 3 element uniform linear array (ULA) of half-wavelength inter-element spacing. Each user is assigned an unique Gold sequence of length $\mathcal{N}_c = 31$ with rectangular chip pulse-shaping. The receivers operate in the presence of multipath effects from other users (MAI), as well as the ISI introduced in a frequency-selective fading channel. The multipath parameters of the 3 users are listed in Table 3.1. Assuming QPSK modulation. The decision variables at the output of MMSE, ST-1 and ST-2 receivers are plotted in Figure 3.12.

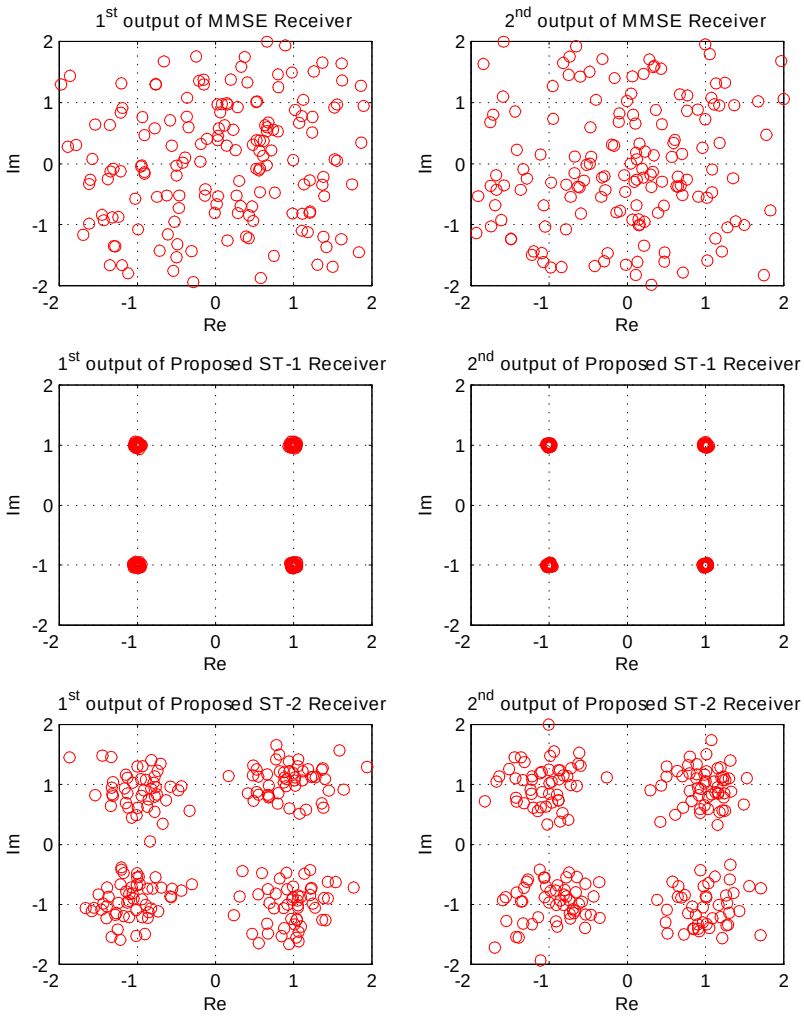


Figure 3.12: Diagram of decision variables at the output of different receivers of the MIMO-CDMA systems with QPSK modulation. for a single run of 200 data symbols. The subspace-based ST receivers show significant near-far resistant ability.

Chapter 4

Precoder and Decoder Optimization in Arrayed MIMO-CDMA Downlink Systems

4.1 Introduction

The explosive demand for wireless internet and multimedia services requires more efficient techniques to be employed to enable high data rate downlink transmission in the next generation wireless communication systems. MIMO systems using antenna arrays at both receiver and transmitter have shown great potential to provide high bandwidth efficiency [12] [11] [2].

In a single-stream multiple-access environment, numerous receiver and/or transmitter beamforming schemes have been developed to efficiently enhance the signals of the desired user while minimizing the effects of multi-access-interference (MAI) from other users and inter-symbol-interference (ISI) caused by frequency-

selective channel [53]-[56].

Recently, the receiver and transmitter optimization in the multiple-stream multiple-access environment has received widespread interest. A generalized framework has been introduced in [57] embracing the most reasonable optimization criteria for multicarrier MIMO design. One of the most popular optimization methods is zero-forcing approach [54][58], which normally requires the number of the transmit antennas to be larger than the sum of the number of receive antennas. Another category of MIMO system design is interference balancing [56]-[59], which normally uses generalized eigendecomposition to obtain suboptimal solutions. The optimal transmit power allocation is carried out separately using, e.g. water-filling method [58].

Most of the above mentioned research assumes frequency-flat channels, and little spatial temporal information of the channel is used to improve the system performance. To fill the gap, investigation of the precoder/decoder optimization schemes in the MIMO-CDMA systems in multipath channels is needed.

In this chapter, the problem under consideration is joint precoding-decoding optimization, with different power allocation schemes, in the downlink MIMO-CDMA systems over multipath fading channels. The study will be based on MIMO-STAR manifold concept, which has been developed in Chapter 3 to conduct blind superresolution channel estimation and multiple-access interference cancellation. The downlink multiuser arrayed MIMO-CDMA system is firstly modelled in Section 4.2. In Section 4.3, different optimization objectives are specified and a criterion on optimal multiplexing order is derived. In Section 4.4, iterative algorithms are proposed for joint precoder/decoder optimization based on the overall MSE criterion with different transmit power allocation schemes. Two close-form algorithms are derived in Section 4.5 to maximize the signal-

to-noise-plus-interference ratio (SNIR) and minimize the transmit power while satisfying predefined symbol error rate (SER) requirements. In Section 4.6, numerical simulations are presented and the paper is concluded in Section 4.7.

Some material in this chapter has been published in [61].

4.2 Channel Modelling

Consider the downlink of an M-user MIMO-CDMA wireless communication system operating in the multipath propagation environment. The receiver of each mobile station employs an array of N antennas whereas the transmitter of base station is equipped with an array of $\overline{N}$ antennas. Remember that a symbol with a 'bar' at the top will denote a transmitter's parameter. It is assumed that the channel is frequency-selective with a delay spread less than one data symbol period T_{cs}.

With reference to Figure 4.1, using a serial-to-parrallel (S/P) processor, the data sequence of the i^{th} user is transformed to a sequence of data vectors of $N_i^{(s)}$ elements, denoted by $\underline{b}_i[n] \in \mathcal{C}^{N_i^{(s)}\times 1}$. The data vectors $\underline{b}_i[n]$ of the i^{th} user are then spread with a unique spreading code $[\alpha_i[k] = \pm 1, k = 1, \cdots, N_c - 1]$ of period N_c and precoded using a precoding matrix $\overline{\mathbb{W}}_i$ before transmission. The overall baseband transmitted signal-vector associated with all M users is given by

$$\begin{aligned} \underline{m}(t) &= \sum_{i=1}^{M} \overline{\mathbb{W}}_i \sum_{n=-\infty}^{\infty} \underline{b}_i[n]\, c_{PN,i}(t - nT_{cs}) \\ & nT_{cs} \le t \le nT_{cs} \end{aligned} \tag{4.1}$$

where T_{cs} and T_c are respectively the data symbol period and the chip period, and $c_{PN,i}(t - nT_{cs})$ has been defined in Eqn. (3.1).

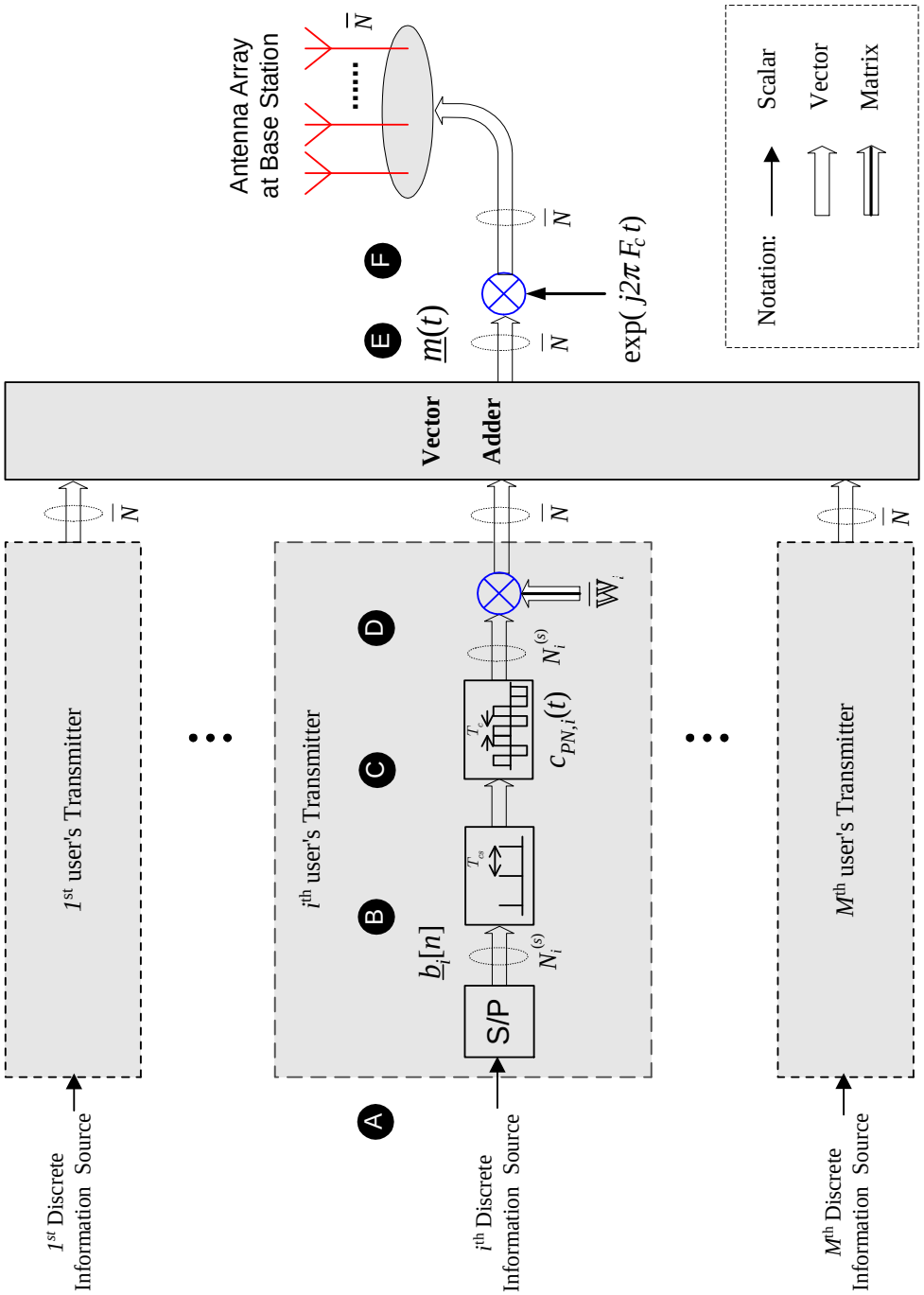


Figure 4.1: System architecture of the transmitter of BS in arrayed MIMO-CDMA downlink communication systems.

Let us assume plane-wave propagation with the transmitted signal arriving at the i^{th} receiver via K_i paths (multipath). Furthermore, consider that the j^{th} path of the i^{th} user's direction of departure (DOD) and direction of arrival (DOA) are denoted as follows:

- DOD: (azimuth, elevation) = $\left(\overline{\theta}_{ij}, \overline{\phi}_{ij}\right)$
- DOA: (azimuth, elevation) = $\left(\theta_{ij}, \phi_{ij}\right)$

In a similar fashion to Figure 3.2, the channel model for the downlink MIMO-CDMA multipath channel is shown in Figure 4.2, where the received complex baseband signal-vector at the antenna array of the receiver (point I) can be expressed explicitly as

$$\underline{x}_i(t) = \sum_{j=1}^{K_i} \beta_{ij} \underline{S}_{ij} \overline{\underline{S}}_{ij}^H \underline{m}(t - \tau_{ij}) + \underline{\mathrm{n}}_i(t) \tag{4.2}$$

where β_{ij} and τ_{ij} represent the fading coefficient and the delay of the j^{th} path of the i^{th} user, and $\underline{\mathrm{n}}_i(t)$ denotes the complex white Gaussian noise vector with zero mean and covariance matrix $\sigma^2 \mathbb{I}_N$. The vectors $\underline{S}_{ij}$ and $\overline{\underline{S}}_{ij}$ represent the array manifold vectors of the receiver and transmitter respectively associated with the j^{th} path of the i^{th} user.

Similar with the procedure described in Chapter 3, at the output of the receiver antenna array, the baseband received signal-vector $\underline{x}_i(t)$ is initially sampled with a period $T_s = T_c$, and then passed through a bank of N tapped-delay lines (TDL) (see [60] for more details). The contents of the bank of N TDLs, each of length $2N_c$, are concatenated to obtain the vector

$$\underline{x}_i[n] = \begin{bmatrix} \underline{x}_{i,1}[n] \\ \vdots \\ \underline{x}_{i,N}[n] \end{bmatrix} \quad \in \mathcal{C}^{2NN_c \times 1} \tag{4.3}$$

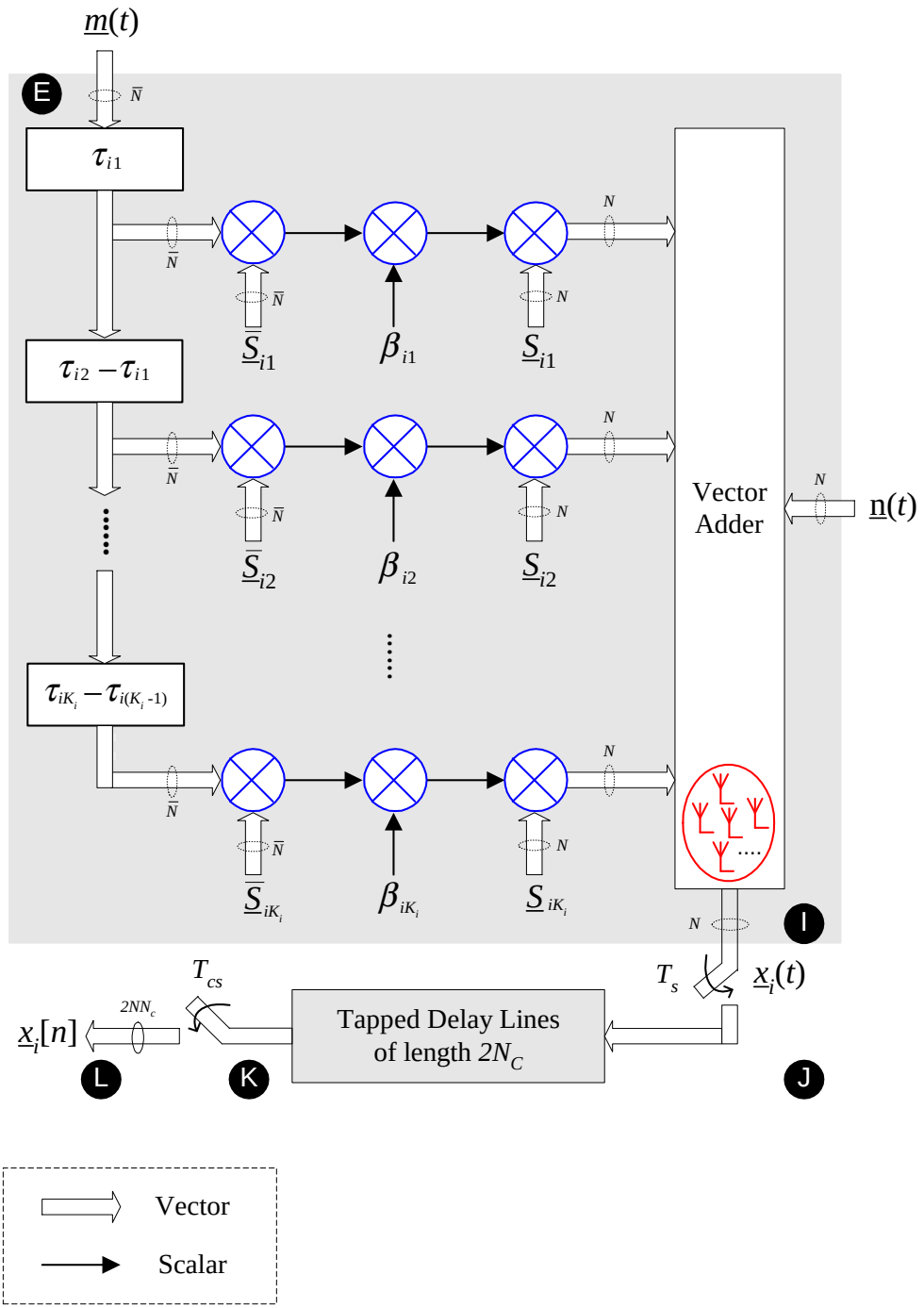


Figure 4.2: Downlink arrayed MIMO frequency selective channel of the i^{th} user.

where $\underline{x}_{i,k}[n] \in \mathcal{C}^{2N_c \times 1}$, $k = 1, \cdots N$, represents the contents of the TDL at i^{th} receiver's k^{th} antenna associated with the n^{th} data-symbol period. Again, to model the j^{th} path arriving at the i^{th} receiver with respect to the transmitted signal of the ξ^{th} user, the MIMO-STAR manifold matrix introduced in previous chapter is extended to

$$\left(\underline{S}_{ij}\overline{\underline{S}}_{ij}^{H}\right) \otimes \left(\mathbb{J}^{l_{ij}}\underline{\mathfrak{c}}_{\xi}\right) \quad \in \mathcal{C}^{2NN_c \times \overline{N}} \tag{4.4}$$

where $\underline{\mathfrak{c}}_{\xi} \in \mathcal{C}^{2N_c \times 1}$ is the ξ^{th} user's spreading code sequence padded with zeros of length N_c defined in Eqn. (3.12), and the matrix $\mathbb{J}$ (or $\mathbb{J}^T$) is a $2N_c \times 2N_c$ time down-shift (or up-shift) operator defined in Eqn. (3.11). The sampled baseband signal-vector $\underline{x}_i[n]$ in Eqn. (4.3) can be rewritten as

$$\underline{x}_i[n] = \sum_{\xi=1}^{M} \left[\mathbb{G}_{i,\xi}^{(\text{prev})}, \mathbb{G}_{i,\xi}, \mathbb{G}_{i,\xi}^{(\text{next})}\right] \left(\mathbb{I}_3 \otimes \overline{\mathbb{W}}_{\xi}\right) \begin{bmatrix} \underline{b}_{\xi}[n-1] \\ \underline{b}_{\xi}[n] \\ \underline{b}_{\xi}[n+1] \end{bmatrix} + \underline{\mathrm{n}}_i[n] \tag{4.5}$$

where $\underline{\mathrm{n}}_i[n] \in \mathcal{C}^{2NN_c \times 1}$ denotes the sampled noise vector during the n^{th} interval and

$$\mathbb{G}_{i,\xi} = \mathbb{H}_{i,\xi}\left(\underline{\beta}_i \otimes \mathbb{I}_{\overline{N}}\right) \quad \in \mathcal{C}^{2NN_c \times \overline{N}} \tag{4.6}$$

$$\mathbb{G}_{i,\xi}^{(\text{prev})} = \left(\mathbb{I}_N \otimes \left(\mathbb{J}^T\right)^{N_c}\right) \mathbb{H}_{i,\xi}\left(\underline{\beta}_i \otimes \mathbb{I}_{\overline{N}}\right) \quad \in \mathcal{C}^{2NN_c \times \overline{N}} \tag{4.7}$$

$$\mathbb{G}_{i,\xi}^{(\text{next})} = \left(\mathbb{I}_N \otimes \mathbb{J}^{N_c}\right) \mathbb{H}_{i,\xi}\left(\underline{\beta}_i \otimes \mathbb{I}_{\overline{N}}\right) \quad \in \mathcal{C}^{2NN_c \times \overline{N}} \tag{4.8}$$

Here,

$$\mathbb{H}_{i,\xi} = \left[\left(\underline{S}_{i1}\overline{\underline{S}}_{i1}^{H}\right) \otimes \left(\mathbb{J}^{l_{i1}}\underline{\mathfrak{c}}_{\xi}\right), \cdots, \left(\underline{S}_{iK_i}\overline{\underline{S}}_{iK_i}^{H}\right) \otimes \left(\mathbb{J}^{l_{iK_i}}\underline{\mathfrak{c}}_{\xi}\right) \right] \in \mathcal{C}^{2NN_c \times \overline{N}K_i} \tag{4.9}$$

and the vector $\underline{\beta}_i$ is composed of the propagation coefficients of these K_i paths which model the effect of path loss, random phase shift due to reflection and

Doppler phase shift due to the possible motion of scatterers, i.e.

$$\underline{\beta}_i = \left[\begin{array}{cccc} \beta_{i1}, & \beta_{i2}, & \cdots, & \beta_{iK_i} \end{array} \right]^T \quad \in \mathcal{C}^{K_i} \tag{4.10}$$

The complete receiver structure is depicted in Figure 4.3. By applying the unit-normalized decoding matrix $\mathbb{W}_i \in \mathcal{C}^{2NN_c \times N_i^{(s)}}$, $i = 1, \cdots, M$, to the sampled baseband signal-vector $\underline{x}_i[n]$, the corresponding decision variable $\hat{\underline{b}}_i[n]$ at point K of Figure 4.3 is obtained,

$$\underline{d}_i[n] = \mathbb{W}_i^H \underline{x}_i[n] \tag{4.11}$$

Consider the covariance matrix of $\underline{x}_i[n]$, the baseband signal-vectors received by the i^{th} UE. That is

$$\begin{aligned} \mathbb{R}_{xx,i} &\triangleq E\left\{\underline{x}_i[n]\,\underline{x}_i^H[n]\right\} && (4.12)\\ &= \sum_{\xi=1}^{M} \left[\mathbb{G}_{i,\xi}^{(\text{prev})}, \mathbb{G}_{i,\xi}, \mathbb{G}_{i,\xi}^{(\text{next})}\right] \left[\mathbb{I}_3 \otimes \left(\overline{\mathbb{W}}_\xi \overline{\mathbb{W}}_\xi^H\right)\right] \left[\mathbb{G}_{i,\xi}^{(\text{prev})}, \mathbb{G}_{i,\xi}, \mathbb{G}_{i,\xi}^{(\text{next})}\right]^H \\ &\quad + \sigma_i^2 \mathbb{I}_{2NN_c}. && (4.13) \end{aligned}$$

Based on Eqn. (4.13), the SNIR at the j^{th} output of the i^{th} user's receiver, $i = 1, 2, \cdots, M$, $j = 1, 2, \cdots, N_i^{(s)}$ is given by

$$\text{SNIR}_{ij} = \frac{\left|\underline{w}_{ij}^H \mathbb{G}_{i,i} \overline{\underline{w}}_{ij}\right|^2}{\underline{w}_{ij}^H \mathbb{M}_{ij} \underline{w}_{ij}} \tag{4.14}$$

where $\underline{w}_{ij}$ and $\overline{\underline{w}}_{ij}$ are the j^{th} column of decoding matrix $\mathbb{W}_i$ and precoding matrix $\overline{\mathbb{W}}_i$, respectively, and the matrix $\mathbb{M}_{ij}$ takes into account the effect of MAI, ISI, noise, and the interference introduced by desired user's other substreams. This matrix is defined as follows:

$$\begin{aligned} \mathbb{M}_{ij} &\triangleq \mathbb{G}_{i,i} \left(\sum_{\eta \neq j, \eta=1}^{N_i^{(s)}} \overline{\underline{w}}_{i\eta} \overline{\underline{w}}_{i\eta}^H \right) \mathbb{G}_{i,i}^H \\ &\quad + \left[\mathbb{G}_{i,i}^{(\text{prev})}, \mathbb{G}_{i,i}^{(\text{next})}\right] \left(\mathbb{I}_2 \otimes \overline{\mathbb{W}}_i \overline{\mathbb{W}}_i^H\right) \left[\mathbb{G}_{i,i}^{(\text{prev})}, \mathbb{G}_{i,i}^{(\text{next})}\right]^H \\ &\quad + \sum_{\xi \neq i, \xi=1}^{M} \left[\mathbb{G}_{i,\xi}^{(\text{prev})}, \ \mathbb{G}_{i,\xi}, \ \mathbb{G}_{i,\xi}^{(\text{next})}\right] \left[\mathbb{I}_3 \otimes \left(\overline{\mathbb{W}}_\xi \overline{\mathbb{W}}_\xi^H\right)\right] \left[\mathbb{G}_{i,\xi}^{(\text{prev})}, \ \mathbb{G}_{i,\xi}, \ \mathbb{G}_{i,\xi}^{(\text{next})}\right]^H \\ &\quad + \sigma_i^2 \mathbb{I}_{2NN_c}. \end{aligned} \tag{4.15}$$

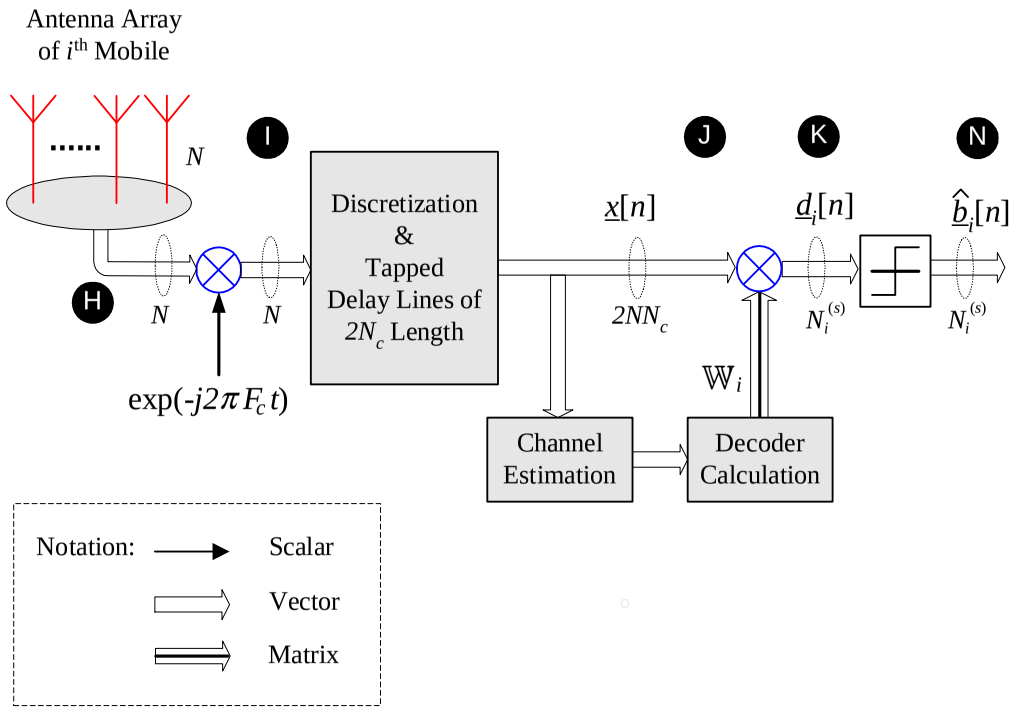


Figure 4.3: System architecture of the receiver in arrayed MIMO-CDMA downlink communication systems.

The MSE matrix of the i^{th} user is defined as [2]

$$\begin{aligned}\mathbb{E}_i &\triangleq \mathcal{E}\left\{\left(\underline{d}_i[n]-\underline{b}_i[n]\right)\left(\underline{d}_i[n]-\underline{b}_i[n]\right)^H\right\} &(4.16)\\ &= \mathbb{W}_i^H\left\{\sum_{\xi=1}^{M}\overline{\mathbb{G}}_{i,\xi}\left[\mathbb{I}_3\otimes\left(\overline{\mathbb{W}}_\xi\overline{\mathbb{W}}_\xi^H\right)\right]\overline{\mathbb{G}}_{i,\xi}^H+\sigma_i^2\mathbb{I}_{N_i^{(s)}}\right\}\mathbb{W}_i+\mathbb{I}_{N_i^{(s)}}\\ &\quad -\mathbb{W}_i^H\mathbb{G}_{i,i}\overline{\mathbb{W}}_i-\overline{\mathbb{W}}_i^H\mathbb{G}_{i,i}^H\mathbb{W}_i, &(4.17)\end{aligned}$$

which, with MMSE reception, can be rewritten as (proof is in Appendix 4.C)

$$\mathbb{E}_i=\left(\mathbb{I}_{N_i^{(s)}}+\overline{\mathbb{W}}_i^H\mathbb{G}_{i,i}^H\mathbb{M}_i^{-1}\mathbb{G}_{i,i}\overline{\mathbb{W}}_i\right)^{-1} \tag{4.18}$$

4.3 Optimization Objectives

In Chapter 3, it is assumed that the number of transmitted substreams equals the number of transmit antennas. Given that all channel parameters have been successfully estimated, beamformer matrices can then be constructed, separately at the transmitter and the receiver, to improve the system performance (e.g. SNIR or MSE). In this chapter, a more complex problem is addressed:

- For each user, the number of substreams, $N_1^{(s)},\cdots,N_M^{(s)}$, $i=1,\cdots,M$, can be dynamically chosen according to the requirement of the underlying service as well as the instantaneous channel state information (CSI). Thus, the dimensionality of the precoder and decoder matrices can be changed.

- The precoder and the decoder of one user are mutually dependent. Furthermore, by MAI, the performance of one user is affected by the precoder/decoder of other users. When the numbers of substream are defined, the overall system performance will be determined by the selection of precoders $\overline{\mathbb{W}}_i$ and decoders $\mathbb{W}_i$, $i=1,\cdots,M$.

4.3.1 Optimal Multiplexing Order

In future mobile MIMO-CDMA systems, *multiplexing order*[1] need to be reconfigurable to allocated different kind of services, e.g., voice, email, file downloading, etc. The multiplexing order of all users $\left(N_1^{(s)}, \cdots, N_M^{(s)}\right)$ plays a vital role in ensuring different data-rate services coexist. Therefore, a criterion is need to identify the optimum multiplexing order for a particular user.

It is intuitive that there is a so-called inter-user multiplexing trade-off, i.e. multiplexing order of one user can always be increased (if it is less than $\overline{N}$) by sacrificing other users' multiplexing orders. However, in this section, when deriving the optimal criterion on multiplexing order of one user, we assume

- other user's multiplexing orders as well as precoding/decoding matrices remain fixed.
- SNIR threshold γ, is identical for signal detection for every subchannel of every user.

To give the criterion on optimal $N_i^{(s)}$, it is necessary to introduce two lemmas:

Lemma 4.1 *SNIR upper-bound: The SNIR at the output the j^{th} substream of the i^{th} receiver is upper-bounded by $\underline{\overline{w}}_{ij}^H \mathbb{G}_{i,i}^H \mathbb{M}_i^{-1} \mathbb{G}_{i,i} \underline{\overline{w}}_{ij}$, i.e.*

$$SNIR_{ij} \leq \underline{\overline{w}}_{ij}^H \mathbb{G}_{i,i}^H \mathbb{M}_i^{-1} \mathbb{G}_{i,i} \underline{\overline{w}}_{ij} \tag{4.19}$$

where $\underline{\overline{w}}_{ij}$ is the j^{th} column of the i^{th} user's precoding matrix $\overline{\mathbb{W}}_i$, and

$$\mathbb{M}_i \triangleq \mathbb{M}_{ij} - \mathbb{G}_{i,i} \left(\sum_{\eta \neq j, \eta=1}^{N_i^{(s)}} \underline{\overline{w}}_{i\eta} \underline{\overline{w}}_{i\eta}^H \right) \mathbb{G}_{i,i}^H. \tag{4.20}$$

[1] The number of substreams.

Proof. The proof of this lemma can be found in Appendix 4.A. ■

Note that by comparing Eqn. (4.19) and (4.18), SNIR and MSE are connected by

$$\mathrm{SNIR}_{ij} \leq \left[\mathbb{E}_i^{-1} - \mathbb{I}_{N_i^{(s)}}\right]_{jj} \tag{4.21}$$

where $[\mathbb{A}]_{jj}$ stands for the j^{th} diagonal element in the square matrix $\mathbb{A}$.

Lemma 4.2 *Ky Fan's maximum principle: Let $\mathbb{A} \in \mathcal{C}^{n\times n}$ be a Hermitian matrix with eigenvalues $\lambda_1 \geq \lambda_2 \geq \cdots \geq \lambda_n$, then for all $k = 1, 2, \cdots, n$*

$$\sum_{j=1}^{k} \lambda_j = \max \sum_{j=1}^{k} \left|\underline{x}_j^H \mathbb{A} \underline{x}_j\right|^{\frac{1}{2}} \tag{4.22}$$

where the maximum is taken over all orthonormal k-tuples of vectors $\{\underline{x}_1, \cdots, \underline{x}_K\}$ in $\mathcal{C}^n$.

Proof. *See [62].* ■

Therefore, a criterion can be derived to determine if a multiplexing order is optimal or not.

Theorem 4.1 *Criterion on Optimal Multiplexing Order: The optimum number of simultaneously transmitted signal streams $N_i^{\dagger}$ satisfies*

$$\frac{1}{N_i^{\dagger}} \sum_{j=1}^{N_i^{\dagger}} \tilde{\lambda}_j \geq \gamma \geq \frac{1}{N_i^{\dagger}+1} \sum_{j=1}^{N_i^{\dagger}+1} \tilde{\lambda}_j \tag{4.23}$$

where $\tilde{\lambda}_{i,1} \geq \tilde{\lambda}_{i,2} \geq \cdots \geq \tilde{\lambda}_{i,\overline{N}}$ are the (real) eigenvalues of matrix $\mathbb{D}_i^{1/2}\mathbb{G}_{i,i}^H\mathbb{M}_i^{-1}\mathbb{G}_{i,i}\mathbb{D}_i^{1/2}$, and $\mathbb{D}_i$ is a diagonal matrix with elements eigenvalues of the Hermitian matrix $\overline{\mathbb{W}}_i\overline{\mathbb{W}}_i^H$.

Proof. The proof of this theorem can be found in Appendix 4.B. ■

Theorem 4.1 provides a measure on judging how 'far' is a practical (or required) multiplexing order from the optimal. If $N_i^{(s)} > N_i^{\dagger}$, some of the substreams will not be received properly. If $N_i^{(s)} < N_i^{\dagger}$, some spare multiplexing order is available to offer higher-rate services.

4.3.2 Optimal Precoder and Decoder

When $N_1^{(s)}, \cdots, N_M^{(s)}$ have already been chosen, the overall system performance will be determined by the selection of precoders $\overline{\mathbb{W}}_i$ and decoders $\mathbb{W}_i$, $i = 1, \cdots, M$.

It should be noted that, the effect of transmit power allocation is absorbed by the optimization of $\overline{\mathbb{W}}_i$. In this chapter, three transmit power constraints (or Power allocation Schemes, PAS) are considered:

- **PAS-I**: Total transmit power constraint, under which, the power will be dynamically distributed to all users and then to all substreams. That is

$$\sum_{i=1}^{M} \mathrm{Tr}\left(\overline{\mathbb{W}}_i^H \overline{\mathbb{W}}_i\right) \leq \overline{P} \tag{4.24}$$

- **PAS-II**: User's transmit power constraint, under which, the transmit power of each user has been fixed and will be distributed to its substreams. That is

$$\mathrm{Tr}\left(\overline{\mathbb{W}}_i^H \overline{\mathbb{W}}_i\right) \leq \overline{P}_i,\ i = 1, \cdots, M \tag{4.25}$$

- **PAS-III**: Substream's transmit power constraint, under which, the transmit power of each substream of each user has been fixed. That is

$$\overline{w}_{ij}^H \overline{w}_{ij} \leq \frac{\overline{P}_i}{N_i^{(s)}},\ i = 1, \cdots, M,\ j = 1, \cdots, N_i^{(s)} \tag{4.26}$$

  where $\overline{w}_{ij}$ denotes the j^{th} column vector of the precoder matrix $\overline{\mathbb{W}}_i$.

The algorithms of optimization rely on different objectives (cost functions) and constraints. The optimization problems considered in this chapter include:

A. Total Transmit Power Minimization with SNIR requirement

Given the expression of SNIR at the j^{th} output of the i^{th} receiver in Eqn. (4.14), the optimization objective is to minimize the total transmit power

subjected to (s.t.) a minimum receiver SNIR requirement γ, and can be expressed as

$$\boxed{\begin{aligned} J &= \min_{\substack{\overline{\mathbb{W}}_1,\cdots,\overline{\mathbb{W}}_M \\ \mathbb{W}_1,\cdots,\mathbb{W}_M}} \sum_{i=1}^{M} \mathrm{Tr}\left(\overline{\mathbb{W}}_i^H \overline{\mathbb{W}}_i\right) \\ \text{s.t.} \quad & \mathrm{SNIR}_{ij} \geq \gamma,\, \forall i \in [1, M], \forall j \in \left[1, N_i^{(s)}\right] \end{aligned}} \tag{4.27}$$

B. Total Tx Power Minimization with Symbol Error Rate Requirement

Similarly, the optimization objective here is to minimize the total transmit power while supporting a target symbol error rate ε, and can be expressed as

$$\boxed{\begin{aligned} J &= \min_{\substack{\overline{\mathbb{W}}_1,\cdots,\overline{\mathbb{W}}_M \\ \mathbb{W}_1,\cdots,\mathbb{W}_M}} \sum_{i=1}^{M} \mathrm{Tr}\left(\overline{\mathbb{W}}_i^H \overline{\mathbb{W}}_i\right) \\ \text{s.t.} \quad & P_s^{(i)} \leq \varepsilon,\, \forall i \in [1, M] \end{aligned}} \tag{4.28}$$

C. Total SNIR Maximization

In this case, the optimization aiming at maximizing the total received SNIR at the output of the receive decoders can be expressed as

$$\boxed{\begin{aligned} J &= \max_{\substack{\overline{\mathbb{W}}_1,\cdots,\overline{\mathbb{W}}_M \\ \mathbb{W}_1,\cdots,\mathbb{W}_M}} \sum_{i=1}^{M} \mathrm{SNIR}_{ij} \\ \text{s.t.} \quad & \text{Power Allocation Scheme-I/II/III} \end{aligned}} \tag{4.29}$$

D. Total MSE Minimization

The optimization based on minimization of the total MSE can be written

as

$$\boxed{\begin{array}{c} J = \min\limits_{\substack{\overline{\mathbb{W}}_1,\cdots,\overline{\mathbb{W}}_M \\ \mathbb{W}_1,\cdots,\mathbb{W}_M}} \sum\limits_{i=1}^{M} \mathrm{Tr}\left(\mathbb{E}_i\right) \\ \\ \text{s.t.} \quad \text{Power Allocation Scheme-I/II/III} \end{array}} \tag{4.30}$$

Note that, alternatively, the determination of MSE matrix, $\sum\limits_{i=1}^{M} \det\left(\mathbb{E}_i\right)$, can also be used as a MSE performance measure, as in [57] and [63].

4.4 Iterative Optimization

4.4.1 Iterative Joint Precoder-Decoder Optimization With Power Allocation Scheme-I

It is assumed that both the transmitter and receiver have perfect knowledge of the channel. Consider the total MSE minimization problem Eqn. (4.30) with PAS-I. Assuming all $\mathbb{W}_i$, $i \in [1, M]$ are fixed, the augmented cost function using the Lagrange multiplier (LM) μ can be expressed as follows

$$J_{\text{aug}} = \sum_{i=1}^{M} \mathrm{Tr}\left(\mathbb{E}_i\right) + \mu\left(\sum_{i=1}^{M} \mathrm{Tr}\left(\overline{\mathbb{W}}_i^H \overline{\mathbb{W}}_i\right) - \overline{P}\right) \tag{4.31}$$

In this case, $\forall i \in [1, M]$, by defining the first derivative of J_{aug} w.r.t. $\overline{\mathbb{W}}_i$ evaluated at $\overline{\mathbb{W}}_i^{\dagger}$ as the matrix $\mathbb{F}_{\overline{\mathbb{W}}_i^{\dagger}}$, i.e[2].

$$\mathbb{F}_{\overline{\mathbb{W}}_i^{\dagger}} \triangleq \left.\frac{\partial J}{\partial \overline{\mathbb{W}}_i}\right|_{\overline{\mathbb{W}}_i = \overline{\mathbb{W}}_i^{\dagger}} \in \mathcal{C}^{\overline{N} \times N_i^{(s)}} \tag{4.32}$$

the necessary condition for $\overline{\mathbb{W}}_i^{\dagger}$ being the solution of the optimization problem

$$\overline{\mathbb{W}}_i^{\dagger} = \arg\min_{\overline{\mathbb{W}}_i} \left(J_{\text{aug}}\right) \tag{4.33}$$

[2] As J is a scalar function of matrix $\overline{\mathbb{W}}_i \in \mathcal{C}^{\overline{N} \times N_i^{(s)}}$, the dimension of J's first derivative w.r.t. $\overline{\mathbb{W}}_i$ is $\overline{N} \times N_i^{(s)}$.

is Kuhn-Tucker conditions

$$\underline{v}^H \mathbb{F}_{\overline{\mathbb{W}}_i^\dagger} \underline{v} = 0, \ \ \forall \underline{v} \neq \underline{0}. \tag{4.34}$$

This finally results in a matrix with Wiener filter form:

$$\overline{\mathbb{W}}_i^\dagger = \left\{ \mathbb{L}^H \sum_{\xi=1}^{M} \begin{pmatrix} \left[\mathbb{G}_{\xi,i}^{(\text{prev})}, \mathbb{G}_{\xi,i}, \mathbb{G}_{\xi,i}^{(\text{next})} \right]^H \mathbb{W}_\xi \\ \mathbb{W}_\xi^H \left[\mathbb{G}_{\xi,i}^{(\text{prev})}, \mathbb{G}_{\xi,i}, \mathbb{G}_{\xi,i}^{(\text{next})} \right] \end{pmatrix} \mathbb{L} + \mu \mathbb{I}_{\overline{N}} \right\}^{-1} \mathbb{G}_{i,i}^H \mathbb{W}_i \tag{4.35}$$

where

$$\mathbb{L} \triangleq \underline{1}_3 \otimes \mathbb{I}_{\overline{N}} \qquad \in \mathcal{R}^{3\overline{N} \times \overline{N}} \tag{4.36}$$

Eqn. (4.34) can also lead to the expression of the Lagrange multiplier $\mu^\dagger$

$$\mu^\dagger = \frac{1}{\overline{P}} \sum_{i=1}^{M} \text{Tr} \left\{ \begin{array}{l} \overline{\mathbb{W}}_i^H \mathbb{G}_{i,i}^H \mathbb{W}_i \\ -\overline{\mathbb{W}}_i^H \mathbb{L}^H \begin{pmatrix} \sum_{\xi=1}^{M} \left[\mathbb{G}_{\xi,i}^{(\text{prev})}, \mathbb{G}_{\xi,i}, \mathbb{G}_{\xi,i}^{(\text{next})} \right]^H \mathbb{W}_\xi \mathbb{W}_\xi^H \\ \left[\mathbb{G}_{\xi,i}^{(\text{prev})}, \mathbb{G}_{\xi,i}, \mathbb{G}_{\xi,i}^{(\text{next})} \right] \end{pmatrix} \mathbb{L} \overline{\mathbb{W}}_i \end{array} \right\} \tag{4.37}$$

Similarly, if the precoding matrices are fixed, the optimal decoding matrices that minimize the total MSE can be derived

$$\mathbb{W}_i^\dagger = \left\{ \begin{array}{l} \sum_{\xi=1}^{M} \left[\mathbb{G}_{i,\xi}^{(\text{prev})}, \mathbb{G}_{i,\xi}, \mathbb{G}_{i,\xi}^{(\text{next})} \right] \left[\mathbb{I}_3 \otimes \left(\overline{\mathbb{W}}_\xi \overline{\mathbb{W}}_\xi^H \right) \right] \left[\mathbb{G}_{i,\xi}^{(\text{prev})}, \mathbb{G}_{i,\xi}, \mathbb{G}_{i,\xi}^{(\text{next})} \right]^H \\ + \sigma_i^2 \mathbb{I}_{2LN} \end{array} \right\}^{-1} \mathbb{G}_{i,i} \overline{\mathbb{W}}_i \tag{4.38}$$

From the above analysis, it can be seen that the transmitter precoders and the receiver decoders as well as the Lagrange multiplier are functions of each other, which suggests a iterative algorithm to obtain the global solution. The joint transmitter-receiver optimization can be accomplished via the following steps:

Algorithm 4.1 Iterative Precoder-Decoder Optimization With PAS-I

1. Initialization: the iterative index $q = 0$ and for each user $i = 1, \cdots, M$, $\overline{\mathbb{W}}_i$ is constructed by single user transmit scheme, i.e.,

$$\overline{\mathbb{W}}_i [0] = \sqrt{\frac{\overline{P}}{M N_i^{(s)}}} \mathbb{U}_{i, N_i^{(s)}} \tag{4.39}$$

where the columns of $\mathbb{U}_{i,N_i^{(s)}} \in \mathcal{C}^{\overline{N}\times N_i^{(s)}}$ are the eigenvectors of matrix pair $\mathbb{G}_{i,i}^H\mathbb{G}_{i,i}$ corresponding to the $N_i^{(s)}$ largest eigenvalues. The scalar factor $\overline{P}/\left(MN_i^{(s)}\right)$ indicates that the transmitting energy is evenly distributed to every user and then to every substream.

2. For each user $i = 1, \cdots, M$, the MMSE weight vector $\mathbb{W}_i^{\dagger}[q]$ is calculated using Eqn. (4.38).

3. For the current precoders and decoders, the Lagrange multiplier $\mu^{\dagger}[q]$ is calculated using Eqn. (4.37).

4. Using receive decoder matrices $\mathbb{W}_i^{\dagger}[q]$, $i = 1, \cdots, M$ and $\mu^{\dagger}[q]$ obtained in Step 2 and 3 respectively, the transmit precoder matrices $\overline{\mathbb{W}}_i^{\dagger}[q+1]$, $i = 1, \cdots, M$ can be updated via Eqn. (4.35).

5. $q \longleftarrow q+1$, repeat Steps 2-4 until a predefined convergence criterion is reached.

Please note that a similar iterative method to optimize the precoder and decoder but for flat-fading downlink channel of the multiuser MIMO systems has been reported recently in [64] where a brute search is needed to find the optimum Lagrange multiplier in each iteration procedure. The Lagrange multiplier in our proposed iterative scheme is directly calculated with the channel information and the precoders and decoders obtained in the last iteration, which significantly reduces the algorithm's complexity.

4.4.2 Iterative Precoder-Decoder Optimization With Power Allocation Scheme-II

With power allocation scheme-II, the augmented cost function of optimization problem (4.30) can be rewritten as

$$J_{\text{aug}} = \sum_{i=1}^{M} \text{Tr}\left(\mathbb{E}_i\right) + \sum_{i=1}^{M} \mu_i \left[\text{Tr}\left(\overline{\mathbb{W}}_i^H \overline{\mathbb{W}}_i\right) - \overline{P}_i\right] \tag{4.40}$$

where $\overline{P}_i$ is the pre-defined transmitting power for the i^{th} user.

The solutions can be obtained by applying the necessary condition of local minimization on (4.40),

$$\overline{\mathbb{W}}_i^{\dagger} = \left\{ \begin{array}{l} \mathbb{L}^H \left(\sum_{\xi=1}^{M} \left[\mathbb{G}_{\xi,i}^{(\text{prev})}, \mathbb{G}_{\xi,i}, \mathbb{G}_{\xi,i}^{(\text{next})}\right]^H \mathbb{W}_\xi \mathbb{W}_\xi^H \left[\mathbb{G}_{\xi,i}^{(\text{prev})}, \mathbb{G}_{\xi,i}, \mathbb{G}_{\xi,i}^{(\text{next})}\right] \right) \mathbb{L} \\ +\mu_i \mathbb{I}_{\overline{N}} \end{array} \right\}^{-1} \mathbb{G}_{i,i}^H \mathbb{W}_i \tag{4.41}$$

and

$$\mu_i^{\dagger} = \frac{1}{\overline{P}_i} \text{Tr} \left\{ \begin{array}{l} \overline{\mathbb{W}}_i^H \mathbb{G}_{i,i}^H \mathbb{W}_i \\ -\overline{\mathbb{W}}_i^H \mathbb{L}^H \left(\begin{array}{c} \sum_{\xi=1}^{M} \left[\mathbb{G}_{\xi,i}^{(\text{prev})}, \mathbb{G}_{\xi,i}, \mathbb{G}_{\xi,i}^{(\text{next})}\right]^H \mathbb{W}_\xi \mathbb{W}_\xi^H \\ \left[\mathbb{G}_{\xi,i}^{(\text{prev})}, \mathbb{G}_{\xi,i}, \mathbb{G}_{\xi,i}^{(\text{next})}\right] \end{array} \right) \mathbb{L} \overline{\mathbb{W}}_i \end{array} \right\} \tag{4.42}$$

and expression of $\mathbb{W}_i^{\dagger}$ is the same as in Eqn. (4.38). A recursive algorithm can then be developed in the similar fashion to the one introduced in last section.

4.5 Sub-optimal Close-form Optimization

The algorithms proposed so far is based on a primary assumption that the feedback channel is error-free and speedy enough to ensure that the convergence can be achieved before the channel changes. In some cases, this is relatively impractical. Moreover, in a system with very large number of users, the computation load

of the proposed iterative algorithms, even for the base station, may be unacceptable. To cope with these, in this section, two sub-optimization precoder/decoder construction algorithms that do not require feedback information or iteration are developed.

4.5.1 Close-form SNIR Optimization

As in Section 4.4.2, the inter-user transmitted power distribution is assumed to be pre-determined. Furthermore, for each user, the transmitted power is evenly distributed to all sub-channels. Otherwise, the maximal SNIR objective can always be achieved by assigning all the power to the sole subchannel with maximum channel gain, leaving all other subchannels unused, which is practically unreasonable.

With Lemma 4.1, instead of directly maximizing SNIR, the objective of this algorithm is to find the maximum of the upper-bound of total SNIR for all receivers. That is

$$\left(\overline{\mathbb{W}}_1, \cdots, \overline{\mathbb{W}}_M; \mathbb{W}_1, \cdots, \mathbb{W}_M\right) = \arg \max_{\substack{\overline{\mathbb{W}}_1, \cdots, \overline{\mathbb{W}}_M \\ \mathbb{W}_1, \cdots, \mathbb{W}_M}} \sum_{i=1}^{M} \mathrm{Tr}\left(\overline{\mathbb{W}}_i^H \mathbb{G}_{i,i}^H \mathbb{M}_i^{-1} \mathbb{G}_{i,i} \overline{\mathbb{W}}_i\right)$$

$$\text{s.t. Power Allocation Scheme III} \quad (4.43)$$

The augmented cost function (using Lagrange multipliers) can be expressed as follows:

$$J_{\text{aug}} = \sum_{i=1}^{M} \mathrm{Tr}\left(\overline{\mathbb{W}}_i^H \mathbb{G}_{i,i}^H \mathbb{M}_i^{-1} \mathbb{G}_{i,i} \overline{\mathbb{W}}_i\right) + \sum_{i=1}^{M} \sum_{j=1}^{N_i^{(s)}} \left(\lambda_{ij} \underline{\overline{w}}_{ij}^H \underline{\overline{w}}_{ij} - \frac{\overline{P}_i}{N_i^{(s)}}\right) \quad (4.44)$$

In this case, $\forall i \in [1, M]$, the necessary condition for $\overline{\mathbb{W}}_i$ to be the local optimal solution is

$$\frac{\partial J}{\partial \underline{\overline{w}}_{ij}} = \underline{0}, \forall j = 1, ..., N_i^{(s)} \quad (4.45)$$

This leads to

$$\mathbb{G}_{i,i}^H \mathbb{M}_i^{-1} \mathbb{G}_{i,i} \underline{\overline{w}}_{ij} = \lambda_{ij} \underline{\overline{w}}_{ij} \tag{4.46}$$

which suggests that the Lagrange multipliers λ_{ij} are the eigenvalues of the semi-positive matrix $\mathbb{G}_{i,i}^H \mathbb{M}_i^{-1} \mathbb{G}_{i,i}$, and the optimal solutions $\underline{\overline{w}}_{ij}$ are the corresponding eigenvectors scaled by $\sqrt{\overline{P}_i / N_i^{(s)}}$. Apparently, as the aim is to find the maximum of the bound, the $N_i^{(s)}$ largest eigenvalues and their corresponding eigenvectors will be chosen.

Based on the above analysis, the eigendecomposition based close-form algorithm can then be developed as follows:

Algorithm 4.2 Eigendecomposition-based Close-form Precoder-Decoder Optimization

1. For first selected user, $\overline{\mathbb{W}}_1$ is constructed by

$$\overline{\mathbb{W}}_1 = \sqrt{\frac{\overline{P}_1}{N_1^{(s)}}} \mathcal{A}_{N^{(s)}} \left\{ \mathbb{G}_{1,1}^H \tilde{\mathbb{M}}_1 \mathbb{G}_{1,1} \right\} \tag{4.47}$$

   where $\mathcal{A}_k \{\mathbb{X}\}$ is a matrix of k columns which are the eigenvectors corresponding to the k largest general eigenvalues of semi-positive matrix $\mathbb{X}$, and

$$\tilde{\mathbb{M}}_1 = \left[\mathbb{G}_{1,1}^{(\text{prev})}, \mathbb{G}_{1,1}^{(\text{next})} \right] \left[\mathbb{G}_{1,1}^{(\text{prev})}, \mathbb{G}_{1,1}^{(\text{next})} \right]^H. \tag{4.48}$$

2. For user $i = 2, \cdots, M$, the precoder is obtained by

$$\overline{\mathbb{W}}_i = \sqrt{\frac{\overline{P}_i}{N_i^{(s)}}} \mathcal{A}_{N_i^{(s)}} \left\{ \mathbb{G}_{i,i}^H \tilde{\mathbb{M}}_i^{-1} \mathbb{G}_{i,i} \right\} \tag{4.49}$$

   where

$$\begin{aligned} \tilde{\mathbb{M}}_i \;=\; & \left[\mathbb{G}_{i,i}^{(\text{prev})}, \mathbb{G}_{i,i}^{(\text{next})} \right] \left(\mathbb{I}_2 \otimes \overline{\mathbb{W}}_i \overline{\mathbb{W}}_i^H \right) \left[\mathbb{G}_{i,i}^{(\text{prev})}, \mathbb{G}_{i,i}^{(\text{next})} \right]^H \\ & + \sum_{\xi=1}^{i-1} \left[\mathbb{G}_{i,\xi}^{(\text{prev})}, \mathbb{G}_{i,\xi}, \mathbb{G}_{i,\xi}^{(\text{next})} \right] \left[\mathbb{I}_3 \otimes \left(\overline{\mathbb{W}}_\xi \overline{\mathbb{W}}_\xi^H \right) \right] \left[\mathbb{G}_{i,\xi}^{(\text{prev})}, \mathbb{G}_{i,\xi}, \mathbb{G}_{i,\xi}^{(\text{next})} \right]^H \end{aligned} \tag{4.50}$$

3. While $\overline{\mathbb{W}}_i$, $i = 1, \cdots, M$, are determined, the precoder matrices $\mathbb{W}_i$, $i = 1, \cdots, M$, can be obtained analytically by Eqn. (4.38).

The eigendecomposition-based algorithm is suboptimal but, because of the "close-form", is practically more efficient than the optimal iterative algorithms.

4.5.2 Close-form Tx Power Minimization

Consider the covariance matrix (4.13) of the i^{th} UE's received baseband signal-vector $\underline{x}_i[n]$, the upper bound of the symbol error rate at the i^{th} receive can be obtained

$$P_{s,\text{ bound}}^{(i)} = \alpha \left[\det\left(\mathbb{I}_{\overline{N}} + g\mathbb{G}_{i,i}\overline{\mathbb{W}}_i\overline{\mathbb{W}}_i^H\mathbb{G}_{i,i}^H\mathbb{M}_i^{-1}\right)\right]^{-1} \tag{4.51}$$

where α and g are constellation-specific positive constants [59]. Recalling the property of the determine of matrix: for matrices $\mathbb{A} \in \mathcal{C}^{m\times n}$ and $\mathbb{B} \in \mathcal{C}^{n\times m}$.

$$\det(\mathbb{I}_m + \mathbb{A}\mathbb{B}) = \det(\mathbb{I}_n + \mathbb{B}\mathbb{A}) \tag{4.52}$$

Eqn. (4.51) can be rewritten as

$$P_{s,\text{ bound}}^{(i)} = \alpha \left[\det\left(\mathbb{I}_{N_i^{(s)}} + g\overline{\mathbb{W}}_i^H\mathbb{G}_{i,i}^H\mathbb{M}_i^{-1}\mathbb{G}_{i,i}\overline{\mathbb{W}}_i\right)\right]^{-1} \tag{4.53}$$

Observing the similarity of Eqn. (4.18) and Eqn. (4.51), by absorbing g into the transmit $\overline{\mathbb{W}}_i$, the optimize problem to minimize the total symbol error rate bound is equivalent to minimize the determine of overall MSE matrix Eqn. (4.30).

Based on the Rayleigh-Ritz Theorem (see 4.2.2 in [65]),

$$\begin{aligned} P_{s,\text{ bound}}^{(i)} &= \alpha \det\left(\mathbb{I}_{N_i^{(s)}} + g\overline{\mathbb{W}}_i^H\mathbb{G}_{i,i}^H\mathbb{M}_i^{-1}\mathbb{G}_{i,i}\overline{\mathbb{W}}_i\right)^{-1} &(4.54)\\ &\geq \alpha \prod_{j=1}^{N_i^{(s)}} \left(1 + g\rho_{ij}\lambda_{ij}\right)^{-1}. &(4.55)\end{aligned}$$

where $\lambda_{i1} \geq \cdots \geq \lambda_{iN_i^{(s)}}$ are the decreasing-ordered eigenvalues of semi-positive definite matrix $\mathbb{G}_{i,i}^H\mathbb{M}_i^{-1}\mathbb{G}_{i,i}$, ρ_{ij} is the power allocated to the j^{th} subchannel of the

i^{th} user. In the last inequation, the equation is obtained when $\mathbb{E}_i$ is a diagonal matrix, or

$$\overline{\overline{\mathbb{W}}}_i = \left[\rho_{i1}\underline{v}_{i1}, \cdots, \rho_{iN_i^{(s)}}\underline{v}_{iN_i^{(s)}}\right]^H \tag{4.56}$$

with $\underline{v}_{ij}$ denoting the eigenvector associated with eigenvalue λ_{ij}.

Furthermore, the power allocation scheme $\left\{\rho_{i1}, \cdots, \rho_{iN_i^{(s)}}\right\}$ can be derived by

$$\left\{\rho_{i1}, \cdots, \rho_{iN_i^{(s)}}\right\} = \arg\min \sum_{j=1}^{N_i^{(s)}} \rho_{ij} \tag{4.57}$$

$$\text{s.t.} \quad \alpha \prod_{j=1}^{N_i^{(s)}} \left(1 + g\rho_{ij}\lambda_{ij}\right)^{-1} \leq \varepsilon$$
$$\rho_{ij} \geq 0, \forall i, j \tag{4.58}$$

Taking the logarithm of both side of (4.58), the augmented Lagrangian cost function can be expressed as

$$J = \sum_{j=1}^{N_i^{(s)}} \rho_{ij} + \mu \left[\ln\frac{\alpha}{\varepsilon} - \sum_{j=1}^{N_i^{(s)}} \ln\left(1 + g\rho_{ij}\lambda_{ij}\right)\right] \tag{4.59}$$

The Karush-Kuhn-Tucker (KKT) condition of the optimization problem Eqn. (4.57) leads to:

$$1 - \mu\frac{g\lambda_{ij}}{1 + g\rho_{ij}\lambda_{ij}} = 0 \tag{4.60}$$

and

$$\prod_{j=1}^{N_i^{(s)}} \left(1 + g\rho_{ij}\lambda_{ij}\right)^{-1} = \frac{\alpha}{\varepsilon} \tag{4.61}$$

Finally, the optimal power allocation coefficients are obtained (proof can be found in Appendix 4.D)

$$\rho_{ij} = \max\left(0, \left(\frac{\varepsilon}{\alpha}\right)^{N_i^{(s)}} \prod_{\eta=1}^{N_i^{(s)}} \frac{1}{g\lambda_{i\eta}} - \frac{1}{g\lambda_{ij}}\right) \tag{4.62}$$

4.6 Numerical Studies

In this section, the performance of the joint optimization algorithms proposed in this chapter is investigated through a number of numerical simulations. The

transmit array and the various receiver arrays are 2-element ULA with half-wavelength inter-element spacing. Each user employs a unique Gold sequence of length $N_c = 15$, and transmit $N_i^{(s)} = 2$ substreams. Signals are transmitted to the receiver via $K_i = 3$ paths. The DOD and DOA of each path are randomly selected from $[0, 180^\circ)$ and the TOA are randomly selected from $[0, 15T_c)$. The array is assumed to collect a block of 200 data symbols for processing at each time, during which the channel is assumed to be stationary with the channel state information available to both BS transmitter and mobile receivers.

Firstly the convergence curves of the proposed Lagrange multiplier based iteration algorithms are studied for various transmit SNR levels in a 6-user MIMO-CDMA scenario. Note that as $\sum_{1}^{M} N_i = 12 > \overline{N}$, the condition of conventional zero-forcing approach [54] is no longer satisfied. The numerical results representing the average MSE over all substreams for all users are shown in Figure 4.4 as the function of the iteration loops by which the precoders and decoders are iteratively obtained, with different power allocation schemes. From Figure 4.4 it is clear that the convergence property of the proposed algorithms improves with SNR. The convergence MSE level of the optimized system with power allocation scheme-I is better than that with power allocation scheme-II.

To investigate the effect of the number of the transmit antennas on the convergence property of the proposed iterative schemes, similar simulations are carried out with $\overline{N} = 6$ and 3, and the convergence curves are depicted in Figure 4.5. As shown in the figure, iterative algorithm in the system with larger number of transmit antennas achieves smaller total MSE than those with less transmitter antennas.

In Figure 4.6, the BER performance of the two iterative algorithms proposed in Section 4.3 (page 129-131) is compared with the eigendecomposition-based close-

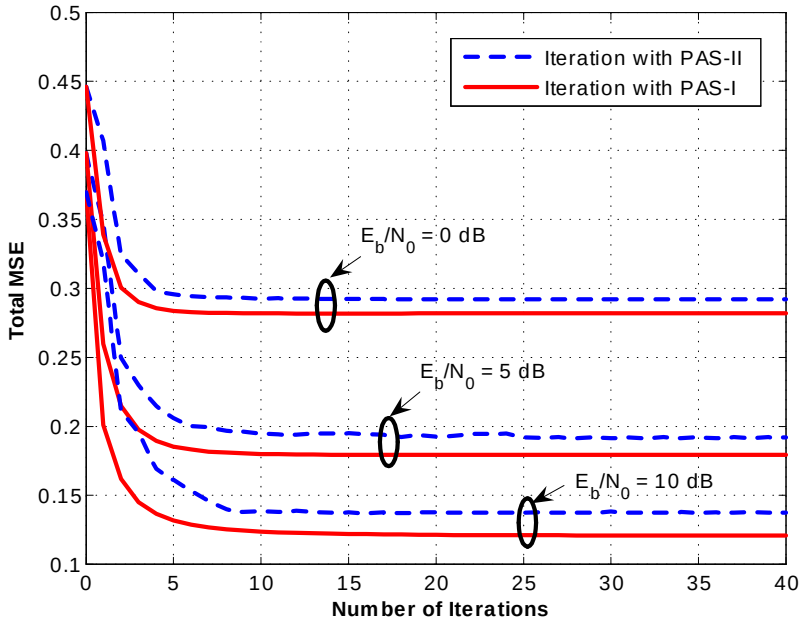


Figure 4.4: Convergence study for the proposed iterative LM-based optimization algorithm with and without power distribution in a 6-user MIMO-CDMA system, with input $E_b/N_0 = 0$, 5, and 10 dB.

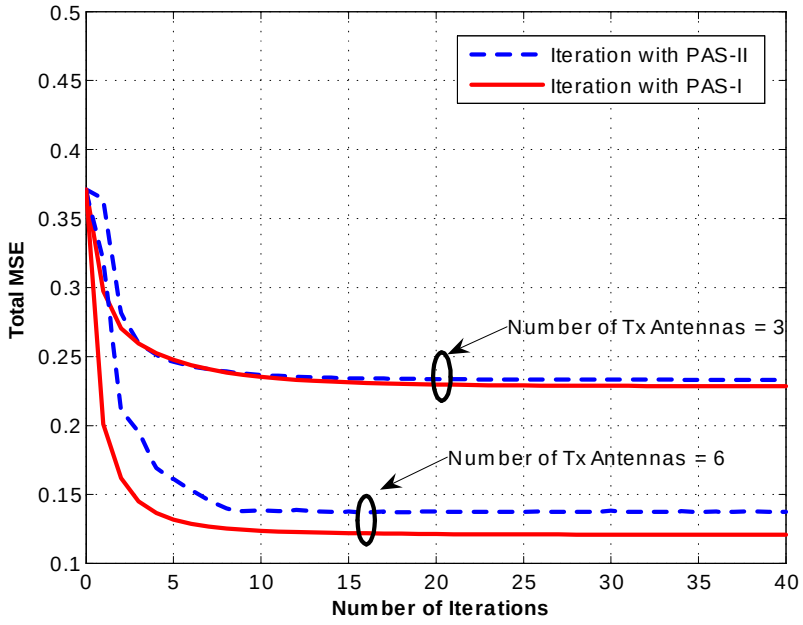


Figure 4.5: Convergence study for the proposed iterative LM-based optimization algorithms with different number of transmit antennas, in a 6-user MIMO-CDMA system, with input $E_b/N_0 = 10$ dB.

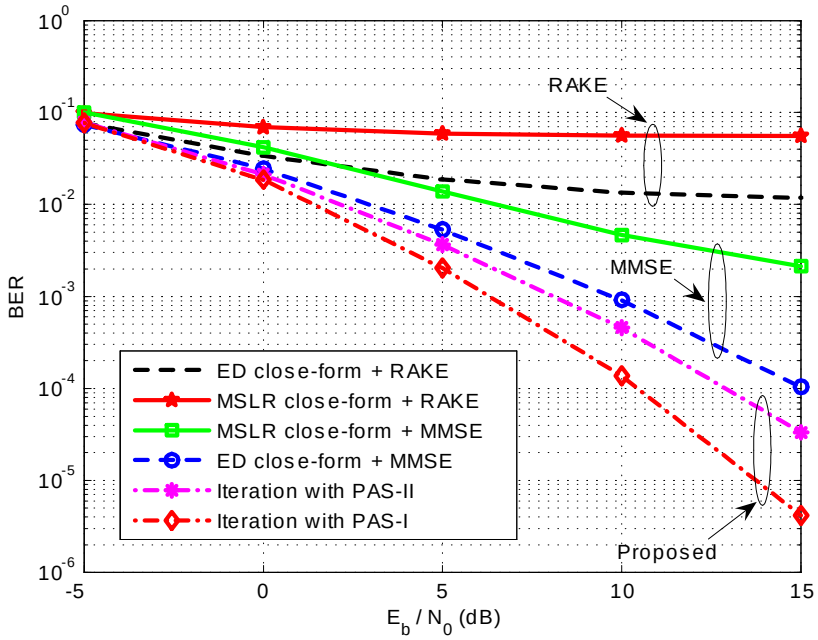


Figure 4.6: BER performance of different optimization schemes for a 6-user MIMO-CDMA system with 6 element Tx ULA and 2 element Rx ULA, $N_c = 15$, $K_i = 3$.

form approach of Section 4.5, as well as the precoding scheme proposed in [56] maximizing the signal-to-leakage ratio (MSLR). It is obvious that the proposed iterative algorithms outperform all other schemes at the cost of computer complexity. Among all close-form approaches, the eigendecomposition-based schemes show considerable advantage against MSLR approaches. Furthermore, at the receiver side, MMSE receivers always achieve better BER performance than RAKE receivers.

In Figure 4.7 and Figure 4.8, with different number of users in the system, the BER performance of the proposed iterative algorithms with power distribution scheme-I and scheme-III is compared with the generalized eigendecomposition (ED) based precoding scheme proposed in [57] and RAKE/MMSE decoder (see Section 3.4.1). The transmit power is distributed using water-filling algorithm. From these two figures, it is clear that BER of all schemes degrade with the

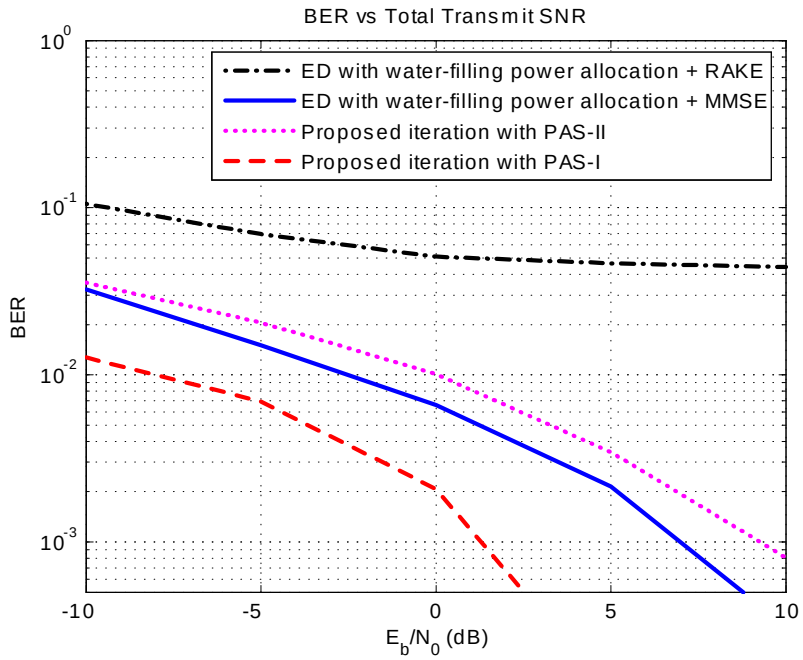


Figure 4.7: BER performance of the proposed iterative algorithms (by 30 iterations) with power allocation scheme I/II, and the eigendecomposition-based transmit precoding with RAKE/MMSE decoding. There are 6 users in the MIMO-CDMA system.

expanding user number. However, the proposed iterative algorithm with power distribution achieves the best performance in all scenarios. Furthermore, even the proposed algorithm without inter-user power distribution outperforms the conventional scheme when the number of users is large enough.

When the geometry of the transmit and receive arrays are uncertain, a downgrade of the system performance can be expected. To investigate the robustness of the proposed algorithms against the array geometry uncertainty, numeric simulation is carried out, assuming 10% random geometry error existing at both the transmitter and the receivers. The BER performance of such uncertain systems is compared in Figure 4.9 with that assuming complete accurate array geometry knowledge. It can be found that the proposed iterative algorithms are relatively robust.

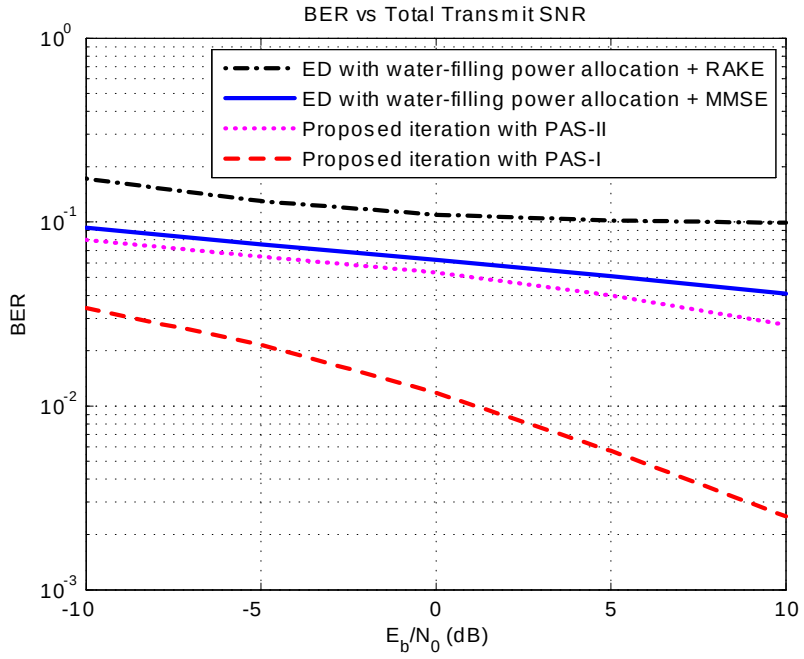


Figure 4.8: The same as Fig. 4.7 except there are 10 users in the MIMO-CDMA system.

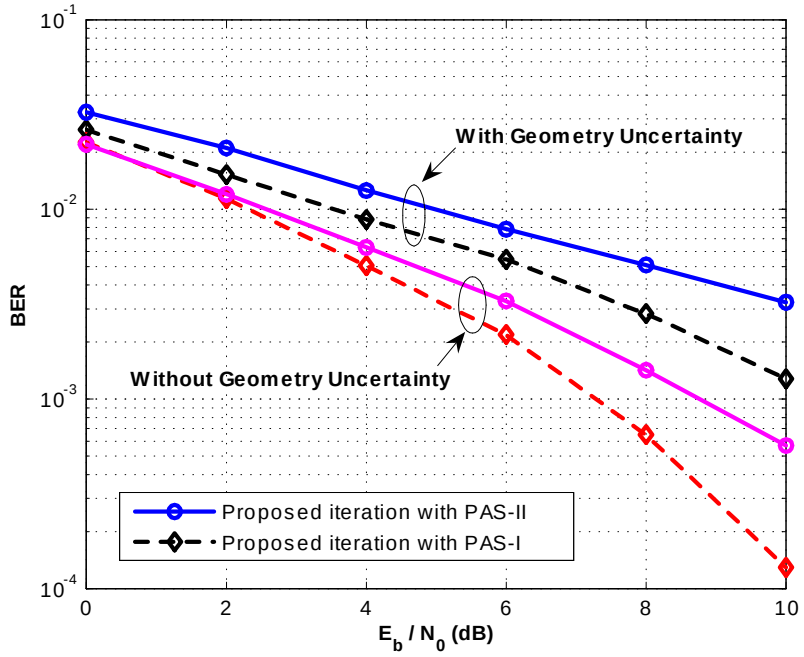


Figure 4.9: BER performance of the proposed iterative schemes (by 30 iterations) with and without array geometry uncertainty, for a 5-user MIMO-CDMA system with 6 element Tx ULA and 2 element Rx ULA, $N_c = 15$, $K_i = 2$.

4.7 Summary

In this chapter, the problem of joint precoding and decoding optimization in the downlink of MIMO-CDMA systems over frequency-selective multipath fading channels has been studied. It has been shown that by utilizing the MIMO-STAR manifold concept, the channel can be properly exploited in both space and time domain. Criterion of optimal multiplexing order has been derived based on predefined SNIR threshold. An upper-bound of SNIR has been given. Two Iterative optimal iterative algorithms have been proposed based on minimizing the overall MSE under the different power allocation schemes. Furthermore, the close-form sub-optimization algorithm has been derived by maximizing the SNIR with user Tx power constraint. Furthermore, by using the upper-bound of symbol error rate, another close-form sub-optimization algorithm has been proposed to minimize the total Tx power while satisfying symbol error rate requirement. The performance of the proposed schemes is supported by simulation results. The proposed iterative algorithms are found robust against array geometry uncertainty compared with conventional approaches.

Appendix 4.A Proof of Lemma 4.1

Proof. From the Cauchy-Schwarz Inequality (0.6.3 in [65]),

$$\begin{aligned}
\mathrm{SNIR}_{ij} &= \frac{\overline{\underline{w}}_{ij}^H \mathbb{G}_{i,i}^H \mathbb{M}_{ij}^{-1/2} \mathbb{M}_{ij}^{1/2} \underline{w}_{ij}}{\underline{w}_{ij}^H \mathbb{M}_{ij}^{1/2} \underline{w}_{ij}} && (4.63)\\
&\leq \frac{\left(\overline{\underline{w}}_{ij}^H \mathbb{G}_{i,i}^H \mathbb{M}_{ij}^{-1} \mathbb{G}_{i,i} \overline{\underline{w}}_{ij}\right)\left(\underline{w}_{ij}^H \mathbb{M}_{ij} \underline{w}_{ij}\right)}{\underline{w}_{ij}^H \mathbb{M}_{ij} \underline{w}_{ij}} && (4.64)\\
&= \overline{\underline{w}}_{ij}^H \mathbb{G}_{i,i}^H \mathbb{M}_{ij}^{-1} \mathbb{G}_{i,i} \overline{\underline{w}}_{ij} && (4.65)
\end{aligned}$$

By substituting $\mathbb{M}_{ij}$ with Eqn. (4.15) and (4.20), inequation (4.65) can be rewritten as

$$\mathrm{SNIR}_{ij} \leq \overline{\underline{w}}_{ij}^H \mathbb{G}_{i,i}^H \left[\mathbb{M}_i + \mathbb{G}_{i,i} \left(\sum_{\eta \neq j, \eta=1}^{N_i^{(s)}} \overline{\underline{w}}_{i\eta} \overline{\underline{w}}_{i\eta}^H \right) \mathbb{G}_{i,i}^H \right]^{-1} \mathbb{G}_{i,i} \overline{\underline{w}}_{ij} \quad (4.66)$$

By the inversion lemma:

$$(\mathbb{A} + \underline{u}\,\underline{v}^H)^{-1} = \mathbb{A}^{-1} - \frac{\mathbb{A}^{-1}\underline{u}\,\underline{v}^H\mathbb{A}^{-1}}{1 + \underline{v}^H \mathbb{A} \underline{u}} \quad (4.67)$$

$$\begin{aligned}
\mathrm{SNIR}_{ij} &= \overline{\underline{w}}_{ij}^H \mathbb{G}_{i,i}^H \left[\underbrace{\mathbb{M}_i + \sum_{\eta \neq j, \eta=2}^{N_i^{(s)}} \mathbb{G}_{i,i} \overline{\underline{w}}_{i\eta} \overline{\underline{w}}_{i\eta}^H \mathbb{G}_{i,i}^H}_{\triangleq \tilde{\mathbb{M}}_{i,j}^{(2)}} + \mathbb{G}_{i,i} \overline{\underline{w}}_{i1} \overline{\underline{w}}_{i1}^H \mathbb{G}_{i,i}^H \right]^{-1} \mathbb{G}_{i,i} \overline{\underline{w}}_{ij} && (4.68)\\
&= \overline{\underline{w}}_{ij}^H \mathbb{G}_{i,i}^H \tilde{\mathbb{M}}_{i,j}^{(2)^{-1}} \mathbb{G}_{i,i} \overline{\underline{w}}_{ij} - \overline{\underline{w}}_{ij}^H \mathbb{G}_{i,i}^H \underbrace{\frac{\tilde{\mathbb{M}}_{i,j}^{(2)^{-1}} \mathbb{G}_{i,i} \overline{\underline{w}}_{i1} \overline{\underline{w}}_{i1}^H \mathbb{G}_{i,i}^H \tilde{\mathbb{M}}_{i,j}^{(2)^{-1}}}{1 + \overline{\underline{w}}_{i1}^H \mathbb{G}_{i,i}^H \tilde{\mathbb{M}}_{i,j}^{(2)^{-1}} \mathbb{G}_{i,i} \overline{\underline{w}}_{i1}}}_{\text{semi-definite-positive}} \mathbb{G}_{i,i} \overline{\underline{w}}_{ij} && (4.69)\\
&\leq \overline{\underline{w}}_{ij}^H \mathbb{G}_{i,i}^H \tilde{\mathbb{M}}_{i,j}^{(2)^{-1}} \mathbb{G}_{i,i} \overline{\underline{w}}_{ij} && (4.70)\\
&\leq \cdots && (4.71)\\
&\leq \overline{\underline{w}}_{ij}^H \mathbb{G}_{i,i}^H \tilde{\mathbb{M}}_{i,j}^{(N_i^{(s)})^{-1}} \mathbb{G}_{i,i} \overline{\underline{w}}_{ij} && (4.72)\\
&= \overline{\underline{w}}_{ij}^H \mathbb{G}_{i,i}^H \left(\mathbb{M}_i + \mathbb{G}_{i,i} \overline{\underline{w}}_{iN_i^{(s)}} \overline{\underline{w}}_{iN_i^{(s)}}^H \mathbb{G}_{i,i}^H \right) \mathbb{G}_{i,i} \overline{\underline{w}}_{ij} && (4.73)\\
&\leq \overline{\underline{w}}_{ij}^H \mathbb{G}_{i,i}^H \mathbb{M}_i \mathbb{G}_{i,i} \overline{\underline{w}}_{ij} && (4.74)
\end{aligned}$$

■

Appendix 4.B Proof of Theorem 4.1

Proof. Consider the eigenvalue decomposition of Hermitian matrix

$$\overline{\overline{\mathbb{W}}}_i \overline{\overline{\mathbb{W}}}_i^H = \mathbb{U}_i \mathbb{D}_i \mathbb{U}_i^H \tag{4.75}$$

where $\mathbb{U}_i$ is unitary matrix composed of orthonormal row vectors $\underline{u}_{i1}, \cdots, \underline{u}_{i\overline{N}}$ and $\mathbb{D}_i$ is a diagonal matrix. It is obviously that the diagonal elements, denoted by $\overline{P}_{ij}$, can be regarded as power distribution factor within the i^{th} transmitter, $\sum_j \overline{P}_{ij} = \overline{P}_i$.

By rewriting $\overline{\overline{\mathbb{W}}}_i = \mathbb{U}_i \mathbb{D}_i^{1/2}$, the total SNIR of the i^{th} receiver

$$\begin{aligned} & \sum_{j=1}^{N_i^{(s)}} \text{SNIR}_{ij} \\ \overset{\text{Lemma 4.1}}{=} & \sum_{j=1}^{N_i^{(s)}} \underline{u}_{ij}^H \mathbb{D}_i^{1/2} \mathbb{G}_{i,i}^H \mathbb{M}_i^{-1} \mathbb{G}_{i,i} \mathbb{D}_i^{1/2} \underline{u}_{ij} \qquad (4.76) \\ \overset{\text{Lemma 4.2}}{\leq} & \sum_{j=1}^{N_i^{(s)}} \hat{\lambda}_j \qquad (4.77) \end{aligned}$$

Combine the above inequality with $\sum_{j=1}^{N_i^{(s)}} \text{SNIR}_{ij} \geq N_i^{(s)} \gamma$, (4.23) can be easily obtained. ■

Appendix 4.C Proof of Eqn. (4.18)

Proof. From Eqn. (4.16), the MSE matrix of i^{th} users can be derived as

$$\begin{aligned}
\mathbb{E}_i &= \mathbb{W}_i^H \mathbb{R}_{xx,i} \mathbb{W}_i + \mathbb{I}_{N_i^{(s)}} - \mathbb{W}_i^H \mathbb{G}_{i,i} \overline{\mathbb{W}}_i - \overline{\mathbb{W}}_i^H \mathbb{G}_{i,i}^H \mathbb{W}_i && (4.78)\\
&= \left(\mathbb{R}_{xx,i}^{-1} \mathbb{G}_{i,i} \overline{\mathbb{W}}_i\right)^H \mathbb{R}_{xx,i} \mathbb{R}_{xx,i}^{-1} \mathbb{G}_{i,i} \overline{\mathbb{W}}_i + \mathbb{I}_{N_i^{(s)}} && (4.79)\\
&\quad - \left(\mathbb{R}_{xx,i}^{-1} \mathbb{G}_{i,i} \overline{\mathbb{W}}_i\right)^H \mathbb{G}_{i,i} \overline{\mathbb{W}}_i - \overline{\mathbb{W}}_i^H \mathbb{G}_{i,i}^H \mathbb{R}_{xx,i}^{-1} \mathbb{G}_{i,i} \overline{\mathbb{W}}_i && (4.80)\\
&= \mathbb{I}_{N_i^{(s)}} - \overline{\mathbb{W}}_i^H \mathbb{G}_{i,i}^H \left(\sum_{\xi=1}^{M} \overline{\mathbb{G}}_{i,\xi} \left[\mathbb{I}_3 \otimes \left(\overline{\mathbb{W}}_\xi \overline{\mathbb{W}}_\xi^H \right) \right] \overline{\mathbb{G}}_{i,\xi}^H + \sigma_i^2 \mathbb{I}_{N_i^{(s)}} \right)^{-1} \mathbb{G}_{i,i} \overline{\mathbb{W}}_i && (4.81)\\
&= \mathbb{I}_{N_i^{(s)}} - \overline{\mathbb{W}}_i^H \mathbb{G}_{i,i}^H \left(\mathbb{G}_{i,i} \overline{\mathbb{W}\mathbb{W}}_i^H \mathbb{G}_{i,i}^H + \mathbb{M}_i \right)^{-1} \mathbb{G}_{i,i} \overline{\mathbb{W}}_i && (4.82)\\
&= \left(\mathbb{I}_{N_i^{(s)}} + \overline{\mathbb{W}}_i^H \mathbb{G}_{i,i}^H \mathbb{M}_i^{-1} \mathbb{G}_{i,i} \overline{\mathbb{W}}_i \right)^{-1} && (4.83)
\end{aligned}$$

where (4.81) is obtained by (4.13), (4.82) is by Eqn. (4.20), and (4.83) is obtained by the inversion lemma:

$$(\mathbb{A} + \mathbb{B}\mathbb{C}\mathbb{D})^{-1} = \mathbb{A}^{-1} - \mathbb{A}^{-1}\mathbb{B}(\mathbb{D}\mathbb{A}^{-1}\mathbb{B} + \mathbb{C}^{-1})^{-1}\mathbb{D}\mathbb{A}^{-1} \tag{4.84}$$

■

Appendix 4.D Proof of Eqn. (4.62)

Proof. From Eqn. (4.60), it can be derived

$$\rho_{ij} = u - \frac{1}{g\lambda_{ij}} \tag{4.85}$$

and

$$1 + g\rho_{ij}\lambda_{ij} = \frac{1}{\mu g\lambda_{ij}} \tag{4.86}$$

Substituting (4.86) into Eqn. (4.61) obtains

$$\prod_{j=1}^{N_i^{(s)}} (\mu g\lambda_{ij})^{-1} = \frac{\alpha}{\varepsilon} \tag{4.87}$$

which lead to

$$u = \left(\frac{\varepsilon}{\alpha}\right)^{N_i^{(s)}} \prod_{j=1}^{N_i^{(s)}} (g\lambda_{ij})^{-1} \tag{4.88}$$

Substituting (4.88) into (4.85), and considering the non-zero condition of power (4.58), the optimal power allocation coefficient can be obtained

$$\rho_{ij} = \max\left(0, \left(\frac{\varepsilon}{\alpha}\right)^{N_i^{(s)}} \prod_{\eta=1}^{N_i^{(s)}} (g\lambda_{i\eta})^{-1} - (g\lambda_{ij})^{-1}\right) \tag{4.89}$$

■

Chapter 5

Conclusions and Further Work

5.1 Thesis Summary

The work described in this thesis starts from answering why there is correlation between MIMO channels and how to model it. From the viewpoint of array processing, a novel spatial discrete channel model for spatial correlated MIMO system is proposed using the concept of array manifold of both Tx and Rx arrays. By implementing the first-order Taylor approximation, the diffused MIMO channel is approximated by modified point-source channel and the MIMO channel matrix is expressed explicitly by multipath characteristics, such as DODs, DOAs and complex path gains, and the geometry of both Tx and Rx arrays. The spatial correlation matrix is then derived, which is inconsistent with the conventional Kronecker-based correlation model. Further numeric studies prove that the proposed arrayed MIMO model gives more accurate capacity estimation of spatial correlated MIMO channel compared with Kronecker-based model. In the arrayed MIMO system, the number of resolvable multipaths is found of great important on bounding of the effective degree of freedom and MIMO capacity. However, the most important factor influencing the spatial correlation is the array geometry,

which can only be well taken into account by the proposed arrayed-MIMO model.

In the uplink of a multiuser asynchronous MIMO-CDMA wireless communication system operating in frequency selective fading channel, the (space-only) arrayed-MIMO model proposed in Chapter 2 has extended to STAR MIMO model using the concept of MIMO-STAR manifold matrix. A blind subspace-based joint DOA-TOA estimation algorithm and Tx beam rotation based DOD estimation scheme have been developed. Furthermore, given the complete estimation of the multipath parameters, two linear subspace-based (single user and multi-user) space-time receivers have been proposed by transforming the received signal-vector using the complement projection operator of the unwanted signal (e.g. MAI and ISI) subspace. Simulation results show that, by exploiting the array geometry and spatial-temporal information of the multipath fading channel, the proposed subspace-based receivers outperform RAKE and MMSE receivers, e.g., on interference cancellation.

In the downlink of MIMO-CDMA systems over multipath fading channels, the problem of precoding and decoding optimization have been studied. It has been shown that by utilizing the STAR manifold concept, the channel can be properly exploited in both space and time domain. A novel criterion is proposed to determine the optimal multiplexing order for each user. Optimal iterative algorithms have been proposed based on minimizing the overall MSE under the different power allocation schemes. Furthermore, close-form sub-optimization algorithms have been derived by maximizing the SNIR without power allocation and minimizing the transmit power while satisfying symbol error rate requirement. The performances of the proposed schemes are supported by simulation results.

5.2 List of Contributions

The list below states the main novel contributions in this thesis and some of them are supported by the publications:

- Proposal of a novel arrayed MIMO model based on the idea of array manifold vectors associated with both transmitter and receiver. It enables the geometrical investigation of spatial correlated MIMO system using classical array processing techniques.
- Proposal of a new spatial correlation model of MIMO channels represented by array manifold vectors. Compared with the widely-used Kronecker model, it provides a better estimation of the spatial correlation as well as the capacity.
- Derivation of a theory on the upper-bound of spatial degree of freedom based on the arrayed MIMO model.
- Extension of STAR manifold vector to MIMO-STAR manifold matrix.
- Development of a multiuser uplink asynchronous arrayed MIMO-CDMA model based on the idea of MIMO-STAR manifold operating in frequency selective fading channel.
- Estimation algorithms of channel parameters, DOA/TOA and DOD, in the uplink arrayed MIMO-CDMA systems.
- Proposal of the subspace-based space-time receivers for uplink arrayed MIMO-CDMA systems. The single-user ST-1 receiver, although with only the spreading sequence and the channel information of the desired user, provides considerable performance improvement compared with the space-time RAKE and MMSE receivers.

- Development of the system framework for joint precoder/decoder optimization in downlink arrayed MIMO-CDMA systems. Iterative algorithms have been proposed under the criterion of minimizing the total MSE of the entire network.

- Proposal of a theory on the optimal multiplexing order which helps to decide the dimensionality of the precoder/decoder matrices.

- Derivation of two close-form solutions for joint precoder/decoder optimization: one by maximizing the SNIR without inter-user power allocation; another by minimizing the transmit power while satisfying pre-defined symbol error rate requirement. These suboptimal solutions, because of the "close-form", are practically more efficient than the optimal iterative algorithms.

5.3 Suggestions for Further Works

A number of different problems associated with correlated MIMO systems have been investigated in this thesis. Based on the achievements made so far, many topics are opened for additional research effort.

5.3.1 Robust Space Time Processing In Arrayed MIMO

The proposed arrayed MIMO model introduced in this thesis will need many improvements before it can be implemented into commercial system.

- Noise in feedback channel: In conventional $\left(\overline{N}, N\right)$-MIMO, the number of channels needs to be estimated simultaneously is $\overline{N}N$. With the negative effect of channel noise and various interferences, the cost of estimation results feedback increases exponentially with $\overline{N}$ or N. The transmit space

time processing should be robust to the feedback information which may be corrupted by the noise.

- Partial feedback: In the majority of scenarios, the covariance matrix of the channels changes more slowly than the channels; and the knowledge of the covariance matrix is enough for the receiver to improve the system performance to a sufficient high level and feedback some partial but useful channel information to the transmitter. An algorithm to facilitate this approach in correlated MIMO using the proposed arrayed model will be an interesting topic.

- Diffused channel: Another problems about the robustness of the proposed MIMO model is about the diffused channel model described in Chapter 2. If the temporal diffusion is large enough, the first-order Taylor approximations made in Chapter 2 may incur large error and higher order terms need to be taken into account. The effect of these higher order terms within the proposed model needs fully investigation.

- Channel parameters estimation error: For some reason, the estimation of the channel parameters may introduce certain errors. For example, pointing error occurs if the estimated DOA is mismatched with the actual DOA of the signal. Such error can cause significant degradation of, e.g. MAI suppression, performance and prevents the implementation of the space time processing proposed in this thesis in commercial mobile system. Thus, it is critical to develop the robust design to minimize the sensitivity of the space time processing algorithms to such errors.

- Geometric uncertainty: Furthermore, as have been shown in Chapter 4, uncertainty of array geometry will degrade the performance of the arrayed

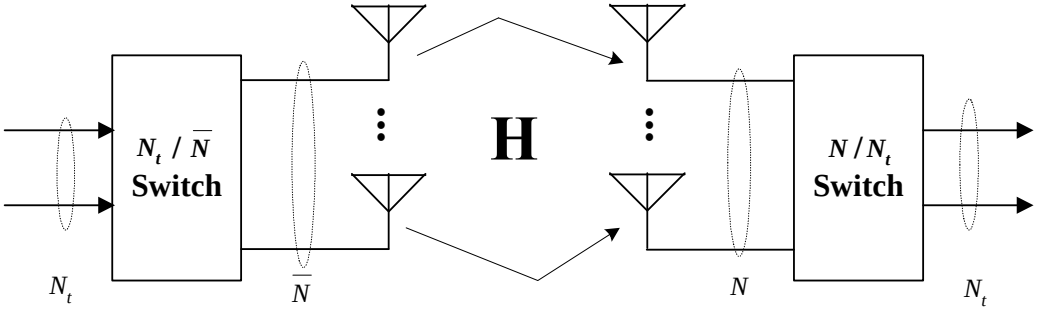


Figure 5.1: MIMO channel with antenna selection

MIMO system. Advance algorithms should be designed to improve the robustness of the precoders/decoders to the geometry errors of the Tx/Rx arrays.

5.3.2 Antenna Selection

In commercial mobile system, as price of antenna is relatively cheaper than that of RF components, e.g., upconversion/downconversion, amplifier, ADC, etc. As shown in Figure 5.1, it would be commercially beneficial to switch a limited number of RF chains to a subset of a large number of available antennas, so-called antenna selection [66].

The core of the antenna selection system is the Antenna Selection Schemes, which select a submatrix of $\mathbb{H}$ to form new $\mathbb{H}_t$ and improve the overall performance significantly. Based on Instantaneous channel state information (CSI), the conventional criterion of selecting $\mathbb{H}_t$ out of $\mathbb{H}$ are

- capacity maximization [67] [68] [69]
- average error probability minimization [70] [71] [72]
- maximize the minimum singular value of $\mathbb{H}_t$.

Drawbacks of these conventional schemes are

- Optimization procedure is computational complex. For example, to select receive antennas, when N is big, we need search $\binom{N_t}{N}$ possibilities
- When CSI varies quickly, precise estimation of CSI is difficult and need too-much additional bandwidth

In correlated MIMO scenario, based on long-term channel statistics, Dai et. al. [73] proposed a selection scheme to minimized the determinate of the transmit/receive channel covariance matrices, $\det\left(\overline{\mathbb{R}}\right)$ and $\det\left(\mathbb{R}\right)$. Drawback of this approach is that it needs probing the complete channel matrix $\mathbb{H}$ (e.g., via additional training procedure), which has been prove to be a very costly task when the number of the multiple antennas are large.

Based on covariance matrix of received signal-vector, $\mathbb{R}_t$=$\mathcal{E}\left\{\underline{x}_t\ \underline{x}_t^H\right\}$the spatial properties, e.g., DOA, of arrival and energy distribution of different multipaths $\underline{\beta}$ can be estimated using the proposed algorithms in Chapter 3, with which the optimal antenna set can be calculated to minimize the spatial correlation, or, the condition number of the covariance matrix $\mathbb{R}_t$,

$$\text{condition number } = \frac{\lambda_{\max}\left(\mathbb{R}_t\right)}{\lambda_{\min}\left(\mathbb{R}_t\right)} \tag{5.1}$$

where $\lambda_{\max}\left(\mathbb{R}_t\right)$ and $\lambda_{\min}\left(\mathbb{R}_t\right)$ are maximal and minimal eigenvalues of $\mathbb{R}_t$ respectively. It will be a blind algorithm without additional training/probing procedure. And, as DOA and optimal antenna set mapping can be set up in advance, the selection procedure does not add computation burden.

5.3.3 STBC in Arrayed Correlated MIMO System

Spatial diversity techniques have been proposed and adopted in 3G standards which are essentially based on the Space-Time Block Coding (STBC) transmission strategy suggested by Alamouti [7]. Space-Time Transmit Diversity (STTD)

scheme first proposed by Texas Instruments has been accepted by 3GPP as the open loop transmit diversity proposal to WCDMA. Two open loop transmit diversity techniques submitted and adopted by CDMA 2000 are the Space-Time Spreading (STS) scheme proposed by Lucent Technologies and the orthogonal transmit diversity (OTD) by Motorola.

Transmit antenna diversity as a means of further enhancing the system capacity and performance can be incorporated into the arrayed MIMO communication system. By using these transmit schemes, additional diversity can be gained without having to exhaust the number of spreading codes available. Many, if not all, reported research works on STBC, including the conventional STTD, STS and OTD schemes, are based on the i.i.d. channel assumption which ignores the spatial correlation of the MIMO channel. Although a few scholars have realized the necessity of taking into account the effect of spatial correlation in STBC, most of their work is based on Kronecker model. The implementation of the arrayed model proposed in this thesis in this area will be an interesting and promising direction.

5.3.4 Ad-hoc distributed precoding/decoding optimization

In Chapter 4, the joint precoder/decoder optimization in the arrayed MIMO-CDMA downlink systems is conducted in so-called centralized fashion, e.g., each user has the information of the spreading code, channel and precoder/decoder of all other users. This requires a significant user cooperation cost.

To cope with this, a suboptimal but distributed precoder/decoder optimization is needed, in which

- receiver of each UE only has the information, such as spreading code and channel, of its own and has to construct the decoding weight matrix based

on this limited information.

- at BS, Tx optimizes the precoding matrices with the information of spreading code and channel of all users, but not the decoding matrices.

One feasible solution to this ad-hoc distributed optimization problem is game theory, in which each user could be considered as a player in a game with multiple players.

References

[1] C. A. Balanis, *Antenna Theory: Analysis and Design*. John Wiley and Sons. Inc., 2nd edition., 1997.

[2] A. J. Paulraj, R. U. Nabar, and D. A. Gore, *Introduction to space-time wireless communications*. Cambridge University Press, 2003.

[3] T. S. Rappaport, *Wireless Communications, Principles and Practice*. Prentice Hall PTR, 2002.

[4] E. Biglieri, J. Proakis, and S. Shamai, "Fading channels: information-theoretic and communications aspects," *IEEE Trans. Information Theory*, vol. 44, no. 6, pp. 2619–2692, 1998.

[5] L. C. Godara, *Smart Antennas*. CRC Press, 2004.

[6] W. Lee and Y. Yu, "Polarization diversity system for mobile radio," *IEEE Trans. Communications*, vol. 20, no. 5, pp. 912–923, 1972.

[7] S. M. Alamouti, "A simple transmit diversity technique for wireless communications," *IEEE J. Select Areas Commun.*, vol. 16, no. 8, pp. 1451–1458, 1998.

[8] V. Tarokh, N. Seshadri, and A. R. Calderbank, "Space-time codes for high data rate wireless communication: performance criterion and code construction," *IEEE Trans. Information Theory*, vol. 44, no. 2, pp. 744–765, 1998.

[9] B. Clerckx, B. Clerckx, and C. Oestges, "Finite-SNR performance analysis of space-time coding in correlated ricean MIMO channels," *IEEE Trans. Information Theory*, vol. 53, no. 12, pp. 4761–4777, 2007.

[10] R. Schmidt, "Multiple emitter location and signal parameter estimation," *IEEE Trans. Antennas and Propagation*, vol. 34, no. 3, pp. 276–280, 1986.

[11] E. Telatar, "Capacity of multi-antenna gaussian channels," *Europ. Trans. Telecommun.*, vol. 10, no. 6, pp. 585–595, 1999.

[12] G. J. Foschini and M. J. Gans, "On limits of wireless communications in a fading environment when using multiple antennas," *Wireless Personal Commun.*, no. 6, pp. 311–335, 1998.

[13] V. V. Veeravalli, L. Yingbin, and A. M. Sayeed, "Correlated MIMO wireless channels: capacity, optimal signaling, and asymptotics," *IEEE Trans. Information Theory*, vol. 51, no. 6, pp. 2058–2072, 2005.

[14] W. C. Jakes, *Microwave Mobile Communications*. New York: Wiley, 1974.

[15] A. Saleh and R. A. Valenzuela, "A statistical model for indoor multipath propagation," *IEEE J. Select Areas Commun.*, vol. 5, no. 2, pp. 128–137, 1987.

[16] K. I. Pedersen, P. E. Mogensen, and B. H. Fleury, "A stochastic model of the temporal and azimuthal dispersion seen at the base station in outdoor propagation environments," *IEEE Trans. Veh. Technol.*, vol. 49, no. 2, pp. 437–447, 2000.

[17] E. Bonek, M. Herdin, W. Weichselberger, and H. Ozcelik, "MIMO - study propagation first!" in *IEEE Proc. Int. Symp. Signal Processing and Information Technology*, pp. 150–153, 2003.

[18] T. Svantesson and J. W. Wallace, "Tests for assessing multivariate normality and the covariance structure of MIMO data," in *IEEE Proc. Conf. Acoustics, Speech, and Signal Processing*, vol. 4, pp. IV–9, 2003.

[19] R. B. Ertel, P. Cardieri, K. W. Sowerby, T. S. Rappaport, and J. H. Reed, "Overview of spatial channel models for antenna array communication systems," *IEEE Pers. Commun. ,*, vol. 5, no. 1, pp. 10–22, 1998.

[20] S. D. Shan, G. J. Foschini, M. J. Gans, and J. M. Kahn, "Fading correlation and its effect on the capacity of multielement antenna systems," *IEEE Trans. Commun.*, vol. 48, no. 3, pp. 502–513, 2000.

[21] J. P. Kermoal, L. Schumacher, K. I. Pedersen, P. E. Mogensen, and F. Frederiksen, "A stochastic MIMO radio channel model with experimental validation," *IEEE J. Select Areas Commun.*, vol. 20, no. 6, pp. 1211–1226, 2002.

[22] M. T. Ivrlac, W. Utschick, and J. A. Nossek, "Fading correlations in wireless MIMO communication systems," *IEEE J. Select Areas Commun.*, vol. 21, no. 5, pp. 819–828, 2003.

[23] W. Weichselberger, M. Herdin, H. Ozcelik, and E. Bonek, "A stochastic MIMO channel model with joint correlation of both link ends," *IEEE Trans. Wireless Communications*, vol. 5, no. 1, pp. 90–100, 2006.

[24] A. M. Sayeed, "Deconstructing multiantenna fading channels," *IEEE Trans. Signal Process.*, vol. 50, no. 10, pp. 2563–2579, 2002.

[25] R. R. Muller, "A random matrix model of communication via antenna arrays," *IEEE Trans. Information Theory*, vol. 48, no. 9, pp. 2495–2506, 2002.

[26] M. Debbah and R. R. Muller, "MIMO channel modeling and the principle of maximum entropy," *IEEE Trans. Information Theory*, vol. 51, no. 5, pp. 1667–1690, 2005.

[27] A. F. Molisch, "A generic model for MIMO wireless propagation channels in macro- and microcells," *IEEE Trans. Signal Processing*, vol. 52, no. 1, pp. 61–71, 2004.

[28] T. D. Abhayapala, T. S. Pollock, and R. A. Kennedy, "Spatial decomposition of MIMO wireless channels," in *Proc. Int. Symp. Signal Processing and Its Applications*, vol. 1, pp. 309–312, 2003.

[29] M. Steinbauer, A. F. Molisch, and E. Bonek, "The double-directional radio channel," *IEEE Mag. Antennas and Propagat.* , vol. 43, no. 4, pp. 51–63, 2001.

[30] X. Hao, D. Chizhik, H. Huang, and R. A. Valenzuela, "A generalized space-time multiple-input multiple-output (MIMO) channel model," *IEEE Trans. Wireless Communications*, vol. 3, no. 3, pp. 966–975, 2004.

[31] A. Manikas and C. Proukakis, "Modeling and estimation of ambiguities in linear arrays," *IEEE Trans. Signal Processing*, vol. 46, no. 8, pp. 2166–2179, 1998.

[32] F. Rashid and A. Manikas, "Diffused multipath vector channels for arrayed MC-CDMA communication systems," in *IEEE Proc. Int. Symp. Wireless Communication Systems*, pp. 154–158, 2006.

[33] Q. H. Spencer, B. D. Jeffs, M. A. Jensen, and A. L. Swindlehurst, "Modeling the statistical time and angle of arrival characteristics of an indoor multipath channel," *IEEE J. Select Areas Commun. ,*, vol. 18, no. 3, pp. 347–360, 2000.

[34] V.Erceg and et al., "TGn channel models," *IEEE P802. 11, 802. 11-03/940r2*, pp. 1–47, 2004.

[35] N. Czink, M. Herdin, H. Ozcelik, and E. Bonek, "Number of multipath clusters in indoor MIMO propagation environments," *Electronics Letters*, vol. 40, no. 23, pp. 1498–1499, 2004.

[36] R. J. M. Cramer, R. A. Scholtz, and M. Z. Win, "Evaluation of an ultra-wide-band propagation channel," *IEEE Trans. Antennas Propogat.*, vol. 50, no. 5, pp. 561–570, 2002.

[37] J. W. Wallace and M. A. Jensen, "Modeling the indoor MIMO wireless channel," *IEEE Trans. Antennas Propogat.*, vol. 50, no. 5, pp. 591–599, 2002.

[38] D. Astely and B. Ottersten, "The effects of local scattering on direction of arrival estimation with music," *IEEE Trans. Signal Processing*, vol. 47, no. 12, pp. 3220–3234, 1999.

[39] M. A. Jensen and J. W. Wallace, "A review of antennas and propagation for MIMO wireless communications," *IEEE Trans. Antennas Propogat.*, vol. 52, no. 11, pp. 2810–2824, 2004.

[40] H. Ozcelik, M. Herdin, H. Hofstetter, and E. Bonek, "A comparison of measured 8x8 MIMO systems with a popular stochastic channel model at 5.2 ghz," in *Proc. Int. Conf. Telecommunications*, vol. 2, pp. 1542–1546, 2003.

[41] R. J. Muirhead, *Aspects of Multivariate Statistical Theory.* Wiley, 1982.

[42] A. S. Y. Poon, R. W. Brodersen, and D. N. C. Tse, "Degrees of freedom in multiple-antenna channels: A signal space approach," *IEEE Trans. Information Theory*, vol. 51, no. 2, pp. 523–536, 2005.

[43] A. S. Y. Poon, D. N. C. Tse, and R. W. Brodersen, "Impact of scattering on the capacity, diversity, and propagation range of multiple-antenna channels," *IEEE Trans. Information Theory*, vol. 52, no. 3, pp. 1087–1100, 2006.

[44] T. M. Cover and J. A. Thomas, *Elements of Information Theory.* New York: Viley, 1991.

[45] I. E. Telatar and D. N. C. Tse, "Capacity and mutual information of wideband multipath fading channels," *IEEE Trans. Information Theory*, vol. 46, no. 4, pp. 1384–1400, 2000.

[46] A. Leon-Garcia, *Probability and Random Processes for Electrical Engineering.* Addison-Wesley, 1989.

[47] X. Wang and A. Manikas, "STAR receiver in MIMO-CDMA multipath channels,", in *IEEE Proc. Int. Conf. Acoustics, Speech, and Signal Processing*, vol. 3, pp. III–229, 2007.

[48] A. Manikas and L. K. Huang, "STAR channel estimation in DS-CDMA communication systems," *IEE Proc. Communications*, vol. 151, no. 4, pp. 387–393, 2004.

[49] M. Wax, M. Wax, and T. Kailath, "Detection of signals by information theoretic criteria detection of signals by information theoretic criteria," *IEEE Trans. Signal Processing*, vol. 33, no. 2, pp. 387–392, 1985.

[50] D. H. Johnson and D. E. Dudgeon, *Array Signal Processing: Concepts and techniques*. Prentice-Hall, Inc., 1993.

[51] P. D. Karaminas and A. Manikas, "Super-resolution broad null beamforming for cochannel interference cancellation in mobile radio networks," *IEEE Trans. Veh. Technol.*, vol. 49, no. 3, pp. 689–697, 2000.

[52] T. Zhang, *Transceiver Design Over Space-Time Fading Channels*. Thesis, Imperial College London, 2008.

[53] W. Xiaodong and H. V. Poor, "Blind multiuser detection: a subspace approach," *IEEE Trans. Information Theory*, vol. 44, no. 2, pp. 677–690, 1998.

[54] U. Lai and R. D. Murch, "A transmit preprocessing technique for multiuser MIMO systems using a decomposition approach," *IEEE Trans. Wireless Communications*, vol. 3, no. 1, pp. 20–24, 2004.

[55] T. Salzer and D. Mottier, "Transmit beamforming for sdma in multi-carrier CDMA downlink on a per subcarrier basis," in *Proc. Int. Conf. Telecommunications*, vol. 1, pp. 793–798, 2003.

[56] A. Tarighat, M. Sadek, and A. H. Sayed, "A multi user beamforming scheme for downlink MIMO channels based on maximizing signal-to-leakage ratios," in *IEEE Proc. Conf. Acoustics, Speech, and Signal Processing*, vol. 3, pp. iii/1129–iii/1132, 2005.

[57] D. P. Palomar, J. M. Cioffi, and M. A. Lagunas, "Joint Tx-Rx beamforming design for multicarrier MIMO channels: a unified framework for convex optimization," *IEEE Trans. Signal Processing*, vol. 51, no. 9, pp. 2381–2401, 2003.

[58] Q. H. Spencer, A. L. Swindlehurst, and M. Haardt, "Zero-forcing methods for downlink spatial multiplexing in multiuser MIMO channels," *IEEE Trans. Signal Processing*, vol. 52, no. 2, pp. 461–471, 2004.

[59] Z. Shengli and G. B. Giannakis, "Optimal transmitter eigen-beamforming and space-time block coding based on channel correlations," *IEEE Trans. Information Theory*, vol. 49, no. 7, pp. 1673–1690, 2003.

[60] A. Manikas and J. W. P. Ng, "Crossed-dipole arrays for asynchronous DS-CDMA systems," *IEEE Trans. Antennas Propogat.*, vol. 52, no. 1, pp. 122–131, 2004.

[61] X. Wang and A. Manikas, "Joint linear precoder-decoder optimization over MIMO-CDMA multipath channels," in *IEEE Proc. Int. Symp. Personal, Indoor and Mobile Radio Communications*, pp. 1–5, 2007.

[62] R. Bhatia, *Matrix Analysis*. Springer, 2004.

[63] J. Yang and S. Roy, "Joint transmitter-receiver optimization for multi-input multi-output systems with decision feedback," *IEEE Trans. Information Theory*, vol. 40, no. 5, pp. 1334–1347, 1994.

[64] Z. Jinfan, W. Yongle, Z. Shidong, and W. Jing, "Joint linear transmitter and receiver design for the downlink of multiuser MIMO systems," *Communications Letters, IEEE*, vol. 9, no. 11, pp. 991–993, 2005.

[65] R. A. Horn and C. R. Johnson, *Matrix Analysis*. Cambridge, U.K.: Cambridge Univ. Press, 1990.

[66] A. F. Molisch and M. Z. Win, "MIMO systems with antenna selection," *IEEE Microwave Magazine*, vol. 5, no. 1, pp. 46–56, 2004.

[67] A. F. Molisch, M. Z. Win, C. Yang-Seok, and J. H. Winters, "Capacity of MIMO systems with antenna selection," *IEEE Trans. Wireless Communications*, vol. 4, no. 4, pp. 1759–1772, 2005.

[68] M. Gharavi-Alkhansari and A. B. Gershman, "Fast antenna subset selection in MIMO systems," *IEEE Trans. Signal Processing*, vol. 52, no. 2, pp. 339–347, 2004.

[69] A. Gorokhov, D. A. Gore, and A. J. Paulraj, "Receive antenna selection for MIMO spatial multiplexing: theory and algorithms," *IEEE Trans. Signal Processing*, vol. 51, no. 11, pp. 2796–2807, 2003.

[70] D. A. Gore and A. J. Paulraj, "MIMO antenna subset selection with space-time coding," *IEEE Trans. Signal Processing*, vol. 50, no. 10, pp. 2580–2588, 2002.

[71] D. A. Gore, J. R. W. Heath, and A. J. Paulraj, "Transmit selection in spatial multiplexing systems," *Communications Letters, IEEE*, vol. 6, no. 11, pp. 491–493, 2002.

[72] D. Gore, R. Heath, and A. Paulraj, "Statistical antenna selection for spatial multiplexing systems," in *IEEE Proc. Int. Conf. Communications*, vol. 1, pp. 450–454, 2002.

[73] L. Dai, S. Sfar, and K. B. Letaief, "Optimal antenna selection based on capacity maximization for mimo systems in correlated channels," *IEEE Trans. Communications*, vol. 54, no. 3, pp. 563–573, 2006.